Differential Role of Caspase-8 in Hepatocytes and Non-Parenchymal Liver Cells in a Model of Chronic Liver Injury and Progenitor Cell Activation

Von der Fakultät für Mathematik, Informatik und Naturwissenschaften
der RWTH Aachen University zur Erlangung des akademischen Grades
eines Doktors der Naturwissenschaften genehmigte Dissertation

vorgelegt von

Master of Science
Kunal Chaudhary
Kota, Indien

Berichter:
Universitätsprofessor Dipl. Ing. Dr. Werner Baumgartner
Privatdozent Dr. med. Konrad Streetz

Tag der mündlichen Prüfung: 5. Dezember 2012

Diese Dissertation ist auf den Internetseiten der Hochschulbibliothek online verfügbar

"It is every man's obligation to put back into the world at least the equivalent of what he takes out of it." — Albert Einstein

Table of contents

List of figures

1 Introduction

1.1 Liver - a unique organ

1.1.1 Physiology of the liver

Liver is the largest glandular organ in terms of its metabolic, synthesizing and detoxifying functions within mammalian body. It performs a plethora of functions in the regulation of blood glucose, synthesizes essential proteins, enzymes, carbohydrates, fatty acids, vitamins and co-factors for digestion and lipid metabolism, produces albumin, as well as prothrombin, fibrinogen, and non-immune α- and β-globulins. Liver serves as a main site for detoxification, eliminating a variety of endogenous and exogenous toxic compounds by metabolic conversion and bile acid excretion, regulation of ammonia, iron and bicarbonate homeostasis.

In adult human, liver makes up only 2% of total body weight (1400-1600 g), and is comprised of four lobes (Fig. 1.1). In adult mice, liver accounts for approximately 5% of total body weight (7-8 g), and is comprised of five lobes.
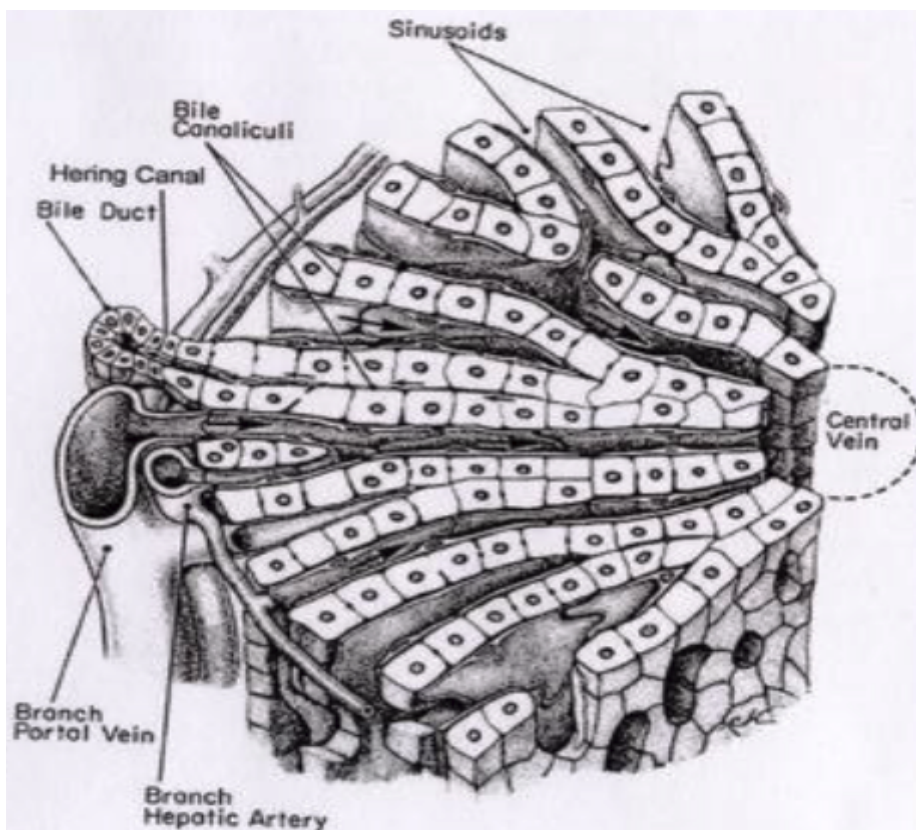
Figure 1.1 Liver anatomy. Diagram depicting the structure of a liver lobule. Each lobule consists of six portal triads surrounding a central vein. Each portal triad consists of a portal vein, a branch of the hepatic artery and a bile duct. Adapted from Junqueira and Carniero, 2002 (1).

The liver is composed of different cell types. Those are parenchymal cells or hepatocytes, which represent about 80% of hepatic cells. The non-parenchymal cells (NPCs) represents the remaining 20% of cells, which include endothelial cell, resident lymphocytes including natural killer (NK) cells and natural killer-T (NKT) cells, T-lymphocytes, Kupffer cells, and the population of mesenchymal cells, stellate cells, liver myofibroblasts and specialized cells like sinusoidal endothelial cells and cholangiocytes and liver progenitor cells (LPCs) (2, 3).

1.1.2 Chronic liver diseases

Correct liver functions are fundamental to human health and loss of these functions can be severely compromising. Chronic liver diseases can be caused by any condition that leads to gradual degradation and disorganization of the lobular architecture, portal hypertension resulting in fibrosis or cirrhosis and can be potentially fatal in cases of chronic liver failure. The word cirrhosis comes from the Greek word kirrhos, which means orange yellow (Rene Laennec, 1781-1826). Cirrhosis is considered to be irreversible and regarded as a possible end stage of many liver diseases and occurs only when a healthy liver tissue becomes damaged and is replaced by a scar tissue. The replacement process does not happen at once, but takes place over a gradual course of time. The new-scarred tissue prevents the regeneration or healing of the liver. The liver will lose the ability to function as the scarred tissue spreads. The consequences are portal hypertension, intrahepatic shunting of blood and impaired parenchymal function, which affecting protein synthesis, hormone metabolism and excretion of bile and bile salts. The most common complications are gastrointestinal hemorrhage, ascites, encephalopathy, bacterial infections, renal failure, hepatocellular carcinoma and hepatic failure (4, 5).

The underlying immunological response has usually been acting for months or years where inflammation and tissue repairing are in progress simultaneously which leads in the end to fibrosis and cirrhosis (6). The main causes of chronic liver disease or cirrhosis are: viral causes (hepatitis B (HBV), and C (HCV), or cytomegalovirus, metabolic causes (Haemochromatosis or Wilson's disease), autoimmune response causes (primary biliary cirrhosis or primary sclerosing cholangitis), toxin-related causes (alcoholic liver disease (ALD), and non-alcoholic steatohepatitis (NASH), auto-immune hepatitis (AIH), primary biliary cirrhosis (PBC) and primary sclerosing cholangitis (PSC) (7, 8).

1.1.3 Pathophysiology of DDC induced liver injury model

3,5-Diethoxycarbonyl-1,4-dihydrocollidine (DDC) is a porphyrinogenic agent and is a powerful inducer of δ-aminolaevulinate synthetase, the first and rate-limiting enzyme of the haem-biosynthetic pathway, in mouse liver. Chronic feeding of DDC in mice is a well-established model to study the mechanisms of LPCs activation and proliferation (9).

DDC feeding in mice results in disseminated necrosis, apoptotic bodies, ballooning of hepatocytes, deposition of brown pigment in macrophages, pigment plugs in the lumina of bile ducts, ductular proliferation, ductular reaction, periductal fibrosis, and portal-portal septa. This model is associated with significant elevations of serum transaminase, alkaline phosphatase, and serum bile acid levels and therefore useful to investigate the mechanisms of liver fibrosis and to test novel therapeutic strategies for these diseases (10). Within this model the proliferative capacity of hepatocytes is compromised, thus other regenerative mechanisms become activated. As a secondary mechanism here the induction of LPCs becomes important (3, 11).

1.1.4 Liver regeneration

One of the unique potentials of the liver is the capacity to restore its constant mass and cell function despite acute mechanical, chemical or immune-related injury. Liver regeneration and repair during chronic tissue injury is a complex process that is tightly controlled by the precise regulation of cell growth and death. Most knowledge about this comes to date from studies using the partial hepatectomy model, which is quite unique as it enables the synchronous start and shut down of the regenerative response (12). During chronic liver injury the situation is more complex, as individual liver cell types proliferate asynchronous and differ in their biological behaviour. Compensatory liver regeneration after chronic liver injury involves two distinct ways, depending on the nature of the injury and the cellular compartments undergoing proliferation. After partial hepatic resection or chemical injury, residing hepatocytes within the remaining liver tissue proliferates and restore the liver mass (12). Under certain types of severe liver injury the proliferative capacity of hepatocytes is impaired activating a potential stem cell compartment located within the intrahepatic biliary tree, giving rise to bipotential cells that ultimately differentiate to hepatic or biliary epithelial cells (13). These hepatic stem/progenitor cells are referred to by different names including 'LPCs' and 'small hepatocyte-like progenitors' (SHPCs) in rodents (14, 15) and

'intermediate cells' in humans (16-18). This cell population has been shown to have 'bipotential characteristics' expressing morphological and immunophenotypic features typical of both hepatic and biliary epithelial cells. Wilson and Leduc, 1958, were the first to describe the activation of this 'reserve cell compartment', which in humans is described as 'ductular activation' or 'progenitor cell activation' (19).
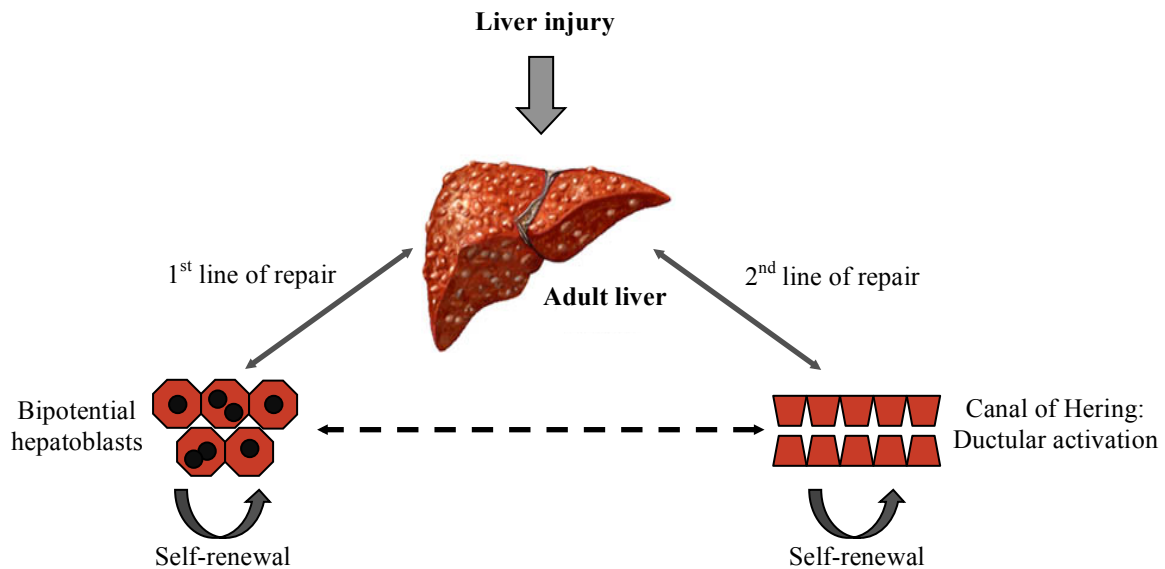
Figure 1.2. Two different cell lineages that contribute to liver regeneration and repair after injury. First line of defense in the face of injury is provided by hepatocytes. When hepatocyte renewal is compromised, or the liver damage is more severe, this calls upon activation of the second line of defence i.e. activation of bipotential stem/progenitor cells in the canal of Hering, located in the intra-hepatic biliary tree that take over the burden of regeneration.

1.2 Liver progenitor cells biology

1.2.1 Liver progenitor cells (LPCs)

LPCs were first observed and reported by Kinosita et al. (20) in rat livers, exposed to the carcinogenic azo dye 'Butter Yellow'. Morphologically, LPCs are small in size (relative to hepatocytes), with a large, ovoid nucleus with high nuclear to cytoplasmic ratio (21). LPCs are localized in the canals of Hering (13, 22, 23), the smallest branches of the intrahepatic biliary tree that constitute the putative hepatic stem cell niche (15) and proliferate in the periportal region of the liver. During LPCs-mediated liver regeneration, they infiltrate into the parenchyma along the periportal regions of the liver (24-26).

1.2.2 Characteristics of LPCs

The rodent model of DDC results in extensive growth of LPCs that share characteristics similar to hematopoietic progenitor cells, such as the receptor for stem cell factor (c-kit), and its ligand stem cell factor and Thy-1 (CD90) (rat) and CD34, a marker of early hematopoietic progenitor cells, stem cell antigen-1 (Sca-1) (mouse), specific for hematopoietic stem cell (HSC) (27-33). LPCs also express different combinations of phenotypic markers from both the hepatocyte and biliary lineage such as OV-6, α-fetoprotein (AFP), and Cytokeratine 19 (CK19) (9, 25, 34, 35). These cells are considered as a progenitor cell types because of their bipotent differentiation capabilities for both hepatocytes and biliary epithelial cells (11, 36-38).

1.2.3 Models of LPCs induction

Different liver injury models are currently used to study biology in rodents, including partial hepatectomy (PH) of two-thirds (70%) of the liver (39, 40), feeding a choline-deficient diet (CDE) supplemented with ethionine (19), feeding N-2-fluorenyl-acetamide (2AAF) in combination with PHx, treatment with pyrrolizidine alkaloids in conjunction with PHx, 2-AAF, and DDC (13, 41, 42). In these chronic liver injury models, the normal regenerative capacity of hepatocyte is blocked (43). A very efficient and extensive murine-specific model described is LPCs induction and expansion by feeding DDC supplemented rodent chow diet (41).

1.2.4. LPCs-mediated liver regeneration

Under conditions of chronic liver injury the liver is crippled by hepatocytes senescence prolife impairing the intrinsic proliferative and clonogenic capacity of inherent hepatocytes resulting in activation of a secondary bipotential amplifying transit compartment of extrinsic stem cells (LPCs) with hepatogenic potentials which are chemo-attracted towards to the site of liver injury, finding a niche and attempt to rescue the liver (11, 12, 44). Given their resistant to the effects of hepatotoxins/carcinogens, LPCs proliferate and migrate throughout the damaged liver lobules to replace lost parenchyma during liver regeneration (Fig. 1.3).
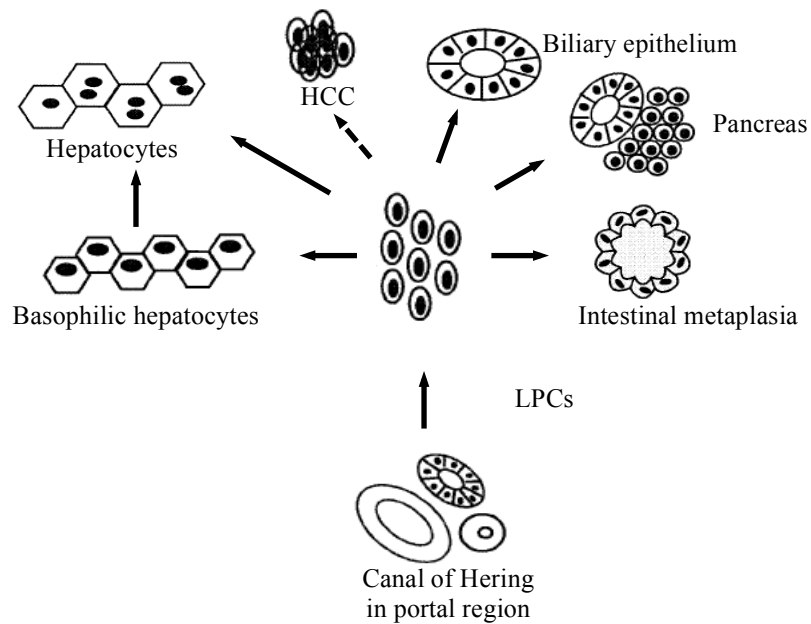
Figure 1.3 Origin and fate of LPCs. LPCs are bipotential stem cells, originating from the canals of Hering, which differentiate to produce cells of either the hepatocytes or biliary epithelia lineage. Under appropriate conditions, LPCs also have the capacity to differentiate into pancreatic cells and intestinal metaplasia, and are associated with hepatocellular carcinoma (HCC). Figure modified and adapted from Lowes K.N., 2003 (45).

1.2.5 Factors influencing LPCs activation, proliferation and differentiation

Microenvironment or liver "stem cell niche" collectively formed by the liver cells (hepatocytes, cholangiocytes, and progenitor cells), mesenchymal cells (Kupffer cells, endothelial cells, hepatic stellate cells) and the liver stroma regulates stem cells (LPCs) proliferation, maintenance and cell fate decisions. Another important factor is the intrinsic genetic regulation of stem cells (46). Multiple signaling pathways and an extensive number of factors such as, the stem cell factor/c-kit system, the interferon-gamma (IFN-γ) network, tumour necrosis factor (TNF), TNF-like weak induction of apoptosis (TWEAK) and Interleukin-6 (IL-6) (9, 47) have been identified to regulate the proliferation and differentiation of rodent LPCs (Fig. 1.4). Other member of the IL-6 family, including leukemia inhibitory factor (LIF) and/or oncostatin M (OSM) (48) levels are increased and remains elevated during LPCs activation, suggesting their role in the expansion and differentiation of the LPCs compartments (49).

Key role of OSM in the maturation of fetal hepatocytes in vitro and in vivo has recently been implicated, pointing to a similar role in the hepatic differentiation of LPCs (50). Interferon (IFN-γ) is another inflammatory cytokine considered to play an integral role in controlling stem cell-mediated liver regeneration (51-53). In addition, growth factors such as

hepatocyte growth factor (HGF), fibroblast growth factor (FGF), transforming growth factor (TGF) (54-56) plays an important role in both early and late events in LPCs activation. With the exception of IFN-α the inflammatory cytokines are pro-proliferative for LPCs (57).

LPCs express the receptors TNF-R1, which binds lymphotoxin alpha and TNF-α, as well Fn14, the receptor for TWEAK (58). Signaling through both of these receptors activates NF-κB, which is mitogenic for LPCs in vitro (59). It was shown that NPCs, such as liver resident macrophages and Kupffer cells, are integral for LPCs proliferation, and their depletion blunts the LPCs response. Both endothelial cells and stellate cells can enhance LPCs growth and differentiation behavior through the production of growth factors including HGF, EGF and TGF-α (60). Stellate cells co-proliferate with LPCs and surround the LPCs in a cellular network and may also direct the LPCs via direct cell-cell interaction. Inflammatory response mediated through resident Kupffer cells, hepatic stellate cells and infiltrating inflammatory cells, which secrete chemokines, growth factors and cytokines in response to liver injury also supports LPCs proliferation (45, 61).
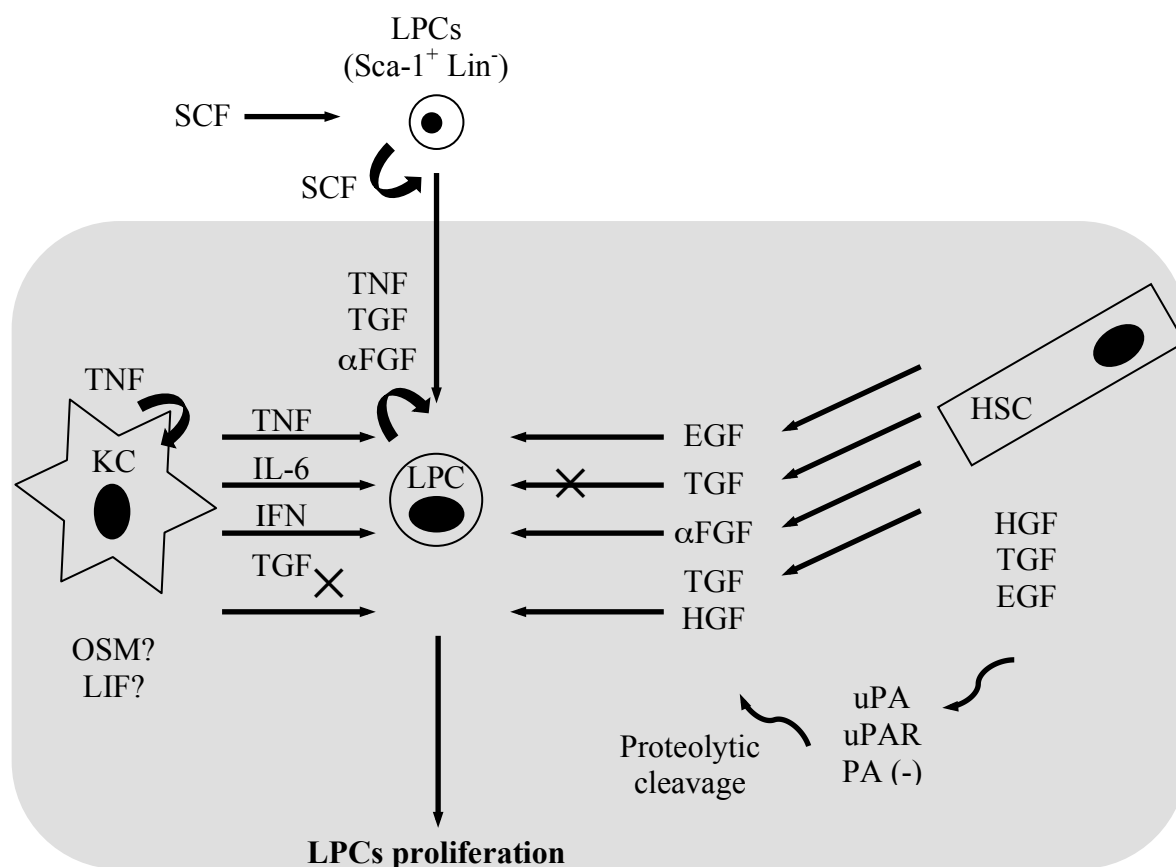
Figure 1.4 Diagram depicting the cytokines, growth factors and transcription factors involved in the development, proliferation and differentiation of LPCs. Figure modified and adapted from Lowes K.N. 2003 (45).

1.2.6 Clinical applications of the LPCs

LPCs existence in liver gives rise to debate and expectations regarding its clinical applications. With increasing number of patients waiting for liver transplantation with relatively lower organ availability, and due to their differentiation potential, LPCs have an enormous potential for new therapeutic treatments to a wide range of liver pathological conditions ranging from congenital metabolic diseases, end-stage liver cirrhosis, and hepatocarcinogenesis. Several obstacles remain to be overcome before the transplantation of LPCs can be used clinically. First, the immediate issue is to determine whether the murine studies can be translated to the human situation. Second, a major problem is the maintenance and expansion of isolated LPCs in an undifferentiated state in ex-vivo prior to transplantation. Third, mechanisms and factors governing differentiation of LPCs selectively to hepatocytes or cholangiocytes remains major concern and have to be addressed. Lastly understanding the mechanism of immune rejection must also be overcome.

1.3 Apoptosis

The process of programmed cell death (PCD) also termed as apoptosis (a term derived from the Greek word describing the falling off leaves from a tree) was classified as a morphological entity in a landmark paper by Kerr and coworkers in 1972 (62), who described the formation of apoptotic bodies from a cell. Apoptosis is a defined opposing process of mitosis and proliferation, which is essential for embryonic morphogenesis and the development of multicellular organisms and in the regulation, and maintenance of the cell populations (63). Apoptosis is defined as a physiological mechanism, occurring in a temporal sequence, which is regulated via distinct signals and signaling pathways (64, 65).

Two fundamentally different forms of cell death are described, apoptosis is a frequent form of programmed cell death, and necrosis is an accidental passive process starting with disruption of the cell membrane and a progressive breakdown of ordered cell structures in response to violent environmental perturbations such as severe hypoxia/ ischaemia, extremes of temperature and mechanical trauma (66).

Typical morphological change that occurs during apoptosis includes chromatin condensation, nuclear fragmentation, condensation of cytoplasm, rounding-up and detachment of cells and subsequently formation of apoptotic bodies containing intact organelles, as well as portions of the nucleus (67).

1.3.1 Molecular mechanisms of apoptosis

The event of apoptosis can be initiated by a set of cysteine proteases that are activated specifically in apoptotic cells, and are part of a large protein family known as the Caspases that are highly conserved through evolution (68-71).

Caspase are activated through two main pathways (72, 73). The first ("extrinsic pathway") begins at the cell surface and involves ligand-induced activation of death receptors, such as members of the TNF receptor family: TNF-R1 (Tumor necrosis factor-receptor 1), Fas/CD95, TRAIL-R1/DR4 (TNF-related apoptosis-inducing ligand receptor 1/2)/ (death receptor 4/5) and TRAIL-R2/DR5 which have death domain (DD) in their cytoplasmic tail (Fig. 1.5).
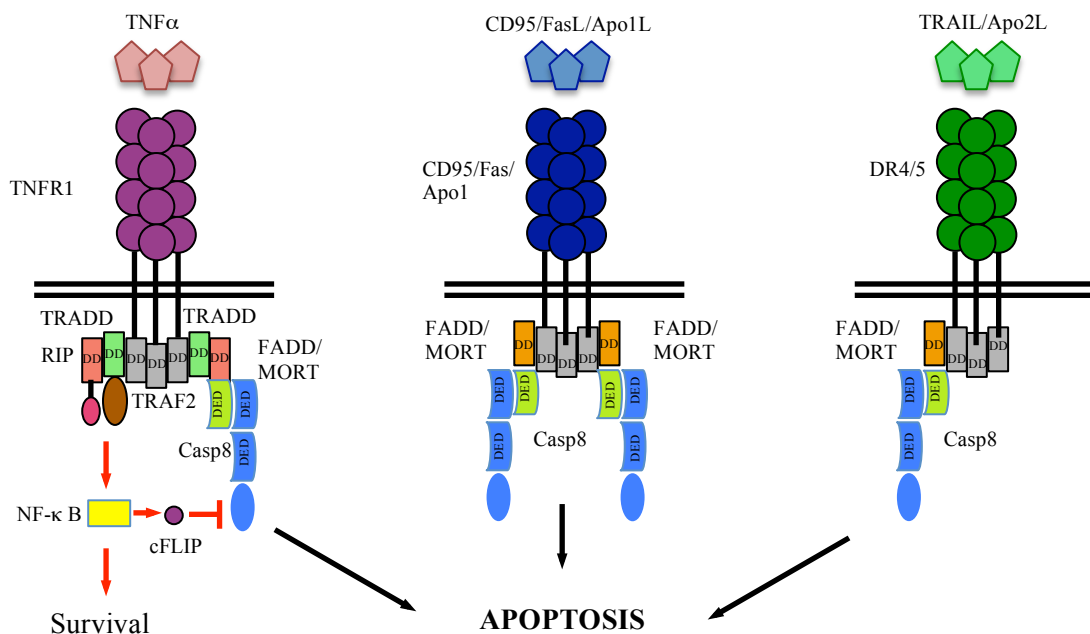
Figure 1.5 Composition of the death-inducing signaling complexes (DISC) of TNF-R1, CD95 and DR4/5. TRADD (TNF-R associated death domain), FADD (Fas associated death domain), TRAF2 (TNF-R associated factor 2), NF-κB (Nuclear factor kappa B), cFLIP (cellular FLICE inhibitory protein). Adapted from Danial, N.N. and Korsmeyer, S.J. 2004 (74).

Activation of Fas caused by binding of the respective ligand leads to a conformational change of the complex and recruits adapter molecule Fas-Associated protein with Death Domain (FADD). Then, via its death effector domain (DED) FADD recruits an inactive form of pro-Caspase-8 resulting in the formation of a death inducing signaling complex (DISC) (75-77). Pro-Caspase-8 gets activated by proteolytic cleavage (78-81) to convert to an active form resulting in the initiation of downstream effector Caspase i.e cleaves Caspase-3 leading to cell death (Fig. 1.6) (82-85).
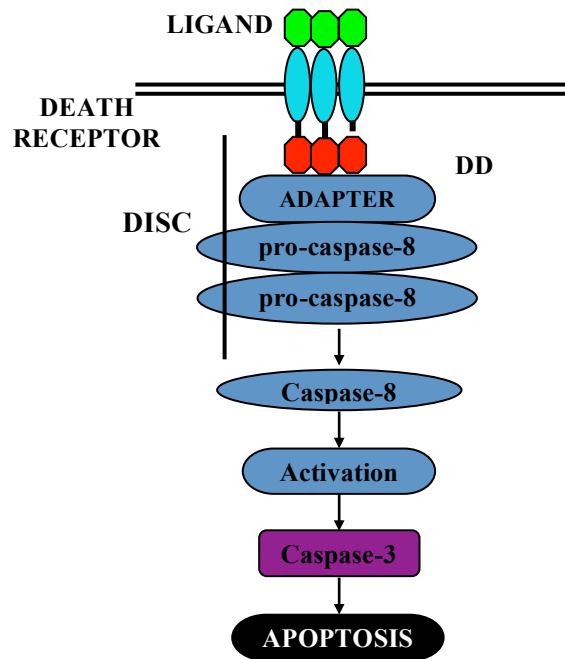
Figure 1.6 Simplified diagram of Caspase-8 induced apoptosis. Death receptor mediated apoptosis activates pro-Caspase-8 to Caspase-8. Activated Caspase-8 then cleaves and activates downstream effetor Caspases such as Caspase-1, 3, 6 and 7. Caspase-3 ultimately leads to apoptosis.

The second ("intrinsic pathway") involves mitochondrial integration of cellular stress signals such as ionizing radiation, heat shock, osmotic stress or chemotherapy, which leads to subsequent cleavage of the cytosolic protein Bid (BH3-interacting domain death agonist) to its active form tBid through Caspase-8. tBid translocates into the mitochondrial membrane causing subsequent release of cytochrome-c into the cytosol, which activates Caspase, initiating the formation of the apoptosome formed by apoptotic protease activating factor-1 (Apaf-1) and Caspase-9 (86) which cleaves and activates pro-Caspase-3, completing the cycle of activation as the initiator Caspase-8 (87). Additionally, more pro-Caspase-8 molecules are cleaved by Caspase-3 releasing a positive feedback loop (88).

1.3.2 Classification of Caspases

Caspases are synthesized as inactive proenzymes composed of a prodomain and a large and small subunit of Caspase catalytic region (CASc), which undergo proteolysis and activation by upstream Caspases or auto-cleaved resulting in the separation of the prodomain and the two subunits leading to the activation of Caspase (89-93).

To date 14 members of the Caspase family, which can be subdivided into three

categories, have been identified (94, 95). Two sub-groups of Caspase are characterized as initiators (Caspase-2, 8, 9 and 10) with long prodomains of more than 90 amino acids. The prodomains consist of either a death effector domain (DED) or Caspase recruitment domains (CARD), that are also present in adaptor molecules of the DISC such as FADD, RAIDD or also Apaf-1 serving as interaction motifs and executioner or effectors (Caspase-3, 6 and 7) in the apoptotic signalling pathway (Fig. 1.5). As the inflammatory Caspase, Caspase-1, 4, 5, 11, 12 and 13 are included in one subfamily. Caspase-14 is a unique Caspase as it belongs to neither apoptotic Caspase nor inflammatory Caspase (96).

2 Aim of the study

Liver regeneration and repair is based on cell proliferation and the concomitant clearing of injured tissue. Receptor mediated cell death has been defined as an important control element of those cellular interactions. Those cell death signals are mediated through the activation of a family of proteases, called initiator and effector Caspases. The particular role of the initiator Caspase-8 however within the complex process of chronic liver injury has not been thoroughly defined yet. Experiments were aimed to characterize the role of receptor mediated cell death in individual liver cell populations with special focus on hepatocytes, liver progenitor cells and immune cells. Within this study we therefore applied hepatocyte-specific conditional Caspase-8 knockout (Casp8$^{\Delta hepa}$) mice and mice carrying a ubiquitous deletion of Caspase-8 (Casp8$^{\Delta Mx}$) to investigate tissue specific effects of this Caspase.

3 Materials and methods

3.1. Materials

3.1.1 Chemicals

Product	Company, Location
Acetic acid 100%	AppliChem, Darmstadt
Acetone	J.T. Baker, Deventer
Agarose	Invitrogen, Karlsruhe
Ammonium persulfate (APS)	Sigma-Aldrich, Steinheim
Bovine Serum Albumin (BSA)	Sigma-Aldrich, Steinheim
5-bromo-2-deoxyuridine (BrDU)	Sigma-Aldrich, Steinheim
Bromophenol blue	Serva, Heidelberg
Chloroform	Merck, Darmstadt
Collagenase Type I	Worthington, Lakewood
Collagenase Type IV	Worthington, Lakewood
DEPC-treated water	Applied Biosystems, Darmstadt
Dexamethasone	Sigma-Aldrich, Steinheim
4′,6-Diamidino-2-phenylindole (DAPI)	St.Katharinen Vector Labs, Burlingame
Diethylether (DTT)	J.T. Baker, Deventer
Dry milk powder	AppliChem, Darmstadt
EDTA ($C_{10}H_{16}N_2O_8$)	AppliChem, Darmstadt
Eosine ($C_{20}H_8Br_4O_5$)	Sigma-Aldrich, Steinheim
Ethanol (CH_3CH_2OH)	Fishar, Saarbrücken
Ethidiumbromide (EtBr)	Sigma-Aldrich, Steinheim
Ficoll 400	Sigma-Aldrich, Steinheim
Formaldehyde 37%	Roth, Karlsruhe
Glucose ($C_6H_{12}O_6$)	AppliChem, Darmstadt
Glycin ($C_2H_5NO_2$)	AppliChem, Darmstadt
Haematoxylin	Roth, Karlsruhe
Hydrochloric acid (HCl)	AppliChem, Darmstadt
4-(2-Hydroxyethyl)-1-piperazineethanesulfonic acid (HEPES)	Roth, Karlsruhe
Isopropyl alcohol (2-Propanol, C_3H_8O)	Merck, Darmstadt

Ketamin ($C_{13}H_{16}CINO$)	Ceva, Duesseldorf
Lymphocyte Separation Medium LSM 1077	PAA, Coelbe
Magnesium chloride ($MgCl_2$)	Sigma-Aldrich, Steinheim
β-Mercaptoethanol, (C_2H_6OS)	AppliChem, Darmstadt
Methanol (CH_3OH)	VWR, Darmstadt
3-(N-Morpholino) propanesulfonic acid (MOPS)	Roth, Karlsruhe
Nicotinamide	Roche, Mannheim
Nonidet P-40	Sigma-Aldrich, Steinheim
Nycodenz	Axis-Shield, Oslo
Orange G ($C_{16}H_{10}N_2Na_2O_7S_2$)	Roth, Karlsruhe
Paraformaldehyde	Roth, Karlsruhe
Penicillin/Streptomycin (pen/strep)	Biochrom AG, Berlin
Phenylmethyl sulfonyl fluoride (PMSF)	Roth, Karlsruhe
Polyacrylamide, poly (2-propenamide)	Roth, Karlsruhe
Ponceau Red	Sigma-Aldrich, Steinheim
Potassium chloride (KCl)	Merck, Darmstadt
Salicylic acid ($C_7H_6O_3$)	Sigma-Aldrich, Steinheim
Sodium-Azide (NaN_3)	AppliChem, Darmstadt
Sodium carbonate (Na_2CO_3)	Merck, Darmstadt
Sodium dodecyl sulfate (SDS)	Roth, Karlsruhe
Sodium fluoride (NaF)	Serva, Heidelberg
Sodium hydrogencarbonate ($CHNaO_3$)	Roth, Karlsruhe
Sodium orthovanadate (Na_3VO_4)	AppliChem, Darmstadt
Sucrose ($C_{12}H_{22}O_{11}$)	Merck, Darmstadt
Tetramethylethylenediamine (TEMED)	Serva, Heidelberg
Triacetic acid	Merck, Darmstadt
Tris ($C_4H_{11}NO_3$)	AppliChem, Darmstadt
Triton X-100	Serva, Heidelberg
Trypan blue stain (0,4%)	Sigma-Aldrich, Steinheim
Tween 20 ($C_{58}H_{114}O_{26}$)	Sigma-Aldrich, Steinheim
Xylazine ($C_{12}H_{16}N_2S$)	Bernburg AG, Bernburg

3.1.2 Ready to use analytical chemicals and reagents

Product	Company, Location
Acrylamide solution 30 %	Biorad, Munich
BioRad Protein Assay	Biorad, Munich
Block and Sample	Promega, Mannheim
Complete Mini®	Roche, Mannheim
Covering solution for cryo sections (Tissue-Tek®)	Sakura, Staufen
Diaminobenzidine (DAB)	Sigma-Aldrich, Steinheim
Dako Pen	Dako, Hamburg
Dulbecco's Modified Eagle's Medium (DMEM)	Invitrogen, Karlsruhe
+4500 mg/l Glucose	
+GlutaMAX	
+Pyruvate	
DMEM F-12	Invitrogen, Karlsruhe
DNA marker 1 kb plus Ladder®	Invitrogen, Karlsruhe
Earles Basic Salt Solution (EBSS) with Ca^{2+} & Mg^{2+}	Gibco/Invitrogen, Karlsruhe
EBSS without Ca^{2+} & Mg^{2+}	Gibco/Invitrogen, Karlsruhe
ECL-Western-Blot-analysis solution®	Pierce/Thermo Scientific, Dreieich
Ethidiumbromid	Invitrogen, Karlsruhe
Fetal Calf Serum (FCS)	PAA, Coelbe
Gluthathione Agarose	Sigma-Aldrich, Steinheim
Oligo dT primer	Qiagen, Hilden
Paraformaldehyde	Roth, Karlsruhe
Penicillin/Streptomycin (P/S)	Gibco/Invitrogen, Karlsruhe
Phospho Buffered Saline (PBS) 1x & 10x	PAA, Marburg
Polyriboinosinic-polyribocytidylic (pIpC)	Amersham, Freiburg
Red Taq	Sigma-Aldrich, Steinheim
Rotiblock	Roth, Karlsruhe
Rotiphorese 10x SDS Page	Roth, Karlsruhe
SDS Running buffer 10x	Roth, Karlsruhe
Tris-Acetate EDTA Buffer (TAE-Buffer) 50x	Gibco/Invitrogen, Karlsruhe
TAE Buffer 10x	Roth, Karlsruhe
Trypsin Inhibitor	Sigma-Aldrich, Steinheim

Vectashield Mounting Medium with Dapi	Vector Laboratories, Burlingame
Williams-E Medium	Gibco/Invitrogen, Karlsruhe

3.1.3 Kit systems

Product	Company, Location
Anti-Sca-1 MicroBead Kit (FITC)	Miltenyi Biotec GmbH, Berg. Gladbach
DNeasy Tissue Kit	Qiagen, Hilden
Hot Star Taq Master Mix Kit	Qiagen, Hilden
Omniscript RT PCR Kit	Qiagen, Hilden
PE Annexin V Apoptosis Detection Kit I	BD Pharmingen, Heidelberg
RNeasy Mini Kit	Qiagen, Hilden
TUNEL Kit	Roche, Mannheim
TUNEL Label Mix	Roche, Mannheim

3.1.4 Consumables

Product	Company, Location
Adhesive Real-time PCR Seals	ABgene, Epsom
Beckman Centrifuge tub	Beckman Coulter, Krefeld
Catheter with injection port (Biovalve®20G: 1.0 x 25 mm)	Vygon, Swindon
Cell scrapers	BD, Heidelberg
Cell strainer, 70 µm nylon mesh	BD, Heidelberg
Coated VICRYL* Plus Sutures (8 x 70 cm: 22 mm ½C)	Ethicon, Norderstedt
Cover slips	Menzel-Gläser, Braunschweig
Cryo tubes	Nunc, Langenselbold
3,5-Diethoxycarbonyl-1,4-dihydrocollidine (DDC)	Sigma-Aldrich, Steinheim
Disposable needles 18G, 20G, 22G	BD, Heidelberg
Disposable scalpels sterile	Feather, Osaka
Disposable weighing boats	Carl Roth, Karlsruhe
Ethibond™ Excel Polyester sutures (75 cm: 17	Ethicon, Norderstedt

mm ½C)

FACS tube	BD, Heidelberg
Falcon tubes 50 ml	BD, Heidelberg
General chow for rodents	Altromin, Lage/Lippe
Glass pasteur pipette	Brand, Wertheim
Glassware	Schott-Duran, Mainz
Hand gloves latex	Semperit, Vienna
Hand gloves nitril	Semperit, Vienna
Haematocrit cappilaries (75 mm/75 µl)	Hirschmann Laborgeraete, Eeberstadt
Hybond-N+ (30 cm × 3 m) membranes	Amersham, Freiburg
Lab-Tek™ Chamber Slides	Nunc, Langenselbold
MACS LS-Columns	Miltenyi Biotec GmbH, Berg. Gladbach
Millex$^®$GP filter unit (0.45 µm)	Millipore, Ireland
Nitrocellulose membrane Protran$^®$	Whatman, Dassel
Parafilm	Pechiney Plastic Packaging, Chicago
Petri dish	Sardest, Nuembrecht
Reaction tubes (0.5-2 ml)	Eppendorf, Hamburg
Reaction tubes (15 ml, 50 ml)	Sarstedt, Nuembrecht
Sterile filter Tipps	VWR, Darmstadt
Sterile pipettes (2-50 ml)	Sarstedt, Nümbrecht
Super Frost slides	Roth, Karlsruhe
Tissue-Tek® III Uni-Cassette® System	Sakura, Staufen
Tranfer pipette (3.5 ml)	Sardest, Nuembrecht
Ultracentrifugation polyallomer tubes	Beckman Instruments GmbH, Munich
Unterpads with absorbent core of 6 cellulose layers	Hartmann, Heidenheim
8 Vial strips for PCR	Sardest, Nuembrecht
Well plates (6; 12; 24 wells)	BD Falcon, Heidelberg
96 Well plates for Protein/ RNA/DNA measurement	Greiner Bio-one, Frickenhausen
96 Well plates for Real-time PCR	StarLAb, Ahrensburg
X-ray films	Amersham, Freiburg

3.1.5 Enzymes, inhibitors and activators

Product	Company, Location
Collagenase Type IV	Worthington Biochemical, Lakewood
Complete Mini Protease Inhibitor	Roche, Mannheim
DNase I	Roche, Mannheim
Omniscript RT	Qiagen, Hilden
Proteinase K	AppliChem, Darmstadt
RNase-free DNase I	Amersham Biosciences, Freiburg
SYBR® GreenER qPCR SuperMix	Invitrogen, Karlsruhe
Taq DNA-Polymerase und Buffer	Roche, Mannheim

3.1.6 Antibodies

3.1.6.1 Primary antibodies

3.1.6.1.1 Western blot

Product	Company, Location
SMA	Merck Millipore, Schwallbach
Caspase-8	Enzo Life Sciences, Loerrach
GAPDH	Biogenesis/AbD Serotech, Kidlington
NF-κB p65 (A)	Santa Cruz Biotechnology, Inc., Heidelberg
p53	Cell Signalling, Danvers
PCNA Ab-1	Dianova GmbH, Hamburg
pSTAT3	Cell Signalling, Danvers

3.1.6.1.2 Fluorescence microscopy

Product	Company, Location
anti-CK19	Santa Cruz Biotechnology, Inc., Heidelberg
anti-Collagen	Abcam, Cambridge

3.1.6.1.3 Flow cytometry (Fluorescent Activated Cell Sorting, FACS)

Product	Company, Location
anti-CD11b PerCP	eBioscience, Frankfurt
anti-CD4 APC	eBioscience, Frankfurt
anti-CD45 PE	BD Pharmingen, Heidelberg
anti-Sca-1 FITC	Miltenyi Biotec GmbH, Berg. Gladbach
anti-OC-1, 2, 3	Kindly provided by Prof. M. Grompe, University of Oregon, USA

3.1.6.2 Secondary antibodies

3.1.6.2.1 Western blot

Product	Company, Location
rabbit anti-goat HRP	Santa Cruz Biotechnology, Inc., Heidelberg
chicken anti-mouse HRP	Santa Cruz Biotechnology, Inc., Heidelberg
anti-rabbit HRP	Cell Signalling, Danvers
chicken anti-rat HRP	Santa Cruz Biotechnology, Inc., Heidelberg

3.1.6.2.2 Fluorescence microscopy

Product	Company, Location
Alexa 488 donkey anti-mouse	Invitrogen, Karlsruhe
Alexa 594 goat anti-rabbit	Invitrogen, Karlsruhe

3.1.7 Primer-sequences

3.1.7.1 Genotyping-primers (all primers are displayed in 5´-3´ direction)

Target	Annealing Temp.	Sequence
Alb-Cre	62°C	**fwd:** CGG GTG AAC GTG CAA AAC AGG CTC
		rev: CTT GCA TGA CCG GTA TTG AAA CTC CAG
Casp8$^{loxP/loxP}$	58°C	**fwd:** AAC TTC GGC CGG CCA ATA ACT TCG

		rev: AGC AGA AAA ACT TGA AGA AAC TTG
Casp8 WT	60°C	**fwd:** CAT ACT GGT TGA GAA CAA GAC CTG G
		rev: GCA GAG GTG ACA AGA GGC CAC TG
Mx-Cre	59°C	**fwd:** CCA CGA CCA AGT GAC AGC AAT
		rev: TTC GGA TCA TCA GCT ACA CCA

3.1.7.2 Real-time PCR primers (all primers are displayed in 5´-3´direction)

Target	Annealing Temp.	Sequence
CK19	60°C	**fwd:** CGT ACC CCC AAA GGA AGA CA
		rev: TCA GAC CTG CGT CCC TTT TT
Cyclin A2	59°C	**fwd:** GTG GTG ATT CAA AAC TGC CA
		rev: AGA GTG TGA GAT GCC CTG G
Cyclin D1	60°C	**fwd:** AAG CAT GCA CAG ACC TTT GTG G
		rev: TTC AGG CCT TGC ATC GCA GC
Cyclin E1	59°C	**fwd:** TCC ACG CAT GCT GAA TTA TC
		rev: TTG CAA GAC CCA GAT GAA GA
FAS	60°C	**fwd:** ATG CTG TGG ATC TGG GCT GT
		rev: TCT CCT CTC TTC ATG GCT GG
FASL	60°C	**fwd:** TGA ATT ACC CAT GTC CCC AG
		rev: AAA CTG ACC CTG GAG GAG CC
Fn14	60°C	**Fwd:** CTA GTT CCT GGT CTG GAA GAT G
		rev: CCC TCT CCA CCA GTC TCC TCT A
GAPDH	60°C	**fwd:** TGT TGA AGT CAC AGG AGA CAA CCT
		rev: AAC CTG CCA AGT ATG ATG ACA TCA
IL-6	60°C	**fwd:** CCG GAG AGG AGA CTT CAC AG
		rev: TCC ACG ATT TCC CAG AGA AC
Pro Collagen-1α	60°C	**fwd:** GAA CAG GGT GTT CCT GAG A
		rev: GGA AAC CTC TCT GCG CTC TT
α-SMA	60°C	**fwd:** ATG AAG CCC AGA GCA AGA GA
		rev: ATG TCG TCC AGT TGG TGA T
TNF-α	60°C	**fwd:** GAA ACA CAA GAT GCT GGG ACA GT

		rev: CAT TCG AGG CTC CAG TGA ATT C
TWEAK	60°C	**fwd:** CGA GCT ATT GCA GCC CAT TAT
		rev: TCC TGC TTG TGC TCC ATC CT

3.1.8 Instruments and equipments

Instruments	Company, Location
Analytical balance	Sartorius, Goettingen
AxioImager Z1 Microscope	Carl Zeiss, Jena
CAT RM5 mixer	Novodirect, Kehl am Rhein
Cell incubator Haereus BB 6220	Thermo Scientific, Dreieich
Cell culture bench BSB6A	Gelaire Flow Laboratories, Meckenheim
Cell culture centrifuge Megafuge 1.0R, Heraeus	Thermo Scientific, Dreieich
Cell culture Incubator, Heraeus	Thermo Scientific, Dreieich
Centrifuge 5415D	Eppendorf, Hamburg
Cooling centrifuge 5417R	Eppendorf, Hamburg
Cryostat HM 550	Microm/Thermo Scientific, Dreieich
Cryotom HM 550 Cryostat	Microm/Thermo Scientific, Dreieich
Deep freezer, -20°C, -80°C	Liebherr, Ochsenhausen
Eppendorf Tabletop 5417 centrifuge	Eppendorf, Hamburg
FACSCanto II flow cytometer	BD, Heidelberg
Fuji LAS mini 4000	GE Healthcare Europe, Freiburg
Gel dryer	Biometra, Goettingen
Heraeus-Kendro Megafuge 1.0R	Thermo Scientific, Dreieich
MilliQ Plus PF Water Purification System	Millipore Corporation, Billerica
Minigel twin gel chamber	Biometra, Goettingen
Multichannel pipette	Eppendorf, Hamburg
Multigel gel chamber	Biometra, Goettingen
NanoDrop; ND-2000c	Peqlab Biotechnologie, Erlangen
Optima™ L-80XP Ultracentrifuge	Beckman Coulter, Krefeld
Overhead shaker REAX 2	Heidolph, Schwabach
Perfusion pump	Ismatec, Wertheim-Mondfeld
pH-Meter Beckman 3500 digital	Beckman, Munich

pH Meter PB-11	Sartorius, Goettingen
Pipettes	Eppendorf, Hamburg
Powersupply PowerPac HC	BioRad, Munich
7300 Real-Time PCR System	Applied Biosystems, Darmstadt
Roller Mixer SRT 9	Stuart, Staffordshire
SDS PAGE electrophoresis system PerfectBlue Twin L	Peqlab Biotechnologie, Erlangen
Semi-Dry-blotter MAXI Blotting chamber	Carl-Roth GmbH, Karlsruhe
Shaking incubator Unimax 1010	Heidolph, Schwabach
Subcell GT gel chamber	Biorad, Munich
Thermocycler T3000 and Tpersonal	Biometra, Goettingen
Thermomixer 5436	Eppendorf, Hamburg
Trans-Blot cell Blotting chamber	Biorad, Munich
QuadroMACS™ Separator	Miltenyi Biotec GmbH, Berg. Gladbach
Vortex Genius 3	IKA, Staufen

3.1.9 Buffer preparation

3.1.9.1 Anesthesia

Ketamin	450 µl
NaCl 0.9%	5 ml
Rompun	50 µl

3.1.9.2 BrdU

5-bromo-2-deoxyuridine (BrdU) solution	300 mg
NaCl 0.9%	100 ml

3.1.9.3 Liver cell isolation buffer

Buffers and media	Additives	Volume
High glucose DMEM	Soybean trypsin inhibitor	0.04 mg/ml
	Penicillin, Streptomycin	5%

	Fetal calf serum (FCS)	5%
Solution I	EBSS without Ca and Mg	50 ml
	EGTA	100 mM
Solution II	EBSS with Ca and Mg	30 ml
	Hepes, pH 7.4	10 mM
Solution III	EBSS with Ca and Mg	50 ml
	Hepes, pH 7.4	10 mM
	Collagenase	0.3 mg/ml

3.1.9.4 Tail lysis buffer

NID buffer	Volume	Final concentration
Gelatine type3 10 mg/ml	10 ml	0.1 mg/ml
KCl 1 M	50 ml	0.05 M
$MgCl_2$ 1 M	2 ml	2 mM
NP-40	4.5 ml	0.45%
Tris 1 M	10 ml	0.01 M
Tween 20	4.5 ml	0.45%
H_2O add	1 l	

3.1.9.5 Whole cell protein extraction buffer

NP40 buffer	Volume	Final concentration
Tris HCl 7.5 pH (1 M)	25 ml	50 mM
NaCl (5 M)	15 ml	150 mM
Nonidet P-40	2.5 ml	0.5%
Sodium fluoride	1.05 g	50 mM
H_2O add	500 ml	
Freshly added:		
Sodium vanadate (100 mM)	100 µl	1 mM
DTT (1 M)	10 µl	1 mM
PMSF (100 mM)	100 µl	1 mM
Complete Mini® (Roche)	1 tablet	

H₂O add	10 ml

3.1.9.6 Buffers for western blot

Ponceau S

For a 10x stock solution, a solution of 2% Ponceau S, 30% trichloracetic acid and 30% sulfosalicylic acid in H_2O was generated. The solution was stable at room temperature for over one year. 1x Ponceau S working solution was diluted in 1% acetic acid.

10x Running buffer	Volume	Final concentration
Tris 15.	1 g	25 mM
Glycine	2 g	192 mM
SDS	5 g	0.5%
dH₂O add	1 l	

10x Transfer buffer	Volume	Final concentration
Tris	24.4 g	
Glycine	112.6 g	
dH₂O add	1 l	
For 1x transfer buffer:		
10x transfer buffer	100 ml	10%
Methanol	200 ml	20%
dH₂O add	1 l	

Buffer A	Volume	Buffer B	Volume
Tris	91.0 g	Tris	30.3 g
SDS	2 g	SDS	2 g
dH₂O add	500 ml	H₂O add	500 ml
adjust to pH 8.8 (6 M HCl)		adjust to pH 6.8 (6 M HCl)	

Separating gel	8%	10%	12.5%	15%
dH$_2$O	21.84 ml	18.5 ml	14.32 ml	10.145 ml
Buffer A	14.8 ml	14.8 ml	14.8 ml	14.8 ml
Acrylamide	13.36 ml	16.7 ml	20.87 ml	25.045 ml
APS 10%	300 μl	300 μl	300 μl	300 μl
TEMED	30 μl	30 μl	30 μl	30 μl

Stacking gel	Volume
dH$_2$O	18 ml
Buffer B	7.5 ml
Acrylamide	4.5 ml
APS 10%	225 μl
TEMED	15 μl

3.1.9.7 Agarose gel

Agarose	1%
Ethidium Bromide	0.00017%
in 1x TAE	

3.1.9.8 BSA solution (30%)

BSA	30 g
PBS	In 100 ml

3.1.9.9 HBSS++

BSA	0.06%
EDTA in HBSS	0.3 mM

3.1.9.10 MACS buffer (degassed)

BSA	1.6%
EDTA	100 mM

3.2 Methods

3.2.1 Animal experimental models

3.2.1.1 Housing and breeding of mice

All mice strains were group-housed (3 to 5 per cage) and bred in a pathogen-free, temperature and humidity controlled facility at the Institute for Laboratory Animal Science (ILAS), University Hospital Aachen with 12 h light-dark cycles and ad libitum access to water and pelleted roden chow. All experimental protocols were approved by the local authority for environment conservation and consumer protection of the state North Rhine–Westphalia (LANUV) and the ILAS guidelines and were performed in accordance with the German legislation on protection of animals and the National Institutes of Health Guide for the Care and Use of Laboratory Animals.

3.2.1.2 Used mouse strains

To reveal Caspase-8 signalling in LPCs induction and proliferation in DDC induced chronic liver injury, we used hepatocyte-specific conditional Caspase-8 knockout (Casp8$^{\Delta hepa}$) mice [97] and mice with ubiquitous deletion of Caspase-8 (Casp8$^{\Delta Mx}$) and Cre (-) (Casp8$^{loxP/loxP}$) littermates as wild-type (WT) controls.

3.2.1.2.1 Generation of hepatocyte-specific conditional Caspase-8 knockout (Casp8$^{\Delta hepa}$) mice

Generation of Casp8$^{\Delta hepa}$ mice was achieved by crossing transgenic mice that express the Cre-recombinase open reading frame (ORF) under the control of both the mouse albumin regulatory elements and the α-fetoprotein enhancers (AlfpCre transgene) [98] with mice expressing loxP-flanked Caspase-8 alleles (Casp8$^{loxP/loxP}$) (Fig. 3.1).
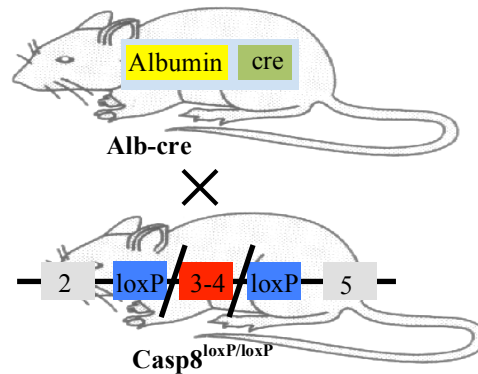
Figure 3.1 Strategy of hepatocyte-specific conditional Caspase-8 knockout (Casp8$^{\Delta hepa}$). For the hepatocyte-specific Caspase-8 deletion, Casp8$^{loxP/loxP}$ mice were crossed with animals expressing a Cre transgene under control of the hepatocyte-specific albumin promoter (98).

3.2.1.2.2 Generation of mice carrying a ubiquitous deletion of Caspase-8 (Casp8$^{\Delta Mx}$) and their use for a ubiquitous or tissue-specific inducible deletion of the Caspase-8 gene

Generation of Casp8$^{\Delta Mx}$ mice was achieved by crossing Casp8$^{loxP/loxP}$ mice with transgenic mice expressing an Mx-Cre transgene under control of the type-1 Interferon (IFN)-sensible myxovirus resistance-1 (*Mx-1*) promoter (Fig. 3.2) (99).
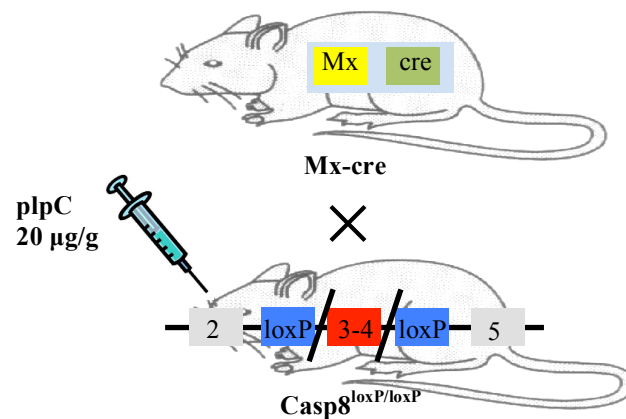
Figure 3.2 Strategy of inducible ubiquitous deletion of Caspase-8 (Casp8$^{\Delta Mx}$). For the ubiquitous deletion of Caspase-8 (Casp8$^{\Delta Mx}$), Casp8$^{loxP/loxP}$ mice were crossed with mice expressing an Mx-Cre transgene under control of the type-1 Interferon (IFN)-sensible myxovirus resistance-1 (*Mx-1*) promoter and transgenic Mx-Cre mice were injected i.p. with 20 μg/g body weight pIpC.

To induce deletion of Caspase-8, transgenic Mx-Cre mice were injected intraperitoneally (i.p.) with 20 μg/g body weight polyriboinosinic-polyribocytidylic (pIpC) (Sigma- Aldrich) three times at 4 d intervals. IFNⲨ-induced activation of the Mx1 promoter led to the expression of Cre and subsequent deletion of exon 3 and 4 of the Caspase-8. In terms of all the parameters tested in this study, the phenotype of the Cre-expressing

Casp8$^{loxP/loxP}$ mice was indistinguishable from that of wild-type mice, irrespective of the Cre strain used. Three weeks after birth, new litters, were separately transferred to new cages and sexually subsequently genotyped.

3.2.2 DNA isolation and analysis

3.2.2.1 DNA isolation from tail biopsis

Total genomic DNA was isolated from tail biopsis with 200 µl of NID buffer + 1 µl of Proteinase K and incubated for 6 h at 56°C with shaking at 800 rpm. After digestion, the lysate was incubated at 95°C for 10 min to inactivate the proteinase K, and was spinned down at 10,000 rpm for 5 min. The supernatant was transferred to fresh eppendorf tube and was used for genotyping PCR.

3.2.2.2 Polymerase chain reaction (PCR)

Genotyping-PCR was performed with specific primers, standard PCR mastermix, and PCR cycling parameters as follows:

Reaction concentration mastermix volume

Red Taq Master Mix	10 µl
Primer sense 100 pmol	1 µl
Primer antisense 100 pmol	1 µl
H$_2$O	6 µl
DNA 100 ng	2 µl
Total	20 µl

Annealing temperature was calculated individually for each primer set (3.1.7.1) according to following formula:

$$Tm = 4x \text{ (number of } G + C) + 2x \text{ (number of } T + A) - 2°C$$

Elongation time was adjusted according to the length of the expected product: 0.5 min/ 500 bp.

PCR cycling parameters:

Step	Temperature	Time	Cycle
Melting	98°C	2 min	35
Denaturing	95°C	30 s	
Annealing	56°C	60 s	
Elongation	72°C	10 min	1
Final elongation	72°C	10 min	1
Conservation	4°C	10 min	1

Each amplified samples were loaded onto a 1% agarose gel with ethidium bromide (EtBr) and the PCR products were separated by applying 120 V for 35 min.

3.2.3 Serum preparation

Transaminase like alanine-aminotransferase (ALT) is an enzyme catalyzing the reversible onversion of α-keto acids to amino acids. This enzyme is qualified as a specific marker for liver damage. In this study, mice were first narcotized using isoflorane and approximately 500 μl blood samples were collected in serum tube by retro-orbital sinus bleeding using glass capillary. Serum was separated from blood by centrifugation at 10,000 rpm for 10 min and stored in fresh tube at -20°C for determination of aminotransferase activities.

3.2.4 LPCs activation and liver injury model

To induce LPCs activation, 6 to 8w old mice were fed Purina 5015 mouse chow diet supplemented with 0.1% wt/wt DDC (Sigma-Aldrich) for 4w (Fig. 3.3) (41). Mice were sacrificed at the indicated time points, one portion of liver from each mice were used for LPCs isolation and other portion were sampled for histological and RNA analysis.

0.1% 3,5-diethoxycarbonyl-
1,4-dihydrocollide (DDC) diet
(consistent and massive LPCs activation)
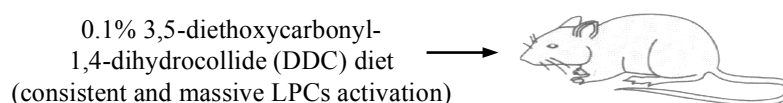
Figure 3.3 LPCs induction model.

3.2.5 Isolation of liver cells

3.2.5.1 Isolation of primary hepatocytes and nonparenchymal cells (NPCs)

NPCs and hepatocytes were isolated from mice 4w after DDC feeding using the collagenase digestion and differential centrifugation method with slight modification (100). Briefly, the liver was perfused with 0.1% collagenase IV (Worthington Biochemical Corporation) in EBBS. After perfusion, one of the smaller lobes was surgically removed for histological and RNA analysis. Rest of the liver tissue was pelleted into small pieces in 0.1% collagenase IV (Worthington) and 0.005% DNase I (Worthington) in EBSS and then incubated at 37°C for 40 min with shaking. After digestion, the liver cell suspension was filtered through 70 mm mesh (BD) and centrifuged twice at 50 g for 5 min at 4°C, to pellet the hepatocytes. The supernatant fraction, which contains NPCs, was then pelleted by centrifugation at 500 g for 10 min at 4°C (Fig. 3.4).

3.2.5.2 Enrichment of LPCs by MACS

LPCs were purified from above obtained NPCs pellet (3.2.5.1). The pellet was resuspended in HBSS with 0.1% BSA and 2 mM EDTA and LPCs were isolated using a FITC-Sca-1 antibody conjugated to magnetic beads (Miltenyi) and eluted through LS columns (Miltenyi) according to the manufacturer´s instructions (Fig. 3.4). Briefly, for isolating LPCs, NPCs pellet (3.2.5.1) was resuspended in 2 ml of MACS buffer. NPCs were incubated with FITC-Sca-1 antibody (Miltenyi) with 1:20 ratio to the volume of the blocking buffer in which they were resuspended for 10 min at 4°C. After incubation, cells were washed with 3 ml of MACS buffer and pelleted. Cell pellet was resuspended in 80 µL of buffer per 10^7 total cells and was incubated with Anti-FITC MicroBeads at 1:40 ratio and further incubated for 15 min at 4°C. Cells were washed with MACS buffer and centrifuged at 1,300 rpm for 10 min at 4°C; the resulting cell pellet was gently resuspended in 2 ml MACS buffer gently and applied through calibrated Miltenyi LS columns under a strong magnetic field. Columns were washed 3 times with 3 ml of MACS buffer at each step and finally the purified cells were collected by positive selection by removing the columns from the magnetic field and flushed with MACS buffer. Cell samples were collected for FACS in order to check the purity.
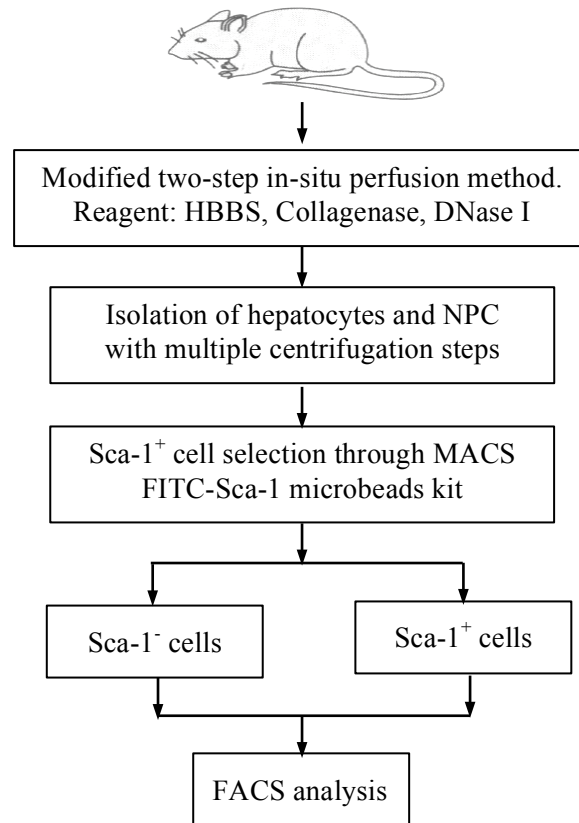
Figure 3.4 Modified two-step in-situ perfusion method.

3.2.5.3 Enrichment of immune cells

Sca-1⁻ (flow through) cells from MACS process (Fig. 3.4) were collected for further characterization of immune cells.

3.2.5.4 Isolation of LPCs through gradient ultracentrifugation

Nycodenz was purchased as Nycoprep from Axis.Shield PoC AS (Oslo, Norway). Nycodenz stock solution at 30% (wt/v) was prepared using Earle´s basic salt solution (EBSS, GIBCO). 26%, 19%, 15%, and 13% solutions were prepared in EBSS by serially diluting the stock solution and sequentially layered in an Ultra-Clear centrifuge tube (Beckman, no. 344059). Then, the NPCs pellet (3.2.5.1) was resuspended in Nycodenz solution of 11% and loaded at the top of the gradient. Centrifugation was set at 8,000 rpm ($\approx$ 8,000 $\times$ g) for 40 min at 4°C in a Beckman L5-50 Ultracentrifuge with a SW41 Ti swinging rotor, slow acceleration, and without brake. After centrifugation, cells were found at the four gradient interphases. The cells at each interphase were named F1, F2, F3, and F4, starting with F1

(11%-13% interphase) at the top. A 16-gauge needle was used to collect the cells in each layer by penetrating the wall of the transparent centrifugation tube. Cells were washed twice with HBSS containing 5% FBS and were cultured (Fig. 3.5). It has been reported that phase F1 and F2 contains LPCs and phase F3 and F4 contains hepatocytes (13).
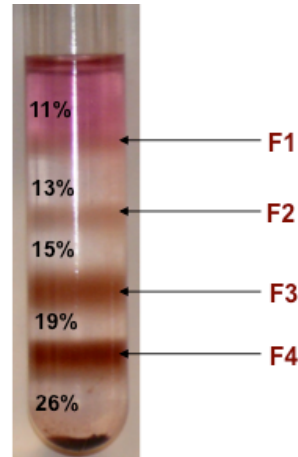
Figure 3.5 Gradient centrifugation. Five different concentrations of Nycodenz gradient solution, cells are resuspended in 11% Nycodenz solution and placed on the top of the gradient. Cell are separated according to sizes and densities.

3.2.6 FACS

3.2.6.1 FACS analysis for LPCs characterization

Single cell suspensions of Sca-1$^+$ cells were obtained as above (3.2.5.2) and were stained for OC-1, OC-2 and OC-3 for 30 min and subsequently analyzed by FACS (Becton Dickinson FACS Canto II).

3.2.6.2 FACS analysis for immune cells characterization

Dissociated Sca-1$^-$ (flow through) liver cells were obtained as described above (Fig. 3.4), and red blood cells were depleted using BD lysis buffer. After washing, Sca-1$^-$ liver cells were incubated at 4°C for 30 min in the dark in 100 ml staining medium (HBSS containing 30% BSA and 100 mM EDTA) with the following fluorochrome-labeled mAbs PE conjugated anti-CD45 Ab, PerCP-conjugated anti-CD11b Ab (eBioscience), and APC conjugated anti-CD4 Ab (BD) and were used according to manufacturer's protocols. Samples were then washed and resuspended in staining medium and were analyzed using Becton Dickinson FACS Canto II. 7AAD staining was used to label dead cells for exclusion. The

mean fluorescence index was calculated using FlowJo software (Treestar, USA). Gating was implemented based on negative control staining profiles.

3.2.6.3 FACS analysis for cell cycle analysis

Hepatocytes, LPCs and immune cells (3.2.5.4) were cultured in 6-well culture plate (BD) for 24 h at 37°C. For FACS analysis, cells were trypsinized, centrifuged and washed three times in PBS. Cells were incubated in 0.05 mg/ml PI, 0.1% sodium citrate and 0.1% Triton X- 100 in the dark overnight at 4°C. After four washes in PBS the cells were sheared by aspirating through a needle (0.5623 mm). The samples were analysed with a Becton-Dickinson FACS Canto II.

3.2.6.4 FACS analysis for apoptosis analysis

Apoptotic cell death was analysed by double staining with annexinV-FITC and PI, where the negative control contained Strep-FITC and Strep-PE to compensate for unspecific binding. As annexinV binding buffer (10 mM HEPES/NaOH. pH 7.4, 140 mM NaCl, 2.5 mM $CaCl_2$), washed once with binding buffer before incubation with annexinV (1 µg/ml) and PI (1 µg/ml) in binding buffer. FACS followed routine procedures. Analysis was performed with an FACS-Canto II fow cytometer. Cell debris was excluded from analysis by gating.

3.2.7 Microscopy

3.2.7.1 Histology

For histological analysis, liver samples were fixed in 4% formalin for 24 h, dehydrated, and embedded in paraffin (The above steps of dehydration and paraffin embedding was performed at Inter-disicplinary Center for Clinical Research (IZKF) Aachen). Sections of 5 µm thickness were cut with an ultra microtome (at a thickness of 1-2 µm) and stored at room temperature.

3.2.7.2 Haematoxylin/Eosin (H&E) staining

To determine the morphological changes, sections were deparaffinized and rehydrated by immersing 3 times in Xylol each for 5 min, 100% ethanol (2 x 10 min) 95 % ethanol (2 x

10 min), 70% ethanol (2 x 10 min) and 5 min in dH$_2$O twice. Immediately samples were immersed in Haemalaun solution, which gave cytoplasm a reddish color for 5 min and then rinsed with tap water. Finally sections were incubated with 1% Eosin for 5 min and then with 70% ethanol for 10 s, 1-3 min with 96% ethanol, 2 x 5 min with 100% ethanol. Finally, the samples were immersed 3 times in Xylol. Slices were examined with a Leica bright field microscope. Pictures were taken with the DS2MV camera from Nikon and analyzed with imaje J imaging software. Data presented in each figure are representative of data obtained from at least three separate experiments.

3.2.7.3 Immunofluorescence

Frozen liver samples embedded in Tissue-Tek were cut in 5 μm thickness sections and were fixed for 5 min in -20°C acetone, and air dried for 30 min. For immunofluorescent staining, sections were rehydrated in PBS, 0.1% Tween 20, blocked in normal donkey serum prepared in 1% BSA in PBS for 1 h to avoid unspecific binding of the antibody. After washing with PBS, the sections were incubated with the primary antibodies diluted in PBS with 1% mouse serum according to manufacturer's recommendation (1:200 - 1:300). Antibodies were incubated for 1 h either at room temperature or 4°C over night in a humid chamber. After incubation, sections were then washed three times in PBS and incubated with a secondary antibody for 1 h at room temperature in the dark. Remaining unbound secondary antibody was removed by rinsing the slides three times in PBS for 5 min. DAPI mounting medium was applied to the sections for counterstaining of the nuclei. Then slides were covered by coverslips and specimens were immediately examined under a fluorescence microscope by using appropriate excitation wavelengths depending on the fluorochrome used. Pictures were taken with a Zeiss fluorescence microscope using AxioVision 4.6 software

3.2.7.3.1 BrdU staining

Cell proliferation was detected by BrdU (Sigma-Aldrich) incorporation. Mice were injected (i.p.) with 30 μg BrdU /g body weight, dissolved in PBS at 2 h prior to euthanasia. Liver samples, frozen in OCT compound (Fischer Scientific) were cut in 5 μm thickness sections and BrdU incorporation was examined with a mouse-anti-BrDU antibody in a 1:40 dilution in PBS /1%BSA over night at 4°C and a secondary antimouse IgG antibody labelled with ALEXA488 flourescent dye in a 1:200 dilution in PBS /1%BSA and incubated for 1 h at

room temperature. BrdU$^+$ cells were counted in 10 different fields at high (400x) magnification, and the percentage of BrdU$^+$ cells was calculated and set into percentage relationship to DAPI-nuclei. All of the histological analysis was performed on an AxioImager Z1 from Zeiss.

3.2.7.3.2 Terminal Deoxynucleaotidyl Transferase dUTP Nick End Labeling (TUNEL) Assay

Terminal deoxynucleotidyltransferase-mediated nick end labeling (TUNEL) staining of deparafinized liver sections was performed using a TUNEL Detection Kit following the manufacturer's instructions (Roche) for detection of apoptosis. In brief, 5 μm thickness of frozen liver sections were treated with H_2O_2, permeabilized for 15 min at 37°C with proteinase K (20 μg/ml, Sigma-Aldrich), and then incubated for 1 h at 37°C with a reaction mixture containing terminal deoxynucleotidyl transferase (Invitrogen) and biotinylated dUTP (Boehringer Ingelheim). Labeled DNA was visualized with an ABC Kit (Vector Laboratories) and diaminobenzidine. Nuclei were stained with DAPI using Vectashield (Vector Laboratories). The liver sections were mounted on glass slides and fluorescence microscopy was performed using a Zeiss fluorescence microscope using AxioVision 4.6 software. TUNEL$^+$ cells were counted by randomly selecting high-power fields (400x) distributed over six independent sections. The numbers of TUNEL$^+$ and TUNEL$^-$ cells were compiled and the percentages of TUNEL$^+$ cells were calculated.

3.2.8 Isolation of nucleic acids

3.2.8.1 Isolation of RNA from liver samples

All work involving RNA was performed using sterile RNase-free single use plastic ware. RNase free or DEPC-treated H_2O was used. All tools and bench were cleaned with RNase Zap before and during usage in order to inactivate RNases. All centrifugation steps were conducted at 4°C. Liver samples were taken out of -80°C storage and were cut in small piece. This liver piece was mixed with 1 ml of peqGOLD RNA-Pure-solution® in a tube. Samples in tube were shredded with an Ultra-Thurax® and incubated for 10 min at room temperature. Chloroform (200 μl) was added to each sample and vortexed to ensure proper mixing and incubated on ice for 10 min. After incubation, samples were centrifuged at 15,000 g for 15 min. Three phases were obtained after centrifugation. The upper supernatant

phase was pipetted and mixed with an equivalent volume of isopropanol. Samples were gently mixed and incubated for 10 min on ice, then pelleted at 15,000 g for 10 min. The RNA-pellet was washed twice with 1 ml 70% ice-cold ethanol (5 min at 10,000 rpm), air-dried and was dissolved in 70 µl 0.1% DEPC water.

To determine RNA purity and concentrations by photometer, each sample was diluted 1:50 in RNase-free dH_2O and OD (optical density) was measured at 260 and 280 nm. dH_2O was used as a blank. A ratio of E260 /E280 between 1.8 and 2.0 accounted for pure RNA.

3.2.8.2 cDNA synthesis

cDNA or complementary DNA was synthesized from 500 ng total RNA template using Omniscript cDNA Kit® from Qiagen according to the manufacturer´s protocol. The RT reaction was done as follows:

Reverse transcription protocol

Step	Duration	Temperature	Number of cycles
Warm up	10 min	25°C	1
Reverse transcription	60 min	50°C	1
Denaturation	5 min	85°C	1
End step	∞	4°C	-

Component	Volume/ reaction
10x Buffer RT	2 µl
dNTP mix (5 mM each dNTP)	2 µl
Oligo-dT primer 10 µM	2 µl
Omniscript Reverse Transcriptase	1 µl
Template RNA (1 µg/µl)	2 µl
dH_2O add	20 µl

PCR program	Temperature
60 min	37°C
5 min	95°C

cDNA was diluted in dH_2O at a ratio of 1:200 and stored at -20°C.

3.2.8.3 Real-time PCR analysis

Real-time quantitative (RT-PCR) was carried out using SybrGreenER quantitative polymerase chain reaction Supermix (Invitrogen) on ABI Prism 7700 Thermal Cycler.

PCR reactions in this study were composed as followed:

Mastermix	Volume/ reaction	Concentration
cDNA	5 μl	
Primer sense	0.5 μl	5 pmol
Primer antisense	0.5 μl	5 pmol
Sybr green	12.5 μl	

dH$_2$O add 25 μl

The program variations were dependent on the annealing temperature of the used primers. Primers for GAPDH were used as loading control, and the level of expression for the genes CK19, Cyclin D1 (CcnD1), CcnE1 and CcnA2, collagen-1α, α-SMA, IL-6, TNF-α was assessed.

General RT-PCR protocol:

Step	Time [min:s]	Temp [°C]	Cycle
Activation	02:00	50	
Denaturation	10:00	95	
Denaturation	00:15	98	
Annealing Tm	00:30	58	40x
Elongation	00:30	60	
Conservation	00:00	4	

Melting curve

The relative gene expression was calculated according to the $2^{-\Delta\Delta Ct}$ method (101). The Ct values of the samples of interest and a control sample were calculated using SDS software version 1.3.1 (Applied Biosystems) and the ΔΔCt values were calculated according to the formula:

$$\Delta\Delta Ct = \Delta Ct \text{ (sample) - } \Delta Ct \text{ (untreated control)}$$

ΔCt (sample) is the Ct value for any sample normalized to endogenous GAPDH housekeeping gene expression and ΔCt (untreated control) is the Ct value for the calibrator also normalized to GAPDH.

From these parameters, the $2^{-\Delta\Delta}$ Ct values of all samples were calculated and interpreted as fold induction compared to untreated controls.

3.2.9 Protein isolation and analysis

3.2.9.1 Extraction of whole cell protein from liver tissue, primary hepatocytes, LPCs and immune cells for western blot

Liver tissues were homogenized on ice in NP-40 lysis buffer (3.1.9.5). The homogenate was centrifuged at 12,000 rpm at 4°C for 10 min. The protein concentrations were determined using a Bradford assay (102) using the following solution:

Bio-Rad Protein Assay solution	200 μl
Aqua select	798 μl
1:5 diluted supernatant	2 μl

The samples were snap frozen in liquid nitrogen and stored at -80°C for further use.

3.2.9.2 Extraction of whole cell protein from liver tissue for Caspase-3 assay with AFC-lysis buffer

For protein extractions, approximately 1 mg of frozen liver tissue was homogenized on ice in 500 μl AFC lysis buffer. Homogenate was centrifuged for 10 min at 12,000 rpm and 4°C. Supernatant was transferred into new tube and concentration was determined. Samples were shock frozen in liquid nitrogen and stored at -80°C.

AFC-Lysis Buffer	Volume	Final concentration
Hepes 1 M pH 7.4	100 μl	10 mM
Chaps 10%	100 μl	0.1%
EDTA 0.5 mM pH 8	40 μl	2 mM

DTT 1 M	50 µl	5 mM
Pefa Block 0.1 M	100 µl	1 mM
Complete Mini®	1 tablet	

dH$_2$O add 10 ml

3.2.9.3 Western blot analysis

Fifty micrograms of liver protein was heated for 5 min at 95°C and subjected to SDS/ polyacrylamide gel and the separated proteins were electrophoretically transferred to a nitrocellulose membrane (PROTRAN©, Whatman) using a western blotting system (BioRad) for 2 h at 385 mA. Nonspecific binding was blocked with 5% nonfat dry milk or 5% BSA in TBS-T buffer for 1 h at room temperature, and incubated at 4°C over night under gentle agitation with primary antibodies at the dilution specified by the manufacturer's recommendations. Following three washes with TBS-T, the membranes were then incubated with the horseradish perooxidase (HRP)-conjugated secondary antibody (5% non-fat milk or BSA in TBS-T) for 1 h at room temperature under gentle agitation. The membrane was washed three times for 10 min with TBS-T and protein bands were visualized with the enhanced chemiluminescence (ECL, GE Healthcare Biosciences) for 5 min and then exposed to a LAS mini 4000 developing machine (Fuji) until specific signals were detectable. GAPDH was used as the loading control.

3.2.9.4 Caspase Assay

Caspase assay was performed as descrbed earlier (103).One hundred micrograms of liver protein lysates were incubated with 20 µM fluorogenic substrates Ac-DEVD-AFC for Caspase-3 (BD Pharmingen) activity for 1 h. The fluorescence signals were quantitated using a fluorescent plate reader (Packard Instrument Co.) at an excitation wavelength of 360 nm and an emission wavelength of 460 nm and the background signals were corrected. The Caspase activities were expressed as fold changes over control samples (from corresponding wild-type mice).

3.2.10 Cell culture

3.2.10.1 LPCs culture

LPCs were isolated as described above (3.2.5.4) and washed three times with PBS (15 min, 13,000 rpm, 4°C). The cell pellet was resuspended in 1 ml culture medium and viability was determined with 0.2% trypan blue using a Neubauer hemacytometer. Cells were cultured at 37°C in air 5% CO_2 in either 6 well cell culture insert companion plate with lid (BD) or 8 well chambered glass slides (Lab-Tek) at a density of 2 x 10^6 cells/mL in culture medium (DMEM-F12 with 10% FBS, 50 U/ml penicillin, 50 µg/ml streptomycin, 10 mM Nicotinamide. 1 x 10^{-7} M Dexamethasone, 2 mM Insulin-Transferrin-Selenium-X, 50 µM ß-Mercaptehnol) for the first 24 h. After 24 h, 50 ng HGF and 20 ng EGF was added until further use.

3.2.10.2 Treatment of LPCs with intrinsic inducers of apoptosis

The cells in culture were treated with (50 ng/ml) Jo2 antibody (BD Pharmingen) for 4-6 h. After 6 h, the cells were harvested and were used for FACS apoptosis analysis. A part of the cells were used for TUNEL staining (see 3.12.2.1) protocol and were analyzed under Zeiss microscope to detect the apoptosis. Also part of cells was used for RNA extraction and was used for detection of FAS and FASL ligand mRNA detection through the Real Time PCR.

3.2.11 Transplantation experiments

3.2.11.1 Irradiation of mice

WT mice were exposed to 12 cGy total body gamma irradiation (Mark I irradiator Model 68, J.L. Shepherd) with a 6,000-Ci source administered in 2 doses of 6cGy each, 4 h apart.

3.2.11.2 Bone marrow isolation

$Casp8^{\Delta Mx}$ mice were were injected intraperitoneally with pIpC dsRNA (5) (20 µg/g body weight; Sigma- Aldrich) three times at 4 d intervals. At day 13, bone marrow was flushed from the tibia and femur with 5 ml HBSS medium (Gibco-BRL; Invitrogen)

containing 2% FCS (Hyclone Laboratories) in 50 ml falcon tube (BD). Cells were filtered through a 70 mm cell-strainer, collected by centrifugation at 15,000 rpm for 5 min at 4°C. The cells were washed twice in HBSS, resuspended in the same medium, counted, and maintained at 4°C until further use.

3.2.11.3 Bone marrow transplantation

Subsequently, 5×10^7 freshly isolated bone marrow cells (Casp8$^{-/-}$) were transplanted via tail vain injection in WT mice at day 2 (Fig. 3.6). From week 5, these mice were subjected to DDC supplemented rodent chow until week 7. At the end of week 7, mice were sacrificed for LPCs (3.2.5.2) and immune cells (3.2.5.3) isolation and were analyzed through flow cytometry.
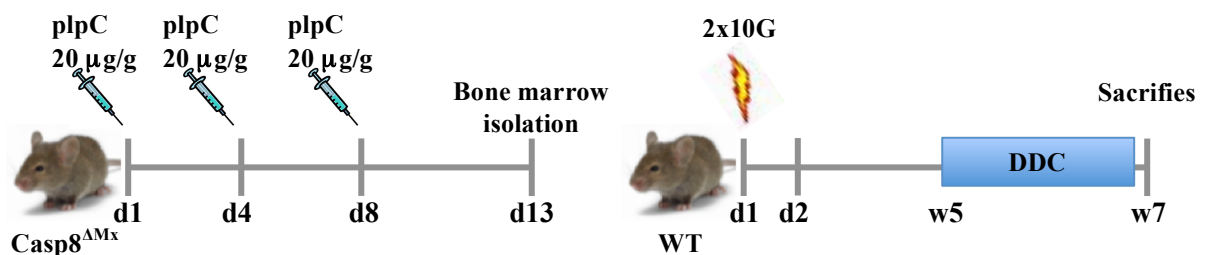
Figure 3.6 Bone marrow isolation and transplantation.

3.2.12 Statistical analysis

All numerical datas are expressed as a Mean ± Standard deviation of the mean (sdm) and represents at least 4-5 animals per time point. All significant p values were determined by unpaired two-tailed Student's t-test implemented in Excel. Statistical analysis was also performed using GraphPad Prism version 5.0 software (GraphPad, La Jolla, CA., USA). A value of $p<0.05$ was considered significant (*$p<0.05$, **$p<0.001$, ***$p<0.0001$). Quantitative analysis of BrdU and TUNEL staining was done by analyzing immunohistochemical slides with Axiovision software (Zeiss). Quantitative analysis of collagen and CK19 staining from immunohistochemical slides was performed via colour-based thresholding using the open source software ImageJ.

4 Results

4.1 Differential role of Caspase-8 in liver cells during chronic liver injury and apoptosis

4.1.1 Cell specific vs. ubiquitous deletion of Caspase-8 leads to a differential phenotype in a model of secondary sclerosing cholangitis

The role of receptor mediated apoptosis and Caspase activation during the development of sclerosing cholangitis is currently unknown. We thus investigated the role of the apical effector Caspase-8 in different liver cell types. Mice with a hepatocyte specific deletion of Caspase-8 (Casp8$^{\Delta hepa}$) (97) and mice with a ubiquitous deletion of Caspase-8 (Casp8$^{\Delta Mx}$) were applied to a model of DDC induced chronic sclerosing cholangitis. Serum transaminases and bilirubin significantly increased in Casp8 WT after DDC treatment as an indication for the development of severe cholestatic liver injury. Mice with a hepatocyte specific deletion of Caspase-8 (Casp8$^{\Delta hepa}$) instead displayed lower ALT and bilirubin levels were thus relatively protected from DDC induced injury after 4w of treatment (Fig. 4.1A-B). In opposite to this both liver function parameters were significantly stronger elevated in Casp8$^{\Delta Mx}$ mice (Fig. 4.1C-D).

To better characterize the differential impact of Caspase-8 deletion on liver injury we next performed H&E staining of liver sections. Tissue damage and fibrotic remodelling became evident at some degree in all animals. In agreement with these findings Casp8$^{\Delta Mx}$ mice displayed more extensive histomorphologic changes including a significantly higher number of infiltrating mononuclear cells, a much stronger induction of the DDC-characteristically periportal cell population as well as increased signs of tissue remodelling (Fig. 4.1E-F).
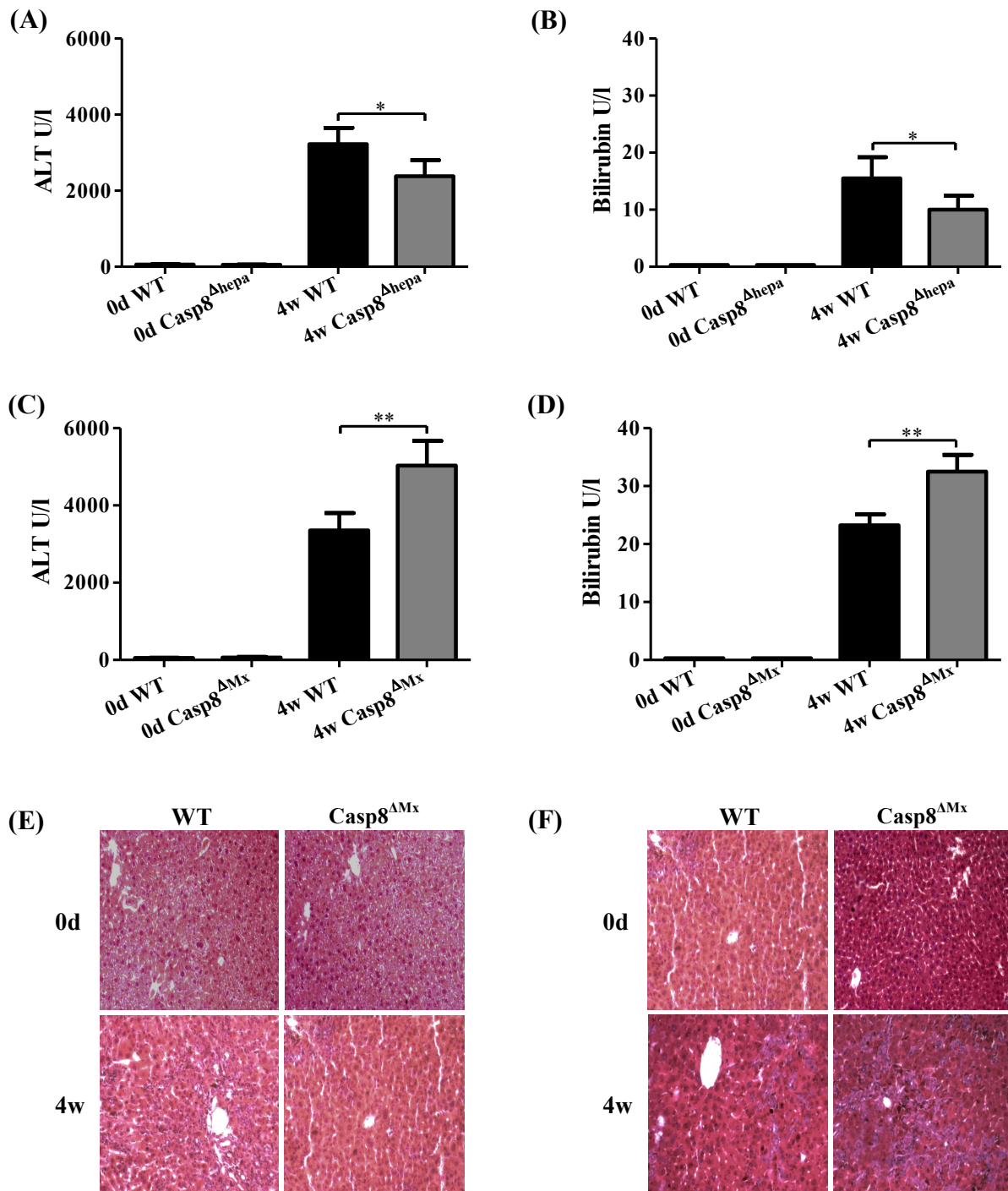
Figure 4.1 Caspase-8 is differentially involved in DDC-mediated liver injury. Displayed are serum transaminases (ALT) and bilirubin levels in Casp8$^{\Delta hepa}$ **(A-B)** and Casp8$^{\Delta Mx}$ **(C-D)** after 4w of DDC treatment. **(E-F)** Hematoxylin/Eosin (H&E) staining of liver sections from untreated and DDC treated controls, Casp8$^{\Delta hepa}$ and Casp8$^{\Delta Mx}$ mice. Results are expressed as mean of at least 4-5 mice per group; error bars indicate SD. *, P < 0.05; **, P < 0.01.

4.1.2 Ubiquitous deletion of Caspase-8 leads to an extensive progression of liver fibrosis

Next, fibrosis progression was investigated by performing collagen immunohistochemistry with collagen as a marker of fibrosis progression. Morphometric quantification of liver tissue from the 4w post DDC treatment time point demonstrated less

collagen accumulation in Casp8$^{\Delta hepa}$ mice after 4w of DDC feeding, which again reflects a better preservation of liver function within this model (Fig. 4.2A,C). Meanwhile, Casp8$^{\Delta Mx}$ mice dislayed extensive progression of liver fibrosis, as evidenced by collagen staining (Fig. 4.2B,D).
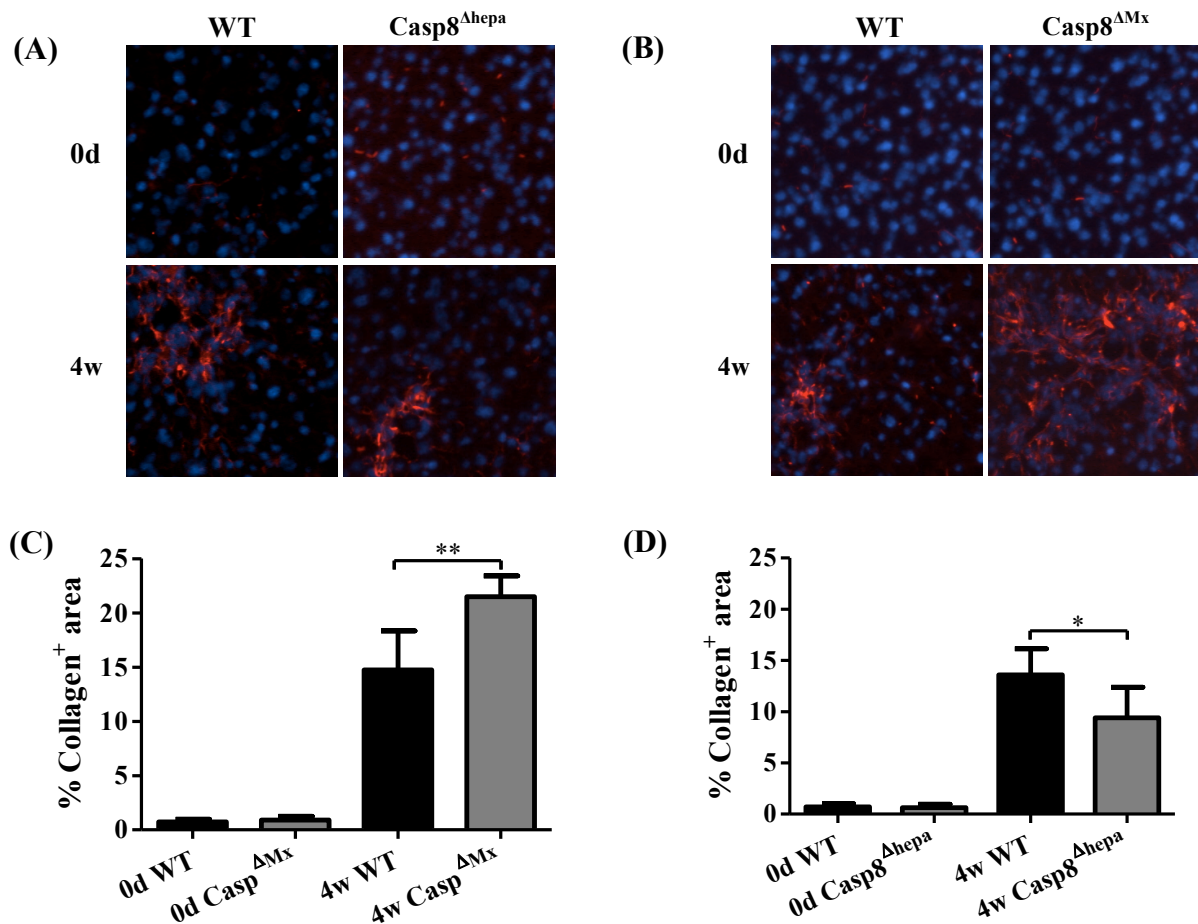
Figure 4.2 Enhanced progression of liver fibrosis in Casp8$^{\Delta Mx}$ mice after 4w of DDC treatment (A-B) Collagen staining of liver tissue derived from livers of Casp8$^{\Delta hepa}$, Casp8$^{\Delta Mx}$ and controls 4w after DDC treatment. Representative photomicrographs are shown for each time point (200x magnification). **(C-D)** Graphical analysis of liver collagen staining in Casp8$^{\Delta Mx}$ mice, Casp8$^{\Delta hepa}$ and controls 4w after DDC treatment. To graphically visualize the difference in collagen fiber accumulation, the intensity of collagen staining in DDC treated mice was determined. Photomicrographs of collagen stained slides were analysed using the open source ImageJ software (livers from untreated mice were used as controls) *=p<0,05 **=p<0,01.

This finding was further strengthened by an enhanced collagen-1α mRNA (Fig. 4.3A-B) and α-SMA mRNA (Fig. 4.3C-D) expression in Casp8$^{\Delta Mx}$ mice compared to Casp8$^{\Delta hepa}$ mice after 4w of DDC treatment.
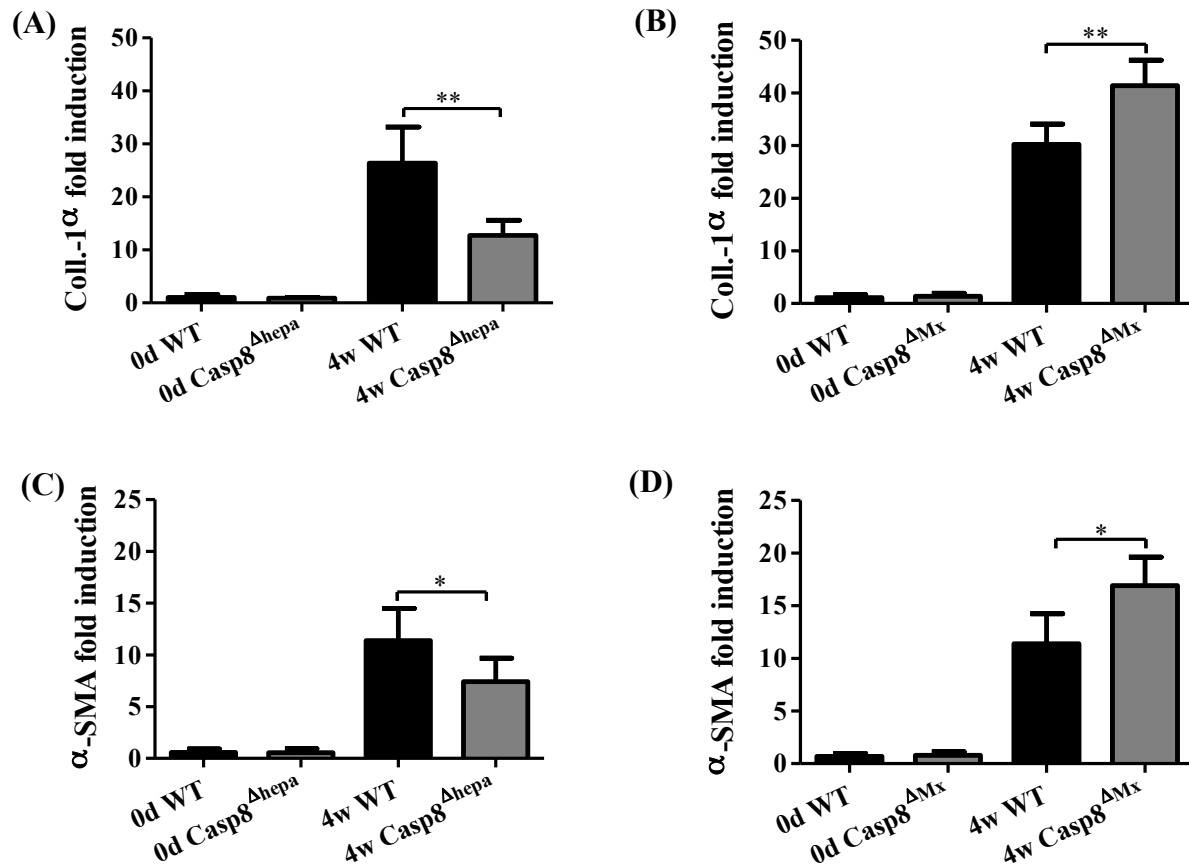
Figure 4.3 Enhanced fibrotic gene expression. (A-B) Collagen-1α and **(C-D)** α-SMA mRNA expression was quantified by real-time PCR before and 4w after DDC treatment as indicated. RNA was extracted separately from individual liver tissues (at least 5 samples/time point were included) at the respective time points, *=p<0,05 **=p<0,01.

4.1.3 Conditional Caspase-8 knockout strains are protected against parenchymal apoptosis

In view of the observed differences in injury and inflammation in livers with conditional Caspase-8 deficiency after 4w of DDC feeding, we next studied the impact of apoptosis in these mice. TUNEL analysis of Casp8$^{\Delta hepa}$ revealed a reduced number of apoptotic cells compared to Casp8 WT mice after 4w of DDC diet (Fig. 4.4A,C). Interestingly Casp8$^{\Delta Mx}$ mice also displayed an overall reduced apoptotic activity, as evidenced by determining TUNEL-positivity (Fig. 4.4B,D). Consistently, the activation of the downstream effector Caspase-3 was reduced in Casp8$^{\Delta hepa}$ and Casp8$^{\Delta Mx}$ mice as well (Fig. 4.4E-F) compared to Casp8 WT mice after 4w of DDC diet.
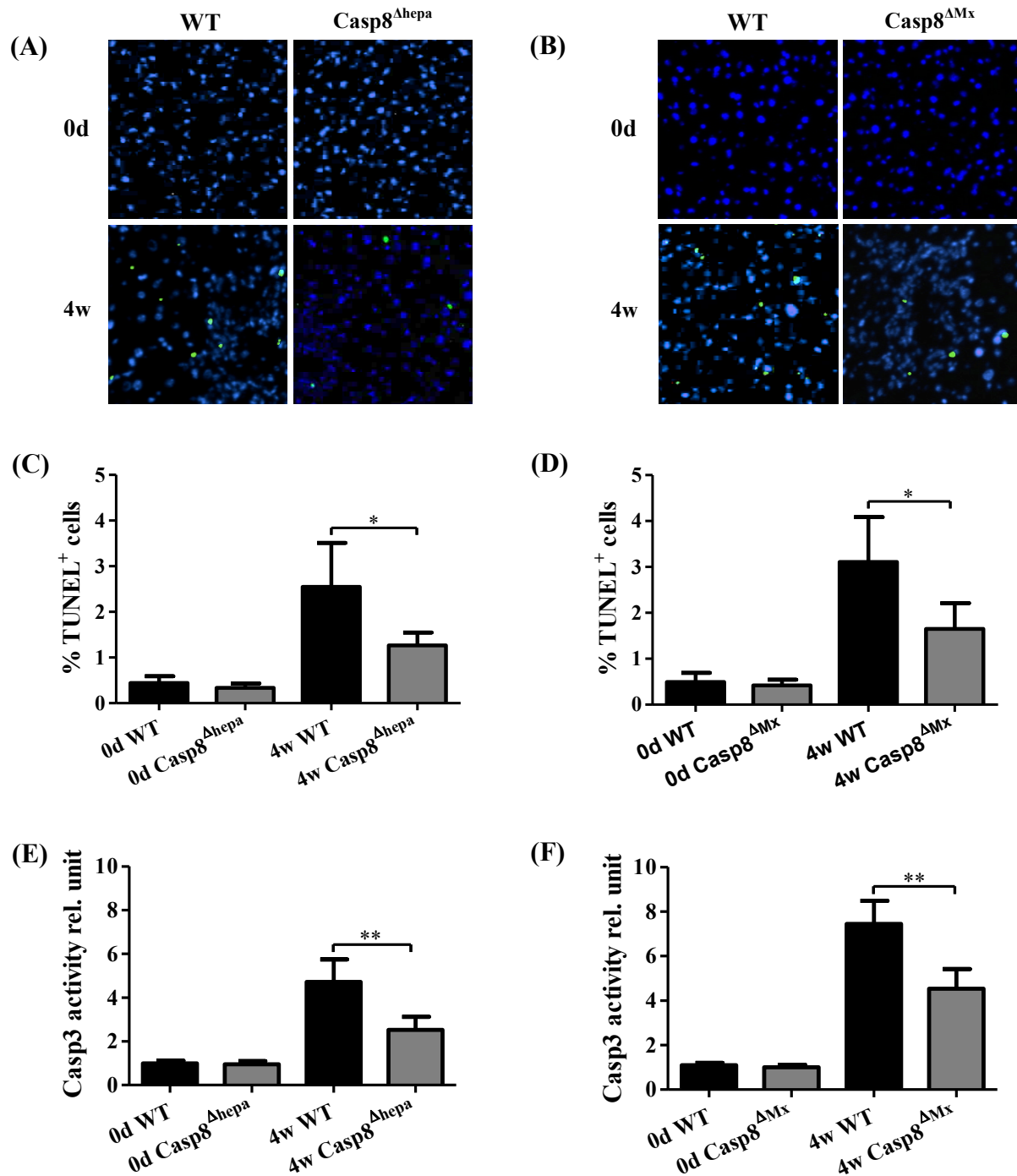
Figure 4.4 Higher apoptosis rate in controls as compared to Casp8$^{\Delta Mx}$ and Casp8$^{\Delta hepa}$ mice. (A-D) Apoptotic cells were analysed by TUNEL staining (green) in livers of Casp8$^{\Delta Mx}$, Casp8$^{\Delta hepa}$ and controls before and after DDC treatment as indicated. Representative pictures are shown for each time point. At least 10 view fields of 5 livers per time point were included in this analysis. **(E-F)** Native protein extracts were isolated from harvested livers and analyzed in Caspase-3 assays for Caspase-3 substrate turnover. The specific Caspase-3 activity was determined and calculated as relative unit. Casp3 activity in the controls (untreated mice) was set to a relative unit of 1. Each bar represents the mean of at least 4-5 mice per group. *, P < 0.05; **, P < 0.01.

These findings were further strengthened by mRNA expression levels of FasR and FasL that were concordantly regulated within the four groups with a stronger induction in treated control mice as compared to either conditional knockout group (Fig. 4.5A-D).
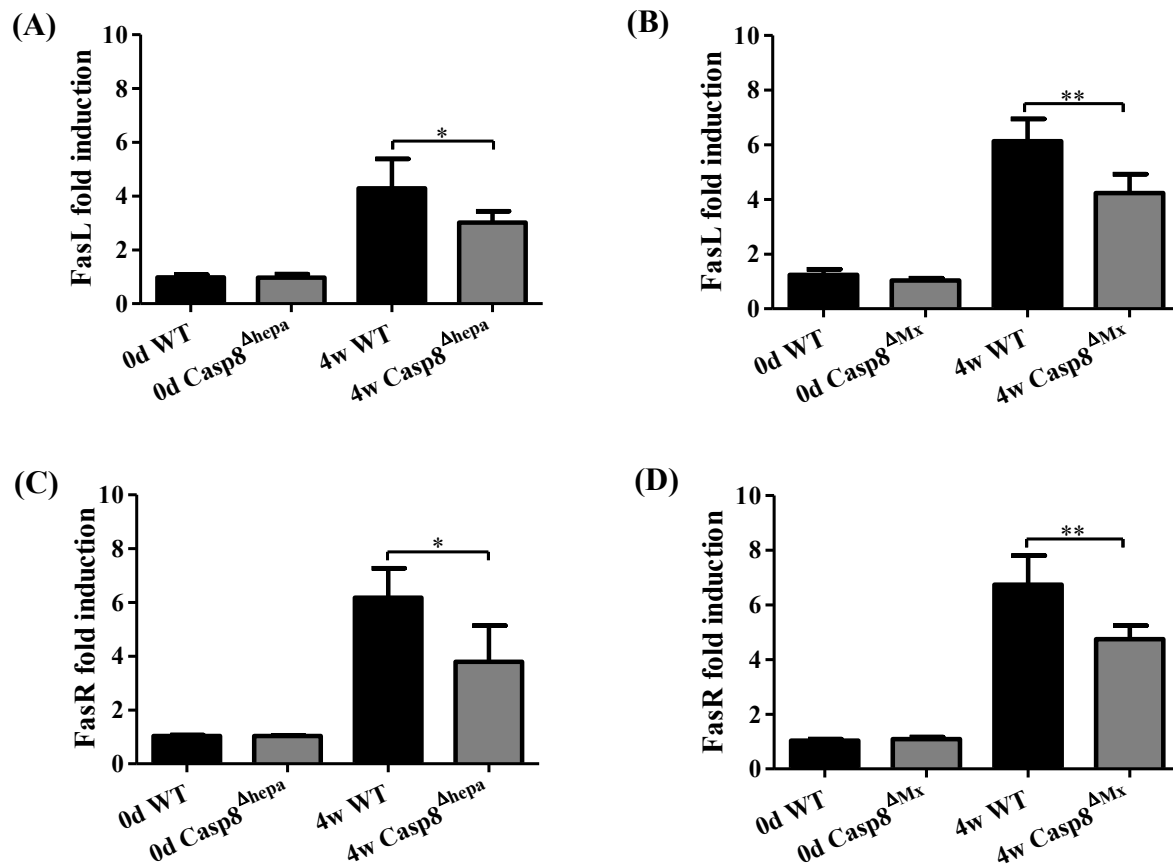
Figure 4.5 Significantly enhanced FasR and FasL mRNA expression in control mice. Real-time PCR for FasR **(A-B)** and FasL **(C-D)** mRNA in Casp8$^{\Delta hepa}$, Casp8$^{\Delta Mx}$ and control mice after 4w of DDC diet treatment demonstrates significant basal mRNA expression in DDC treated Casp8 WT livers. The FasR/ GAPDH and FasL/GAPDH expression ratio was determined for each time point and calculated as fold induction in comparison to untreated controls. Each time point represents the mean of 4-5 mice. *, P < 0.05; **, P < 0.01.

4.2 Ubiquitous deletion of Caspase-8 accelerates the onset of liver regeneration in mice after DDC treatment

4.2.1 Accelerated proliferation in the liver of Casp8$^{\Delta Mx}$ mice compared to Casp8$^{loxP/loxP}$ (Casp8 WT) and Casp8$^{\Delta hepa}$ mice after 4w of DDC diet treatment

Hepatic apoptosis is usually counterbalanced by the proliferation of parenchymal or stem cells. We thus investigated cellular proliferation as a measure for regenerative approaches. While Casp8$^{\Delta hepa}$ (Fig. 4.6A,C) displayed a reduced overall BrdU-incorporation activity, we observed an enhanced proliferation in Casp8$^{\Delta Mx}$ mice (Fig. 4.6B,D). A further

refined analysis in Casp8$^{\Delta Mx}$ mice unraveled that most of the proliferating cells were located within the periportal region (Fig. 4.6E-F), an area known to contain a population of LPCs.
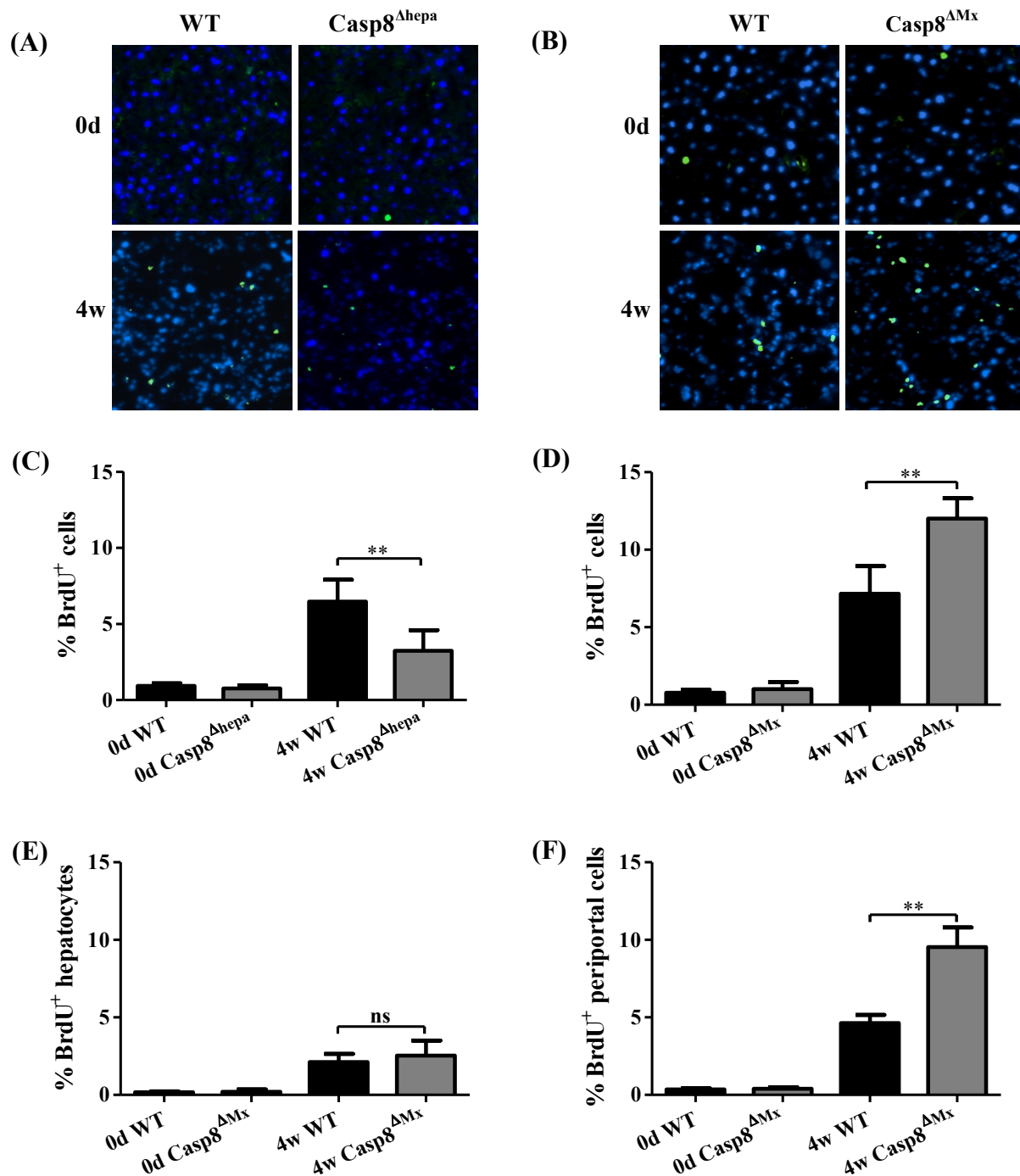
Figure 4.6 Higher proliferative rates in Casp8$^{\Delta Mx}$ as compared to Casp8$^{\Delta hepa}$ and controls mice (A-B) BrdU staining of liver sections from Casp8$^{\Delta Mx}$, Casp8$^{\Delta hepa}$ and their respective control mice after 4w of DDC diet treatment. Two hours before sacrificing, mice were injected with the nucleotide analogue BrdU. Green: BrdU$^+$ nuclei, blue: co-staining total nuclei with DAPI. **(C-D)** Quantification of total BrdU$^+$ cells relative to total nuclei (DAPI) per 200x power field. The amount of BrdU$^+$ nuclei was determined by counting 4 representative high power fields/mice after microscopic examination. **(E-F)** Quantification of BrdU$^+$ hepatocytes and periportal cells in Casp8$^{\Delta Mx}$ mice after 4w of DDC diet. Each value represents the mean of 4-5 mice. *, $P < 0.05$; **, $P < 0.01$.

Corresponding to the counted BrdU incorporation rates we detected a similarly regulated gene expression associated with cell proliferation that was further supported by elevated levels of Cyclin D1 (Fig. 4.7A-B), E1 (Fig. 4.7C-D) and A2 (Fig. 4.7E-F) mRNA expression levels in Casp8$^{\Delta Mx}$ mice compared to control and Casp8$^{\Delta hepa}$ mice after 4w of DDC treatment.
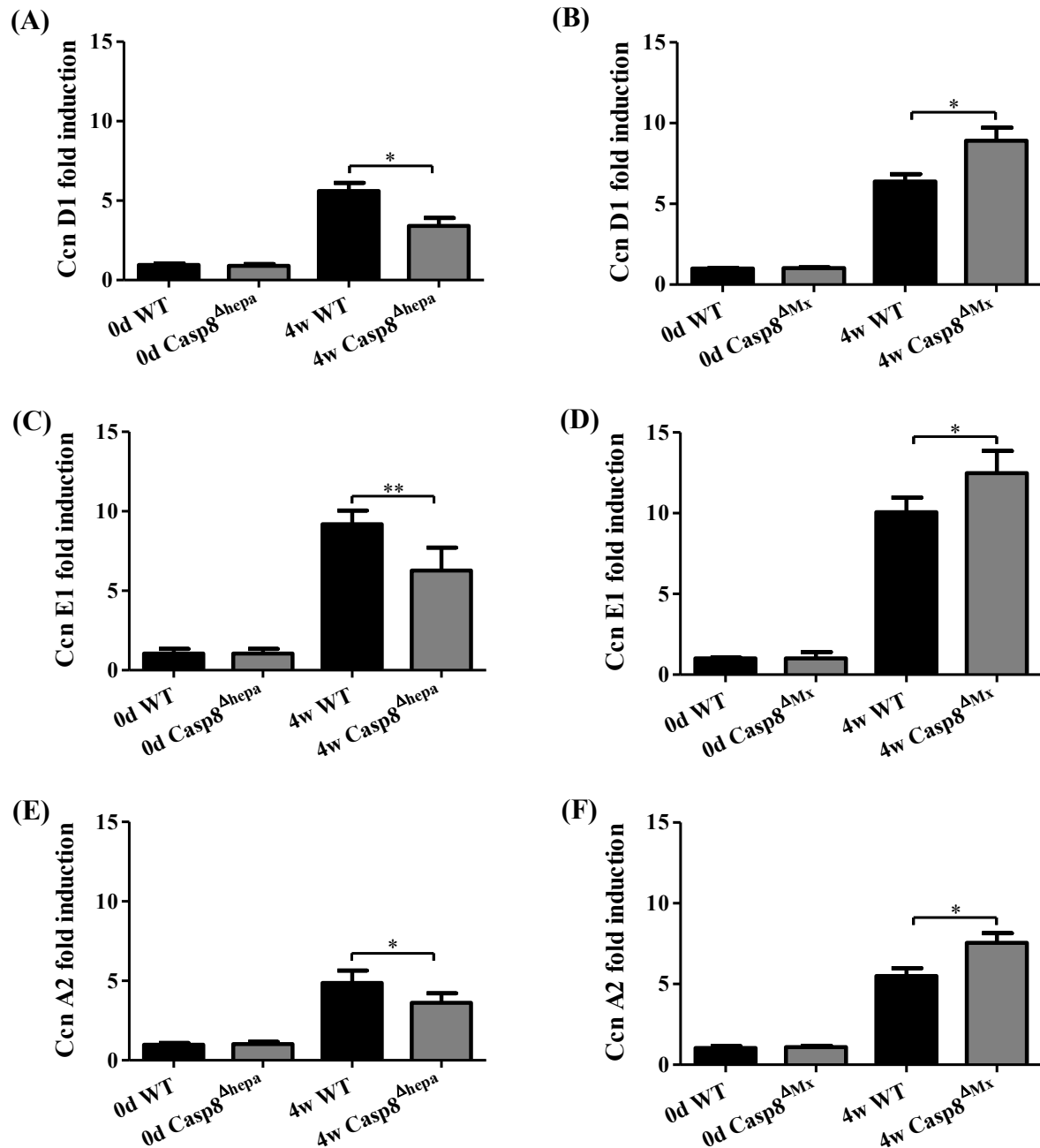
Figure 4.7 Significantly enhanced CcnD1, CcnE1 and CcnA2 mRNA expression in Casp8$^{\Delta Mx}$ mice. Real-time PCR for CcnD1 **(A-B)**, CcnE1 **(C-D)** and CcnA2 **(E-F)** mRNA in Casp8$^{\Delta hepa}$, Casp8$^{\Delta Mx}$ and control mice after 4w of DDC diet treatment demonstrates significant higher mRNA expression in Casp8$^{\Delta Mx}$ livers. The CcnD1/GAPDH, CcnE1/GAPDH and CcnA2/GAPDH expression ratio was determined for each time point and calculated as fold induction in comparison to untreated controls. Each time point represents the mean of 4-5 mice. *, P < 0.05; **, P < 0.01.

This observation could be confirmed at the protein level showing significantly higher PCNA expression 4w after DDC in Casp8$^{\Delta Mx}$ mice compared to Casp8$^{\Delta hepa}$ and controls (Fig. 4.8A-B). p53, another cell cycle regulator was regulated in a similar manner as demonstrated by western blot analysis (Fig. 4.8C-D).
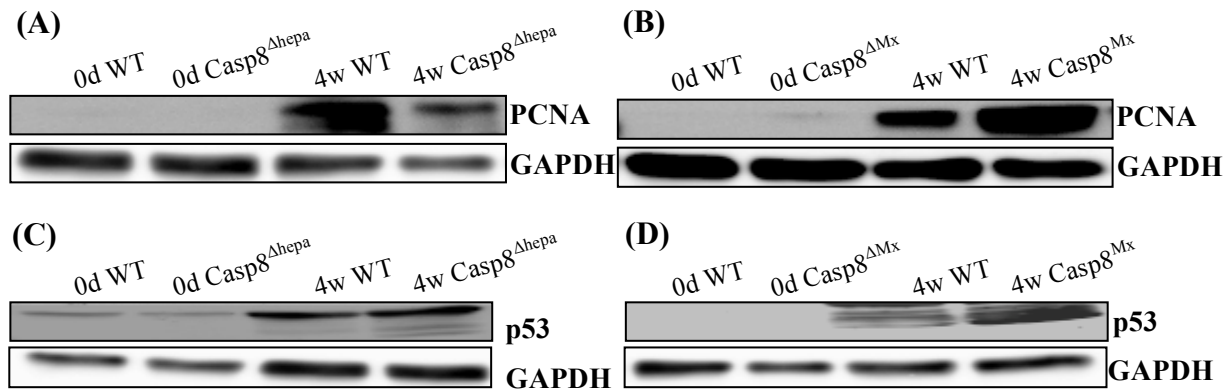
Fig. 4.8 Western blot analysis of total protein levels. PCNA **(A-B)** and p53 **(C-D)** after 4w of DDC diet treatment demonstrating elevated level of proliferation in Casp8$^{\Delta Mx}$ mice compared to Casp8$^{\Delta hepa}$ and controls. GAPDH (lower panel) was used as internal loading control.

4.2.2 Deletion of Caspase-8 results in an enhanced LPCs activation after DDC treatment

Previous studies have demonstrated that Caspase-8-mediated hepatocyte apoptosis plays an important role in liver regeneration (35). However, the role of Caspase-8-mediated apoptosis in LPCs activation has not been studied. LPCs are a known major component of intrinsic liver regeneration within the DDC model. As the periportal cell fraction was enhanced in Casp8$^{\Delta Mx}$ mice we evaluated their contribution under the condition of Caspase-8-deficiency. Immunostaining of liver sections showed the presence of large numbers of CK19^{+} cells branching out from portal areas toward the central regions of the liver lobule and spanning the liver parenchyma (Fig. 4.9A-B). A quantification of the tissue area covered by CK19^{+} cells revealed a significantly enhanced expansion of this population in the injured liver of Casp8$^{\Delta Mx}$ mice compared to controls and Casp8$^{\Delta hepa}$ mice after 4w of DDC treatment (Fig. 4.9C-D). The latter showed even less CK19^{+} cells then their controls (Fig. 4.9A,C). This finding was further supported by quantitative CK19 mRNA expression analysis that demonstrated elevated levels of CK19 expression in the injured liver of Casp8$^{\Delta Mx}$ mice compared to controls and Casp8$^{\Delta hepa}$ mice after 4w of DDC treatment (Fig. 4.9E-F).
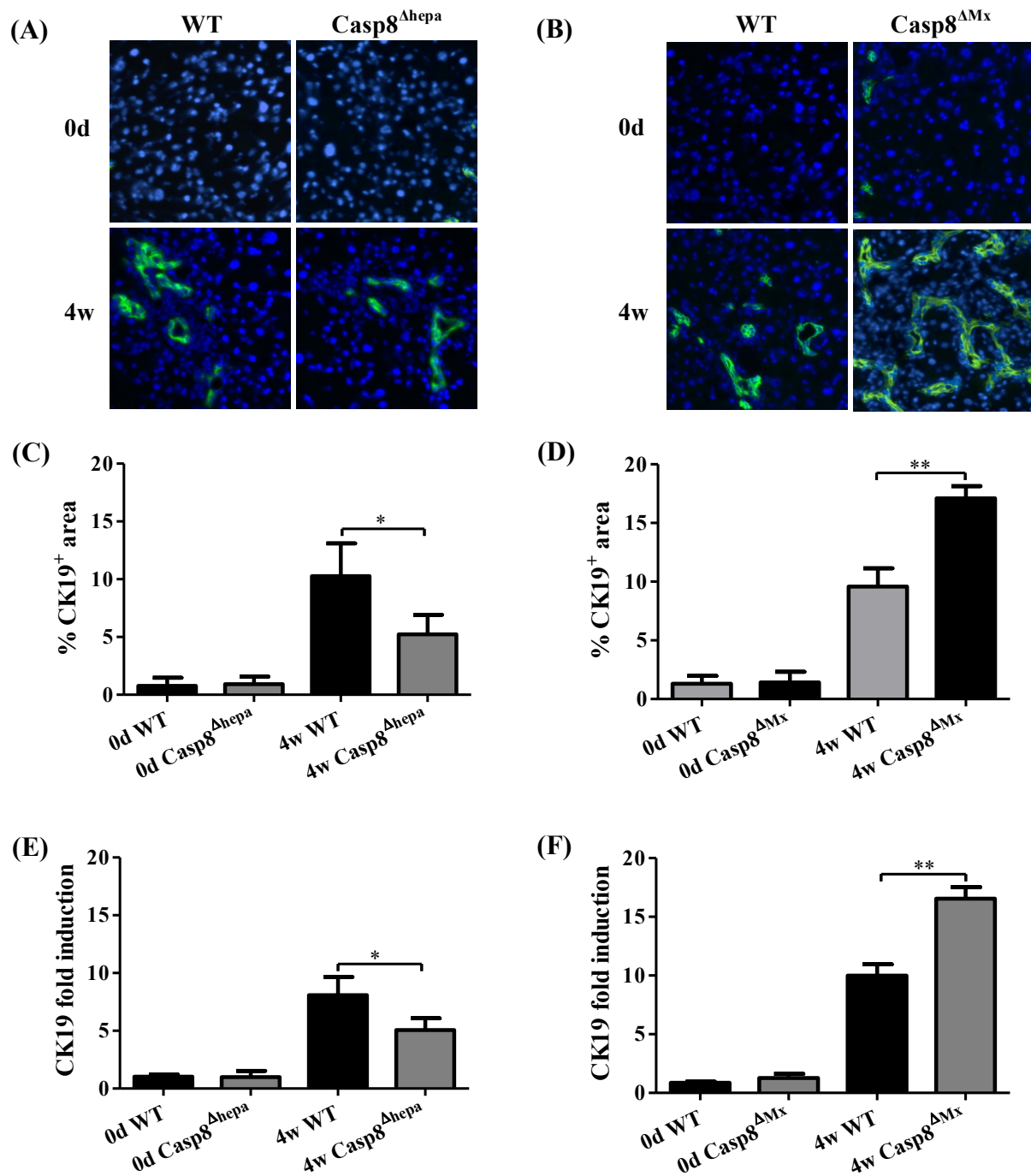
Figure 4.9 Deletion of Caspase-8 results in enhanced LPCs activation after DDC-mediated liver injury in Casp8$^{\Delta Mx}$ mice. (A-B) Immunofluorescence staining for CK19 in liver sections from controls, Casp8$^{\Delta hepa}$ and Casp8$^{\Delta Mx}$ mice after 4w of DDC diet treatment. **(C-D)** Graphical analysis of CK19 staining in Casp8$^{\Delta Mx}$ mice, Casp8$^{\Delta hepa}$ and Casp8$^{loxP/loxP}$ controls 4w after DDC treatment. To graphically visualize the difference in CK19 accumulation, the intensity of CK19 staining in DDC treated mice was determined. Photomicrographs of CK19 stained slides were analysed using the open source ImageJ software (livers from untreated mice were used as controls). **(E-F)** Real-time PCR analysis for CK19 mRNA demonstrating significant basal mRNA expression in Casp8$^{\Delta Mx}$ livers. Each time point represents the mean of 4-5 mice. *, P < 0.05; **, P < 0.01.

Next, further expression profiles of genes involved in the activation of LPCs were undertaken. Analysis of CD133, Fn14 and TWEAK (30, 33) revealed an enhanced expression of both factors in Casp8$^{\Delta Mx}$ mice compared to controls and Casp8$^{\Delta hepa}$ mice after 4w of DDC treatment (Fig. 4.10A-F).
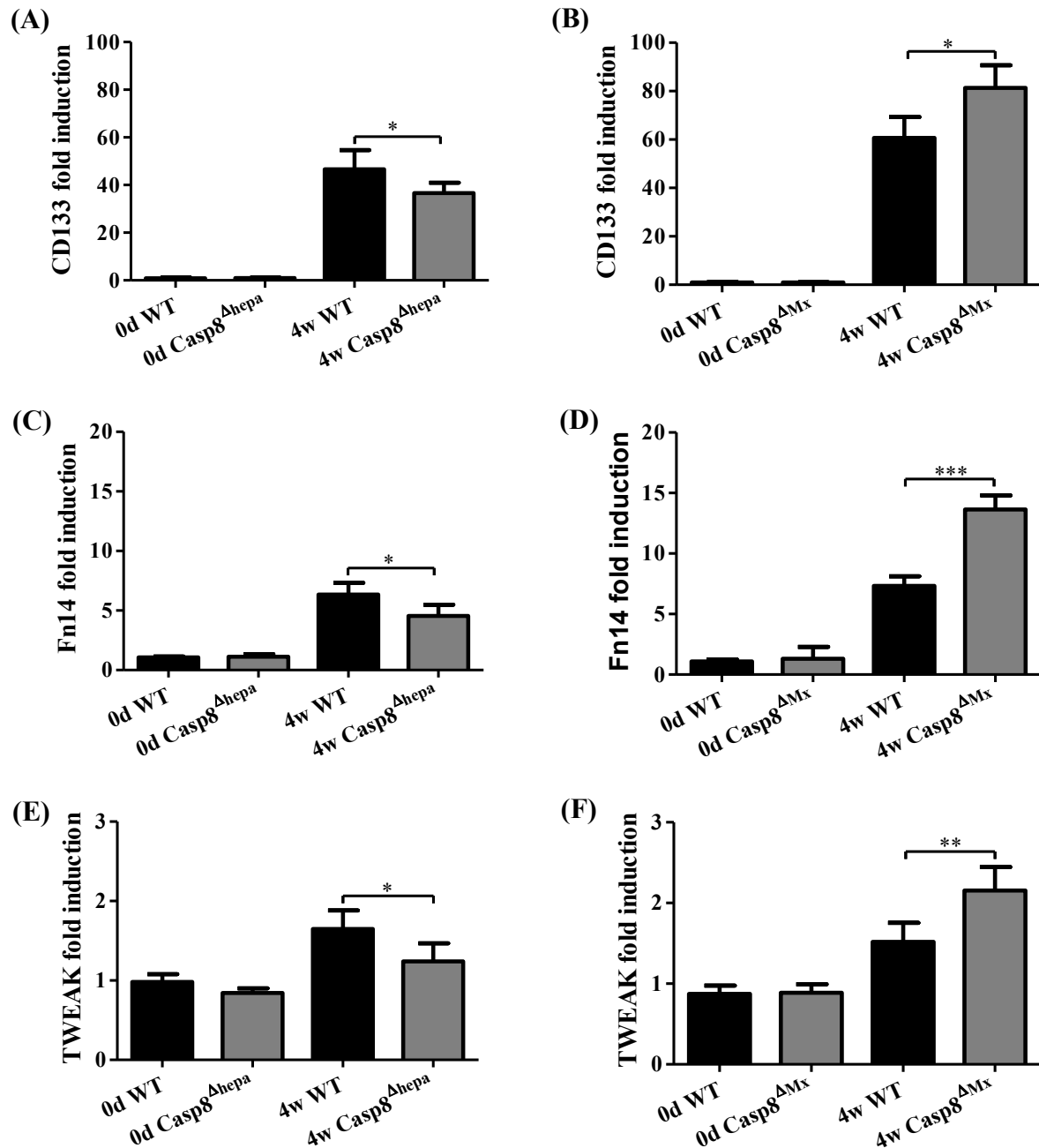
Figure 4.10 Gene expression profiling of LPCs. Displayed is quantitative real-time PCR analysis for CD133 **(A-B)**, Fn14 **(C-D)** and TWEAK **(E-F)** mRNAs of controls, Casp8$^{\Delta hepa}$ and Casp8$^{\Delta Mx}$ mice after 4w of DDC diet treatment. Normalized data are expressed relative to the corresponding value for control mice. mRNA expression was quantified by real-time PCR before and 4w after DDC treatment as indicated. RNA was extracted separately from individual liver tissues (at least 5 samples/time point were included) at the respective time points, *=p<0,05 **=p<0,01.

4.2.3 Characterisation of LPCs through MACS and FACS

Sca-1 expression on fetal liver stem cell generated in DDC injury models has been demonstrated (32). Using FITC-labelled anti-Sca-1 antibody, LPCs were isolated through a MACS process and analysed by FACS. We found >98% Sca-1$^+$ cells from the total cell fraction with >80% viability through MACS process (Fig. 4.11A-D).
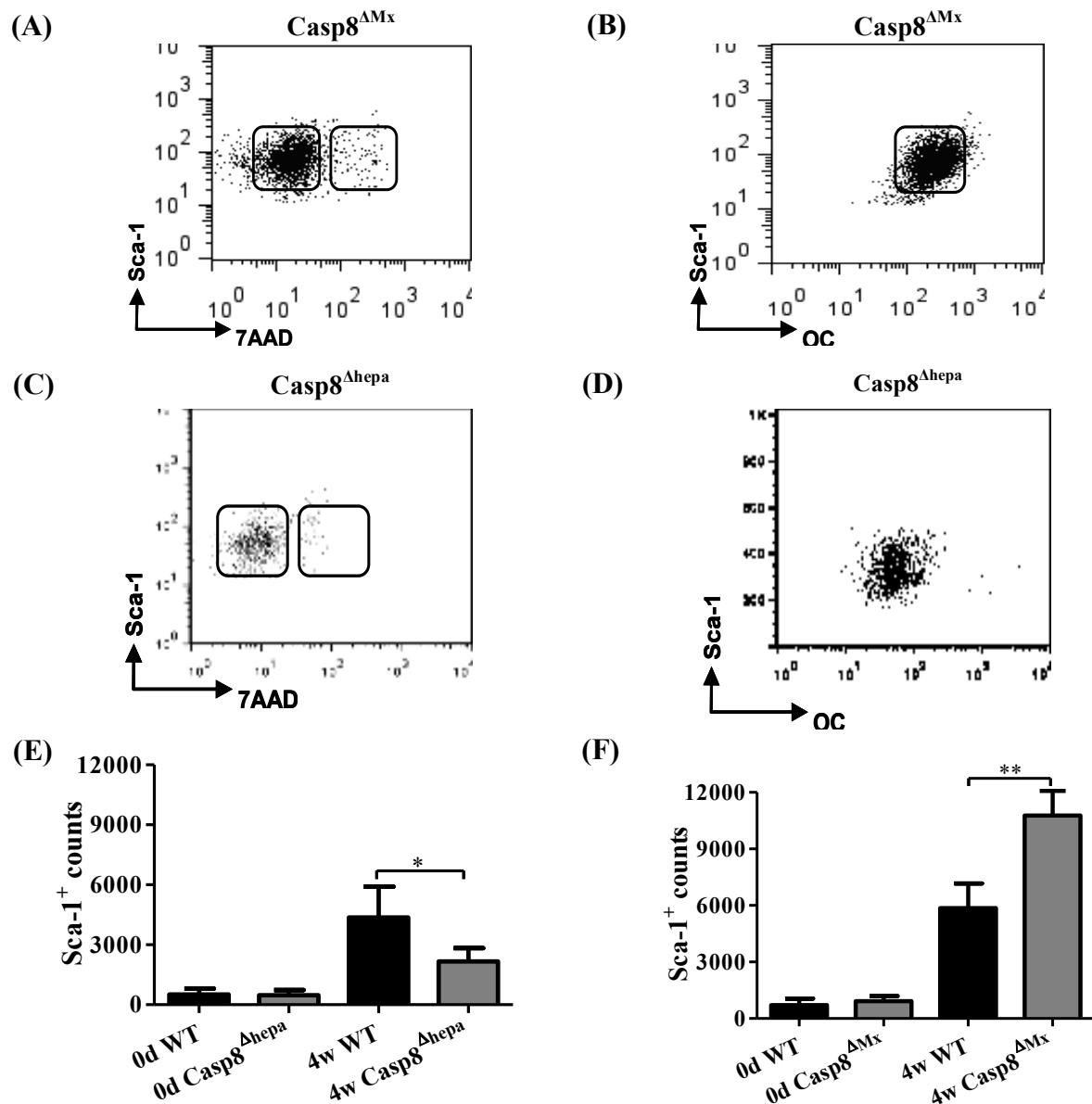
Figure 4.11 Characterization of MACS sorted Sca-1$^+$ cells through FACS assessment. (A-D) Representative FACS plots from a MACS-based isolated liver progenitor cell fraction. Cells isolated from normal and DDC injured livers were enzymatically dispersed, Sca-1 antibody-labeled, and sorted by MACS. Successive gating showed sequential selection of cell-sized events (SSC vs. FSC). Dead cells and debris were excluded using 7-AAD labeling and size exclusion, respectively. (**C**) Sca-1$^+$ displays the gating strategy representing % of the total cell fraction (after depleting mature hepatocytes and corresponding to the NPC population stained with Sca-1). (**E-F**) The analysis represents the percentage of the total cell fraction (after depleting mature hepatocytes and corresponding to the NPC population stained with Sca-1). *, P < 0.05; **, P < 0.01.

WT mice displayed a strong induction of this fetal liver stem cell marker after DDC treatment (Fig. 4.11E). Here again, livers of Casp8$^{\Delta Mx}$ mice showed a significantly stronger activation of LPCs, while Casp8$^{\Delta hepa}$ livers obviously contained less Sca-1$^+$ cells (Fig. 4.11E-F).

Next, we further characterized the isolated LPCs with additional hepatic stem cell related markers OC-1 (Fig. 4.12A-B), OC-2 (Fig. 4.12C-D), and OC-3 (Fig. 4.12E-F) (18). The co-expression was confirmed by FACS analysis (Fig. 4.12).
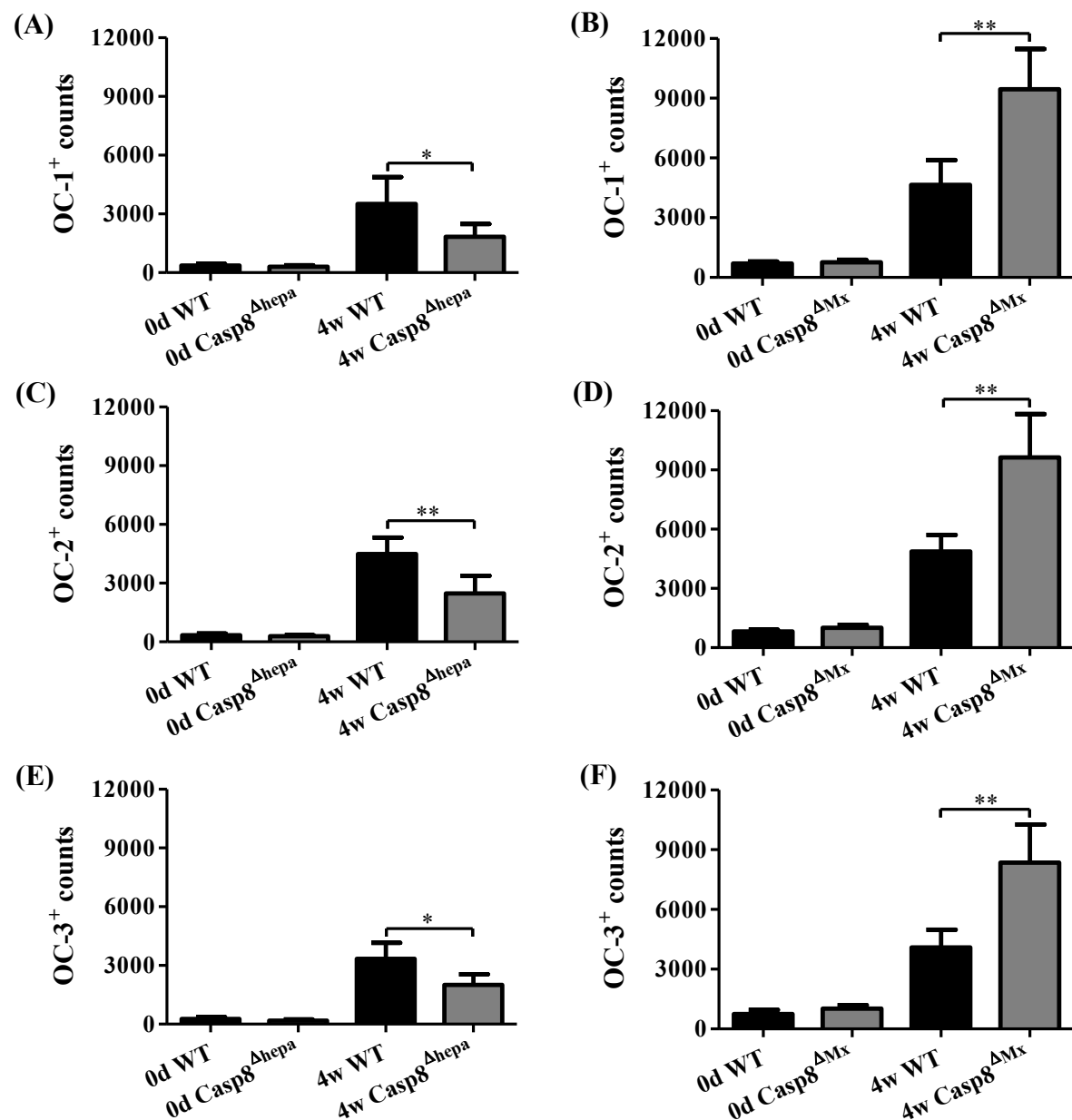
Figure 4.12 Enhanced LPCs marker expression in Casp8$^{\Delta Mx}$ mice. Displayed are representative FACS analysis of MACS-based isolations of LPCs fractions, that were labelled and subsequently analyzed for the expression of OC-1 **(A-B)**, OC-2 **(C-D)** and OC-3 **(E-F)** immediately after isolation. The analysis represents the percentage of the total cell fraction (after depleting mature hepatocytes and corresponding to the NPCs population stained with Sca-1). *, $P < 0.05$; **, $P < 0.01$.

4.2.4 Enhanced LPCs proliferation assessed through PI FACS analysis

To answer the question, whether elevated level of progenitor cells in Casp8$^{\Delta Mx}$ mice are causally related to an enhanced LPCs-proliferation we performed PI-stainings of isolated LPCs-fractions (Fig. 4.13).
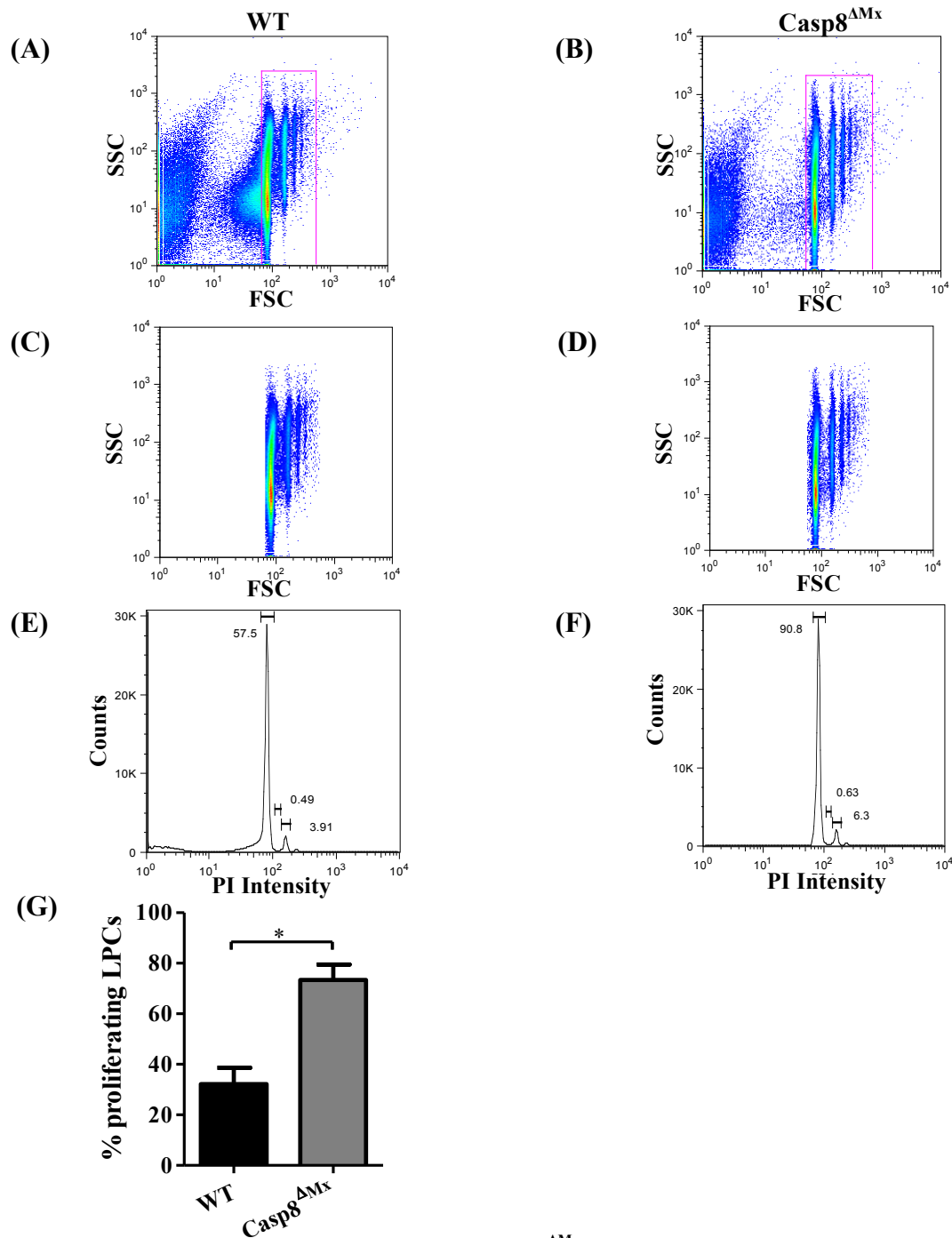
Figure 4.13 Enhanced proliferation of LPCs in Casp8$^{\Delta Mx}$ mice. (A-B) Represantative FACS plots of isolated LPCs stained with PI. Successive gating showed sequential selection of cell-sized events (SSC vs. FSC). **(C-D)** Dead cells were excluded using size exclusion. **(E-F)** The fraction of LPCs isolated from WT (left) and Casp8$^{\Delta Mx}$ (right) mice after 4w of DDC diet treatment labelled with PI (50 µg/ml) were gated on single cells. Single cells were then marked to calculate different phase of the cell cycle G1, S phase and G2-M. **(G)** Representative flow cytometric analysis of DNA content and cell cycle showing that LPCs sustain elevated rate of proliferation potential. *, P < 0.05; **, P < 0.01; ***, P < 0.001.

Here we could demonstrate a significantly stronger PI-uptake in the LPCs-fraction isolated from Casp8$^{\Delta Mx}$ mice (Fig. 4.13A-F), which represents their stronger proliferation. A quantification of this staining is given in Fig. 4.13G.

4.3 Expansion of LPCs is accompanied by enhanced inflammatory response

4.3.1 Enhanced inflammatory response and immune cells infiltration in DDC treated Casp8$^{\Delta Mx}$ mice

The finding of an increased LPCs induction in livers of Casp8$^{\Delta Mx}$ mice after DDC treatment prompted us to investigate the underlying mechanisms in more detail. We thus concentrated in the following mainly on mice with a ubiquitous deletion of Caspase-8 (Casp8$^{\Delta Mx}$), as this group had the strongest ductular-response and LPCs activation. It is known, that LPCs proliferation is related to an inflammatory response in the liver (61). FACS analysis of livers from Casp8$^{\Delta Mx}$ mice being treated with DDC for 4w revealed a strong increase in infiltrating inflammatory cells compared to Casp8$^{\Delta hepa}$ and Casp8 WT mice as well as compared to control diet fed mice. A dramatic increase in the amount of total inflammatory cells (CD45) (Fig. 4.14A-B), macrophages (CD11b) (Fig. 4.14C-D) and T-lymphocytes (CD4) (Fig. 4.14E-F) was observed in Casp8$^{\Delta Mx}$ mice.

(A)

(B)

(C)

(D)

(E)

(F)
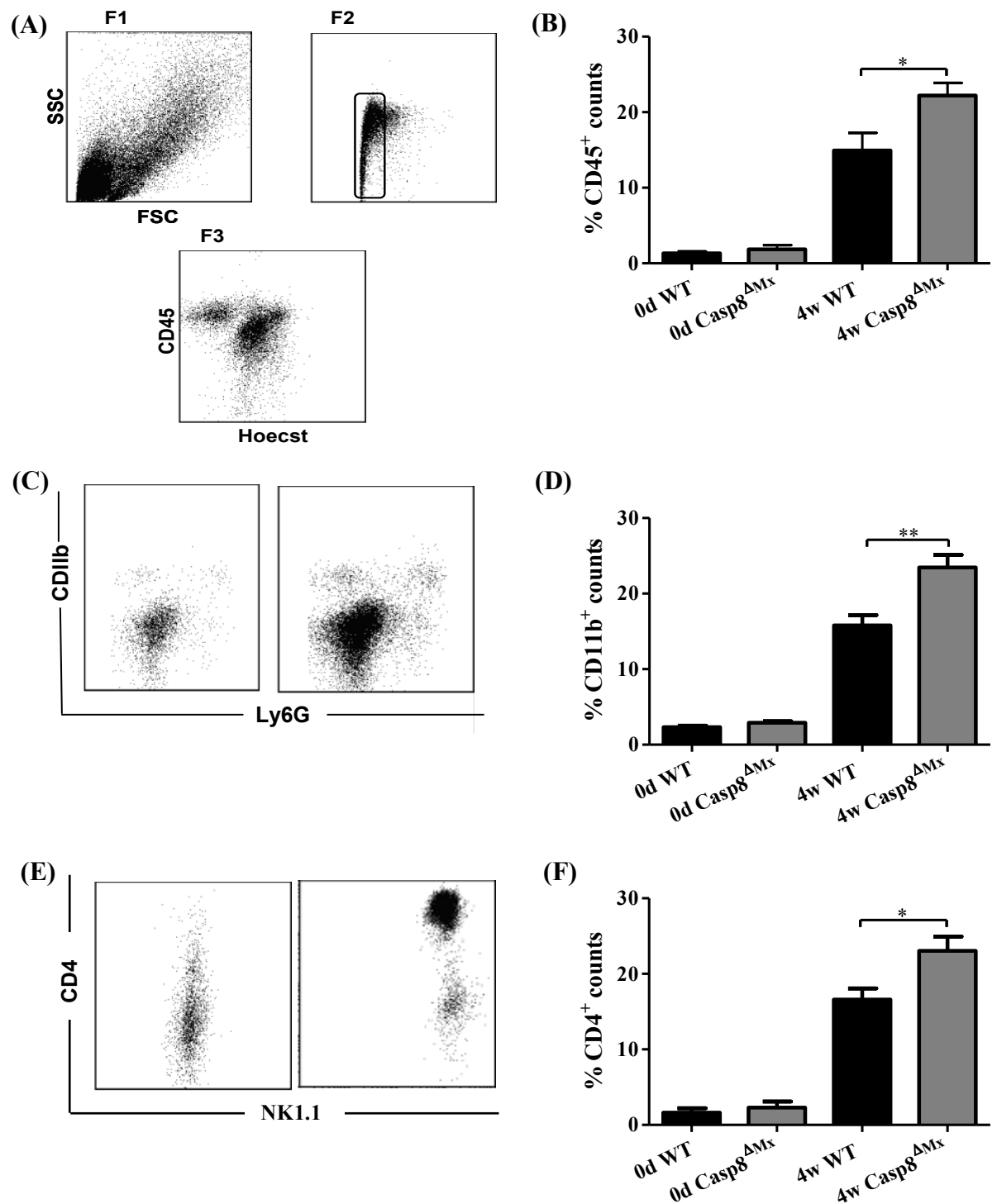
Figure 4.14 Characterization of infiltrating inflammatory cells through FACS assessment. Representative flow cytometric plots from a MACS-based isolated Sca-1$^-$ cell fraction. Successive gating showed sequential selection of cell-sized events (SSC vs. FSC). Dead cells and debris were excluded using 7-AAD labeling and size exclusion, respectively. The gate on CD45 **(A)** represents % of the total immune cell fraction (after depleting mature hepatocytes, Sca-1$^+$ cells and corresponding to the NPC population). **(A-F)** Representative FACS analysis showing dramatic increase in the percentage of total inflammatory cells CD45$^+$, macrophages CD11b$^+$ and T cells CD4$^+$ in Casp8$^{\Delta Mx}$ mice compared to control mice. *, $P < 0.05$; **, $P < 0.01$.

Western blot analysis was thus undertaken, to confirm the efficacy of the Caspase-8 knockout in different cell populations. This revealed an efficient deletion of Caspase-8 (Fig. 4.15) in hepatocytes, immune cells and LPCs.
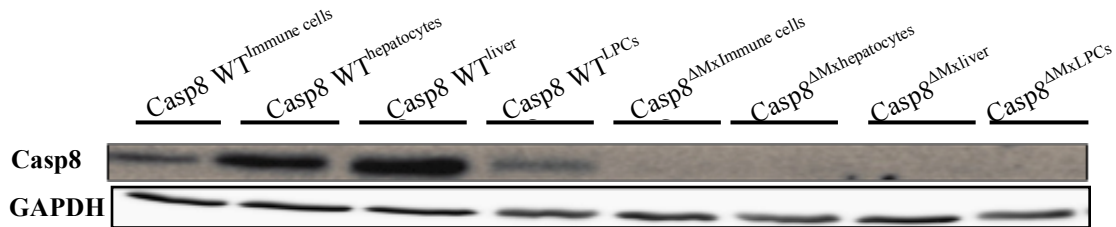
Figure 4.15 Western blot analysis of total protein level for pro-Caspase-8 (55 kDa) expression was performed to monitor Cre-mediated knockout efficiency. GAPDH was detected as loading control.

4.3.2 Apotosis analysis of liver cells through AnnexinV FACS

To proof, that Caspase-8 has a functional effect on cell biology we stimulated freshly isolated NPCs from DDC treated Casp8$^{\Delta Mx}$ and control mice with 50 ng/ml Jo2 antibody in vitro. Here we could observe a relative protection from this apoptosis-inducing antibody in Casp8$^{\Delta Mx}$ mice, while NPCs isolated from control mice went into apoptosis (Fig. 4.16A-B).
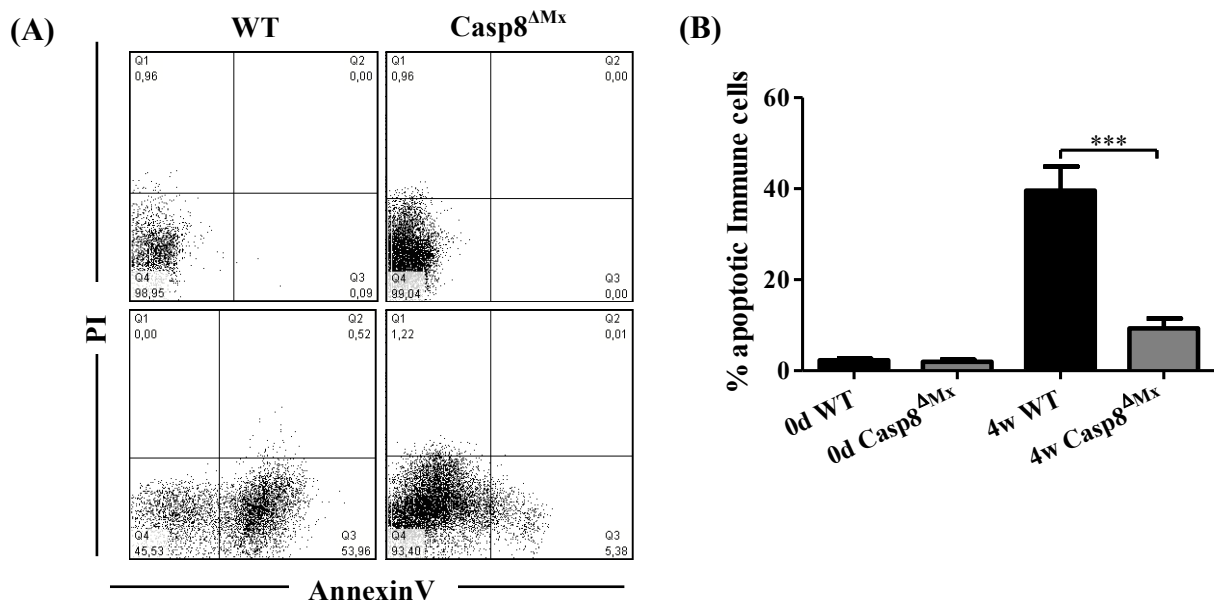
Figure 4.16 Apoptosis analysis in-vitro after Jo2 treatment. (A-B) Representative FACS analysis of the apoptotic index of immune cells in a given sample by dual labelling with FITC-labeled AnnexinV (AV) and propidium iodide (PI). The different labelling pattern in this assay identifies the different cell subpopulations i.e lower right region; apoptotic cell (AV+/PI-), upper left region; necrotic cell (AV+/PI+). *, P < 0.05; **, P < 0.01; ***, P < 0.001.

4.3.3 Enhanced mRNA expression of pro-inflammatory cytokines

Next mRNA levels of pro-inflammatory cytokines were determined by RT-PCR analysis. Those revealed a higher expression of tumor necrosis factor (TNF-α) mRNA (Fig. 4.17A-B) and a significant increase of interleukin-6 (IL-6) mRNA in Casp8$^{\Delta Mx}$ mice compared with Casp8$^{\Delta hepa}$ and controls 4w after DDC diet (Fig. 4.17C-D). Thus the increased expression of proinflammatory cytokines in livers of Casp8$^{\Delta Mx}$ mice after 4w of DDC diet correlated with the stronger occurrence of periportal cellular infiltrates.
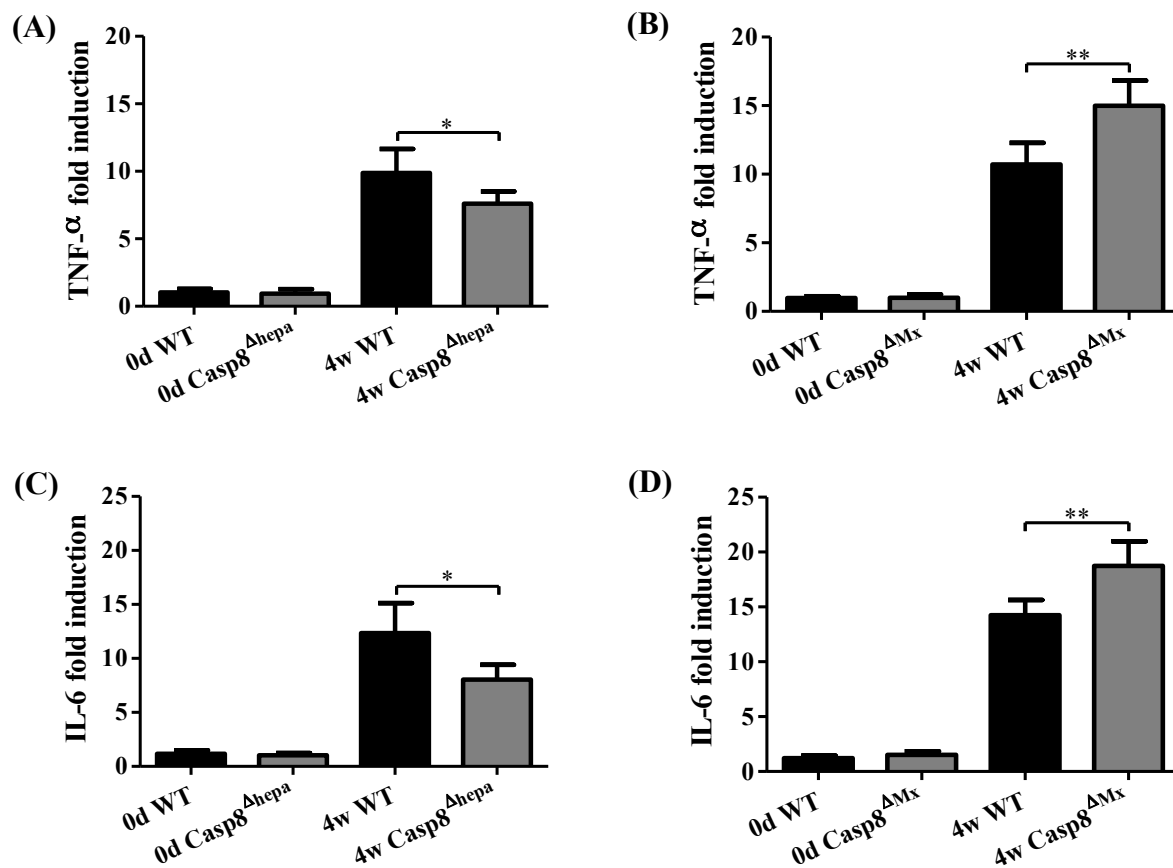
Figure 4.17 mRNA expression of pro-inflammatory cytokines. Quantitative real-time PCR analysis for TNF-α **(A-B)** mRNA and IL-6 **(C-D)** mRNA of WT, Casp8$^{\Delta hepa}$ and Casp8$^{\Delta Mx}$ mice after 4w of DDC diet treatment. Normalized data are expressed relative to the corresponding value for control mice. All data are representative of three independent experiments. n = 4-5 *, $P < 0.05$; **, $P < 0.01$; ***, $P < 0.001$.

This observation could be confirmed at the protein level showing significantly higher NF-κB and pSTAT3 expression 4w after DDC in Casp8$^{\Delta Mx}$ mice compared to Casp8$^{\Delta hepa}$ and controls 4w after DDC diet ((Fig. 4.18A-B).

(A)

(B)
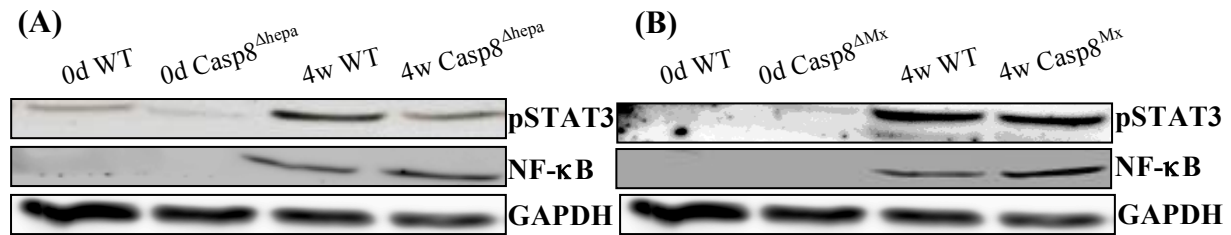
Figure 4.18 Western blot analysis of total protein level for pSTAT3 and NF-κB expression was performed to monitor inflammatory response. GAPDH was detected as loading control.

4.4 Caspase-8 knockout bone marrow transplantation (BMT) aggravates liver damage after chronic liver injury

So far we could provide evidence that under the condition of ubiquitous Caspase-8-deletion mice develop enhanced liver injury after DDC treatment. Based on our finding that Casp8$^{\Delta Mx}$ mice displayed significantly more periportal infiltration, inflammation and also LPCs induction all culminating in the stronger onset of fibrosis progression we aimed to answer the likely question, whether this effect is primarily mediated by BM derived cells. To proof this hypothesis we transplanted lethality-irradiated mice with control and Casp8$^{-/-}$ BM. Those mice then underwent further DDC treatment. Data from this experiments now first showed, that transaminases and bilirubin levels were almost two-fold stronger increased in mice having received Casp8$^{-/-}$ BM compared to recipients of control BM (Fig 4.19A-B). Second, we were able to proof, that this was correlated with a significant increase in the number of infiltrating immune cells. Consistent data were obtained for CD45$^+$, CD11b$^+$ and CD4$^+$ cells (Fig. 4.19C-E). Third, we wanted to analyse, whether this was related to an enhanced LPCs reaction - in analogy to the experiments using Casp8$^{\Delta Mx}$ mice (see Fig. 4.11F). FACS analysis finally confirmed a significantly enhanced number of Sca-1$^+$ cells in the Casp8$^{-/-}$ BM-transplanted group (Fig. 4.19F).
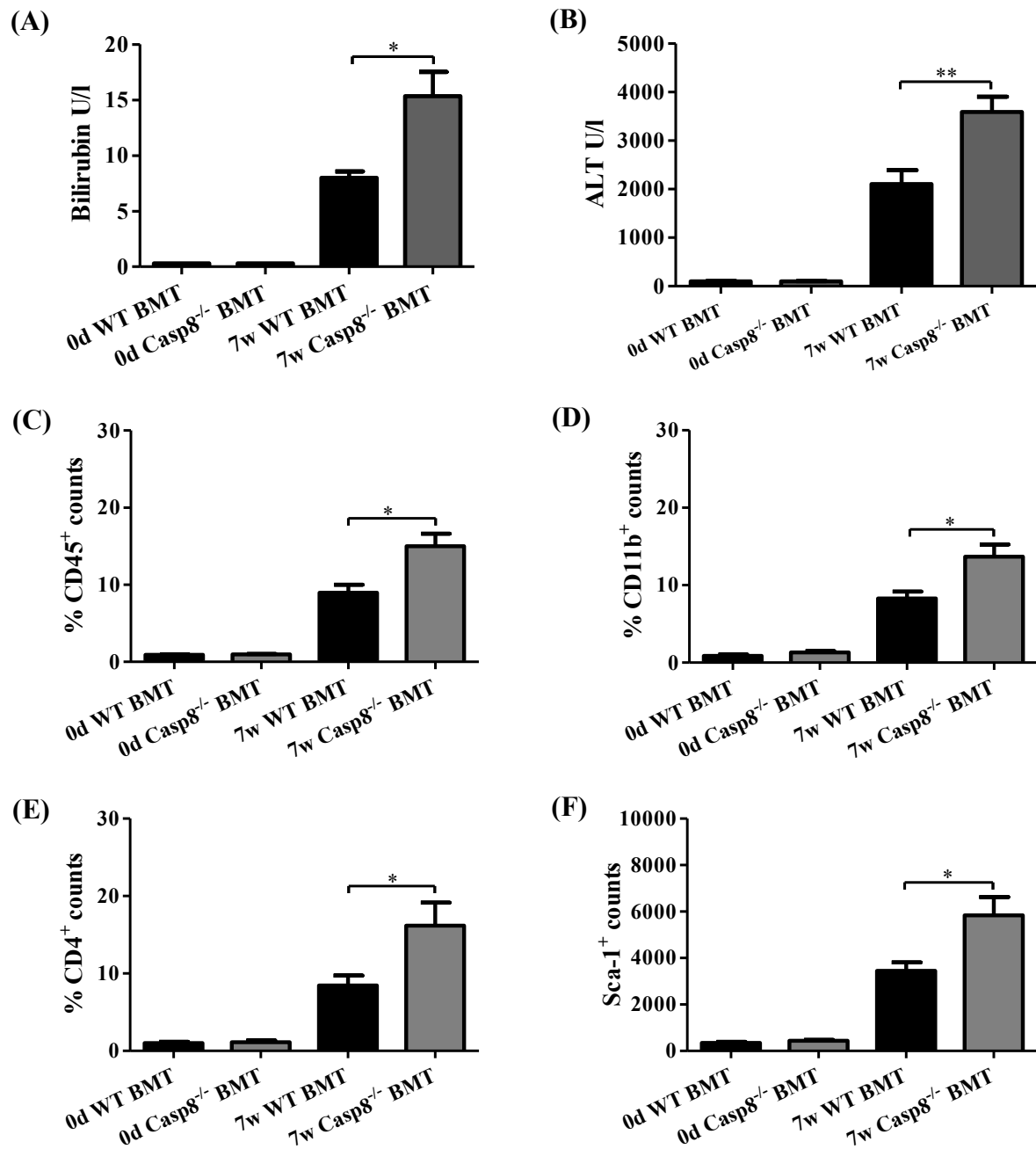
Figure 4.19 Caspase-8 mice bone marrow transplantation (BMT) aggravates liver damage after chronic liver injury. (A-B) Serum transaminases (ALT) and bilirubin levels were almost two-fold stronger increased in mice receiving Casp8$^{-/-}$ BM compared to recipients of control BM. **(C-E)** Representative FACS analysis show a significant increase in the percentage of total inflammatory cells CD45, macrophages CD11b and T cells CD4 in mice receiving Casp8$^{-/-}$ BM compared to recipients of control BM. **(F)** Representative FACS analysis revealed significantly stronger activation of LPCs in mice receiving Casp8$^{-/-}$ BM compared to recipients of control BM. *, $P < 0.05$; **, $P < 0.01$; ***, $P < 0.001$.

5 Discussion

Liver regeneration following chronic injury is controlled through a complex signalling network that regulates the balance between cell proliferation and apoptosis (104-106), inflammation, the proliferation of LPCs and fibrosis (107). Apoptosis has become the focus of many researchers since it became apparent that an imbalance between cell proliferation and cell death in the liver contributes to the pathogenesis of several liver diseases (108-112). During liver regeneration apoptosis and death-receptor induced cell death are thought to play a role in a) the termination of tissue expansion and proliferation and b) to provide space for the expanding new cell population. Involved signalling pathways however have not been thoroughly defined so far. To address this question hepatocyte-specific knockout mouse strains for Caspase-8 (Casp8$^{\Delta hepa}$) and mouse strain for a ubiquitous deletion of Caspase-8 (Casp8$^{\Delta Mx}$) were characterized in a model of DDC induced liver injury. We now investigated the role of Caspase-8 deletion in different liver cells during chronic liver injury and regeneration.

5.1 Hepatocyte specific vs. ubiquitous deletion of Caspase-8 leads to a differential phenotype in a model of secondary sclerosing cholangitis

Caspase-8 is essential for death-receptor mediated apoptosis. The Caspase-8 gene has been shown to be indispensable for embryonic development, as constitutive disruption of Caspase-8 leads to an impaired heart muscle development and hyperemia. In earlier studies the role of receptor-mediated Caspase activation has been investigated through the use of newly generated Caspase-8 knockout mice (97). It has been shown that hepatocyte-specific deletion of Caspase-8 results in moderate basal liver inflammation and protected mice from the induction of apoptosis and liver injury. Interestingly here non-apoptotic liver injury and necrosis were increased if the more immune-dependent model of Concanavalin-A (97) induced liver injury was used. Further evidence for a tissue protective role of Caspase-8 comes from data generated in the NEMO-model of liver injury. Cancer development, based on a chronic hepatic inflammation due to the failing activation of the transcription factor NF-κB could be completely abrogated through the simultaneous ablation of NEMO and Caspase-8 signalling (113). Therefore Caspase inhibition seems to be disease-preventive in certain conditions. We thus aimed to define the cell-specific role of Caspase-8 in a relevant mouse

model of cholangitis based chronic liver injury that models a number of metabolic and toxic liver diseases in mice.

To analyse the role of Caspase-8, a hepatocyte-specific knockout mouse strain for Caspase-8 (Casp8$^{\Delta hepa}$) and a mouse strain for a ubiquitous deletion of Caspase-8 (Casp8$^{\Delta Mx}$) were subjected to DDC treatment for 4w and analysed for molecular and cellular changes during secondary sclerosing cholangitis and liver regeneration compared to appropriate control mice (Casp8$^{loxP/loxP}$).

First we could show a clear liver protective effect if the gene was inactivated solely in hepatocytes (Casp8$^{\Delta hepa}$). Although this might have been somewhat expected, those data contain several interesting points. Interestingly transaminases were only reduced by a quarter of their original elevation in Casp8$^{\Delta hepa}$ mice after DDC feeding, but the degree of the ductular reaction (Fig. 4.9C, Fig. 4.11E) and fibrosis (Fig. 4.2A,C, Fig.4.3A) were even stronger reduced. Thus a greater part of DDC-mediated liver injury is at least partly mediated via the activation of hepatocellular death-receptors. Several reports including our own previous analysis estimated the number of truly apoptotic cells after DDC feeding in a range of 1-3% (114). Although this is a rather moderate number, it is obviously still significantly enough to contribute over time to organ failure and to trigger regenerative approaches. Here now the possibility remains, that Caspase-8 activates besides Caspases other downstream signaling components that are involved in tissue injury, e.g. c-jun N-terminal kinases (JNK) (115), the induction of reactive oxygen species (ROS) (116) and BH3-only proteins (117).

Another likely mechanism, how DDC can harm mouse livers is chemically induced injury. Fickert et al. suggested that DDC metabolites change the expression of transporter molecules, like bile salt export pumps and multi-drug resistance proteins (118). This in term leads to a reduced excretion of glutathione and phospholipids. Subsequently an inflammatory response is triggered, which leads to the recruitment and infiltration of neutrophils and other inflammatory cells. Through this mechanism liver injury gets perpetuated and remodelling occurs. Mice carrying a hepatocyte specific conditional Caspase-8 deletion also showed reduced cholestasis (Fig. 4.1B) during DDC treatment. As we do not see remarkable differences in the expression of bile-salt transporters, we belive that reduced cholestasis in Casp8$^{\Delta hepa}$ mice is an indirect effect of the preserved function of hepatocytes. However, the provided cell protection through the missing activation of the Caspase cascade in Casp8$^{\Delta hepa}$ mice obviously reduces the inflammatory activity in this group.

Consequently we observed in Casp8$^{\Delta hepa}$ mice much less periportal cellular infiltration and a significantly lower rate of LPCs (Fig. 4.9C and Fig. 4.11E) that are typically induced

during DDC treatment under this condition. Biliary epithelial cells most likely are not involved here, as Cre-expression is restricted to hepatocytes. This is consistent with some of our earlier studies showing an enhanced chronic injury in the DDC model, if hepatocellular fitness is impaired (114).

As a possible consequence of the slowed progression towards chronic injury we see in Casp8$^{\Delta hepa}$ mice now a lower degree of LPCs induction and extracellular matrix accumulation. To date it is not fully answered; whether the activation of LPCs follows the accumulation of extracellular matrix, or if LPCs themselves might directly or indirectly contribute to the activation of matrix producing cells. In a recent report it was convincingly shown, that the evolvement of the hepatic stem cell niche and LPCs activation follows collagen-accumulation and not the other way around (119). On the other hand Chobert and co-wrokers demonstrated that liver fibrosis was not the direct consequences of hepatocellular lesions or inflammatory response, but was due to the accumulation of LPCs (120). Further analysis by Chobert et. al. showed that CK19$^+$ LPCs expressed fibrogenic cytokine transforming growth factor-β (TGF-β), which contributed to the accumulation of α-SMA$^+$ myfibroblasts in the ductular reaction leading to enhanced fibrosis. Next, Chobert et. al. showed that LPCs did not expressed α-SMA, desmin or fibroblast-specific protein-1, demonstrating that LPCs did not undergo an epithelial-mesenchmal transition. Thus futher studies have to reveal the exact relationship between LPCs expansion and extracellular matrix deposition leading to hepatic fibrosis.

Accumulating investigations in murine models and chronically diseased human livers have also reported a correlation between the presence of extracellular matrix (ECM) deposition and magnitude of LPCs expansion (107, 121-127). Van Hul et.al. suggested that in addition to the presence of ECM deposition before the expansion of LPCs, LPCs are embedded in matrix and that matrix deposition escort the LPCs, paving the way from the portal tract to the parenchyma and allowing the progenitor cells to invade the deposited matrix. Thus, the established hepatic microenvironment plays an important role in the activation, proliferation and survival of LPCs in a hostile environment (Fig. 5.1) (22, 128, 129). In our study we found a reduced amount of collagen accumulation in Casp8$^{\Delta hepa}$ mice ccompared to WT mice after 4w of DDC feeding as demonstrated by collagen staining in Fig.4.2A-B. This finding was further strengthened by a lower collagen-1α mRNA (Fig. 4.3A) and α-SMA mRNA (Fig. 4.3B) expression in Casp8$^{\Delta hepa}$ mice compared to WT mice after 4w of DDC treatment, thus supporting the correlation between the importance of ECM deposition and the level of LPCs expansion.
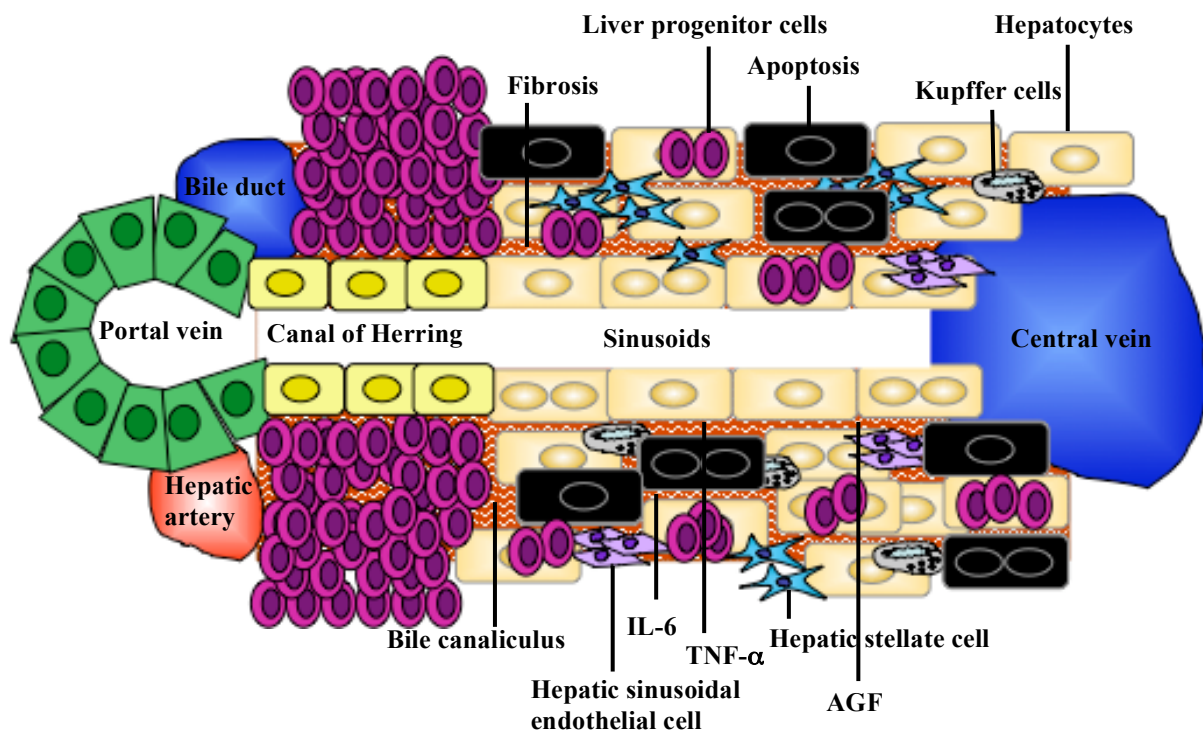
Figure 5.1 Corellation between magnitude of extracellular matrix deposition, inflammation and hepatic microenvironment during activation, proliferation and survival of LPCs in a hostile environment.

Interestingly we observed increased transaminases and bilirubin levels and significantly more cholestasis in the Casp8$^{\Delta Mx}$ mice compared to WT and Casp8$^{\Delta hepa}$ mice after 4w of DDC treatment (Fig. 4.1A-D), thus pointing a different mechanism to be responsible in case of a ubiquitous Caspase-8-deletion. We therefore sought after an explanation how apoptosis resistance against – Caspase-8-mediated – receptor activated cell death in different liver cell types might influence the development of chronic liver injury.

DDC induced liver damage is accompanied by the induction of a strong intrinsic regenerative approach that involves hepatic progenitor cells and a prominent ductular reaction. But it also hampers proliferation (41, 118, 130) and comprises metabolic and excretory functions of hepatocytes through the down regulation of biliary transporters.

5.2 Conditional Caspase-8 knockout mice are protected against parenchymal apoptosis

Measuring of Caspase-3 activity unravelled that receptor mediated apoptotic activity in the liver parenchyma was reduced regardless of the Cre-source, as both Casp8$^{\Delta hepa}$ and Casp8$^{\Delta Mx}$ mice showed a diminished activity (Fig. 4.4E, F). Thus the observed phenotype

must be attributed to other cells then hepatocytes. Here two other cell populations came into the focus of our investigations – hepatic progenitor cells and immune cells, as histological analysis of Casp8$^{\Delta Mx}$ mice unravelled their stronger presence in this group after DDC treatment. The fact, that Mx-Cre mediated deletion of Caspase-8 however was obviously unequivocally quite effective in different tissue compartments (Fig. 4.15) made it further likely that Caspase-8 deletion also in NPCs would provoke a diverse phenotype. Both immune cells and cells of the LPC compartment displayed enhanced proliferation rates in mice with deleted Caspase-8 as compared to their control counterparts.

Our data point to a significant and so far under recognised role of immune cells in the pathogenesis of the DDC model. Indeed isolated immune cells from Casp8$^{\Delta Mx}$ mice showed an intrinsic resistance to apoptosis after Fas-receptor activation through the use of Jo2 antibody (Fig. 4.16A, B). It is known for long, that defective Fas-signalling - either due to defective function of Fas-Ligand or Fas itself - can lead to the development of auto-immune-lymphoproliferative disorders (131). Mice bearing a defective mutation of the Fas-receptor (132) even showed a liver phenotype after reconstitution of BM with Fas-receptor inactive cells.

It has been demonstrated that activated lymphocytes produce a soluble FasL homotimer, which is a potent pathologic agent in tissue injury (133). Under normal conditions, activation induced cell death (AICD) of mature T cells is regulated by Fas-mediated AICD, but in certain chronic liver injury (e.g., a viral infection) a strong antigenic stimulus could result a defect in this autoregulatory apoptosis inducing mechanism and can lead to a deficient activation induced cell death of T lymphocytes. Those in turn over-express FasL which results in nonspecific hepatocyte injury and cytotoxicity leading to autoimmune effects (132).

Another proof for our theory of enhanced immune cell activation comes from the experiments involving BMT of Caspase-8 deficient donor cells. The apoptosis resistant immune cells that repopulate in mice after bone marrow transplantation must act in an auto-aggressive manner on their host livers. This somehow mimics the above-described auto-immune-like phenotype that has been reported before for apoptosis resistant immune cells (134). Given this as an explanation for the observed phenotype one must demand, that inactivation of Caspase-8 in immune cells first provokes them to proliferate and second that their activation can cause harm to resident livers. Here it is important to note, that there is no obvious spontaneous phenotype and that liver damage must occur first.

5.3 Expansion of LPCs in DDC treated Casp8$^{\Delta Mx}$ mice liver is correlated with an enhanced inflammatory response and immune cell infiltration

It has been shown that liver regeneration following the loss of hepatocytes induced by toxins, such as the DDC diet model (13, 30, 118) replication and differentiation of intrahepatic progenitor cells occurs. Analysis of the proliferation of LPCs in WT, Casp8$^{\Delta hepa}$ and Casp8$^{\Delta Mx}$ mice after 4w of DDC treatment as a measure for regenerative approaches, displayed stronger proliferation in periportal areas- where LPCs emerge and reside.

LPCs have been reported to express stem cell antigen (Sca-1) marker, which is also expressed on hematopoietic stem cells (135). Petersen et.al. demonstrated Sca-1 expression on LPCs using an experimental injury model to induce LPCs proliferation (30). In-depth analysis of LPCs demonstrated that a subset of the Sca-1 is positive for stem cell markers (e.g. OC-1, OC-2 and OC-3) each of which has been shown tobe important in various LPCs studies (32). Consistent with previous reports we also demonstrate Sca-1 (Fig. 4.11A-F), OC-1, OC-2 and OC-3 (Fig. 4.12A-F) markers expressing LPCs in Casp8$^{\Delta Mx}$ mice compared to WT, Casp8$^{\Delta hepa}$ and after 4w of DDC treatment.

Important parallel pathophysiologic processes between liver inflammation and regeneration involving hepatic NPCs (endothelial cells, stellate cells, Kupffer cells and lymphoid cells) and hepatocytes during liver regenerative process have been studied (136, 137). Several inflammatory molecular mechanisms used by cancer cells to proliferate effectively may also aply to proliferating liver cells during regeneration, supporting the concept that inflammatory mediators are indeed involved in the regulation of regenerative process (138, 139). It is known, that LPCs proliferation is related to an inflammatory response in the liver (61). Studies have also indicated that DDC diet induced chronic liver injury and LPCs proliferation is correlated with increased inflammation (140). We thus investigated the inflammation profile in WT, Casp8$^{\Delta hepa}$ and Casp8$^{\Delta Mx}$ mice after 4w of DDC treatment.

It has been shown that TNF-α and IL-6, which are produced by macrophages, play an important role in the priming phase of liver regeneration (141, 142). Studies in IL-6-deficient (143, 144) and TNF-α receptor 1 (TNF-R1)-deficient (145) mice have shown that liver regeneration requires this cytokines. Further, specific studies by inhibiting inflammatory cytokines, by treating with dexamethasone or a cyclooxygenase 2-inhibitor, have shown the mitogenic potential of inflammatory cytokines for LPCs in the damaged liver (52, 53, 55). Based on previous observations suggesting a link between inflammation and the proliferation

of LPCs during chronic liver injury, we investigated the effects of an LPCs inducing process in a hepatocyte-specific knockout mouse strain for Caspase-8 (Casp8$^{\Delta hepa}$) and a mouse strain for the ubiquitous deletion of Caspase-8 (Casp8$^{\Delta Mx}$) mice. The analysis of the anti-inflammatory cytokines unrevealed a high expression of interleukin-6 (IL-6) mRNA (Fig. 4.17C-D) and a significant increase of tumor necrosis factor (TNF-α) mRNA in Casp8$^{\Delta Mx}$ mice compared with Casp8$^{\Delta hepa}$ and controls 4w after DDC diet (Fig. 4.17A-B). Further flow cytometry analysis of immune cells in these mice point to an additionally enhanced infiltration of immune cells (CD45, F4/80, CD4) in Casp8$^{\Delta Mx}$ mice. This finally resulted in a stronger fibrosis progression of the underlying sclerosing cholangitis induced by DDC in Casp8$^{\Delta Mx}$ mice, as evidenced by an enhanced expression of collagen-1α and α-SMA. Knight and co-workers have demonstrated a correlation between the magnitude of LPCs response and the intensity of fibrosis supporting the above results (107).

Thus the increased expression of proinflammatory cytokines in livers of Casp8$^{\Delta Mx}$ mice after 4w of DDC diet correlated with the stronger occurrence of periportal cellular infiltrates, liver fibrosis and elevated number of LPCs proliferation.

In summary we demonstrate within the present study, that Caspase-8 has a distinct cell specific impact on the function of individual liver cell types in a mouse model of chronic cholestatic liver injury and progenitor cell activation. While a hepatocyte specific knockout provided protection from liver damage a ubiquitous deletion of Caspase-8 triggered more injury and inflammation. This was related to a significantly stronger activation of the LPCs compartment and more tissue remodelling. Thus new light is shed on the role of death receptor mediated physiological functions in individual cell types, which can lead to unexpected consequences upon disturbance. Caspase-inhibition in hepatocytes seems to be a promising option to at least temporarily preserve organ function of the whole liver. The targeting of Caspase-8 in LPCs can also be a future therapeutic option, as their proliferation and thus repopulation potential can be further enhanced through this strategy. However, if Caspase-inhibition cannot be securely restricted to the target cell and occurs uncontrolled one must be aware of severe side-effects of potential Caspase-8-targeted therapies.
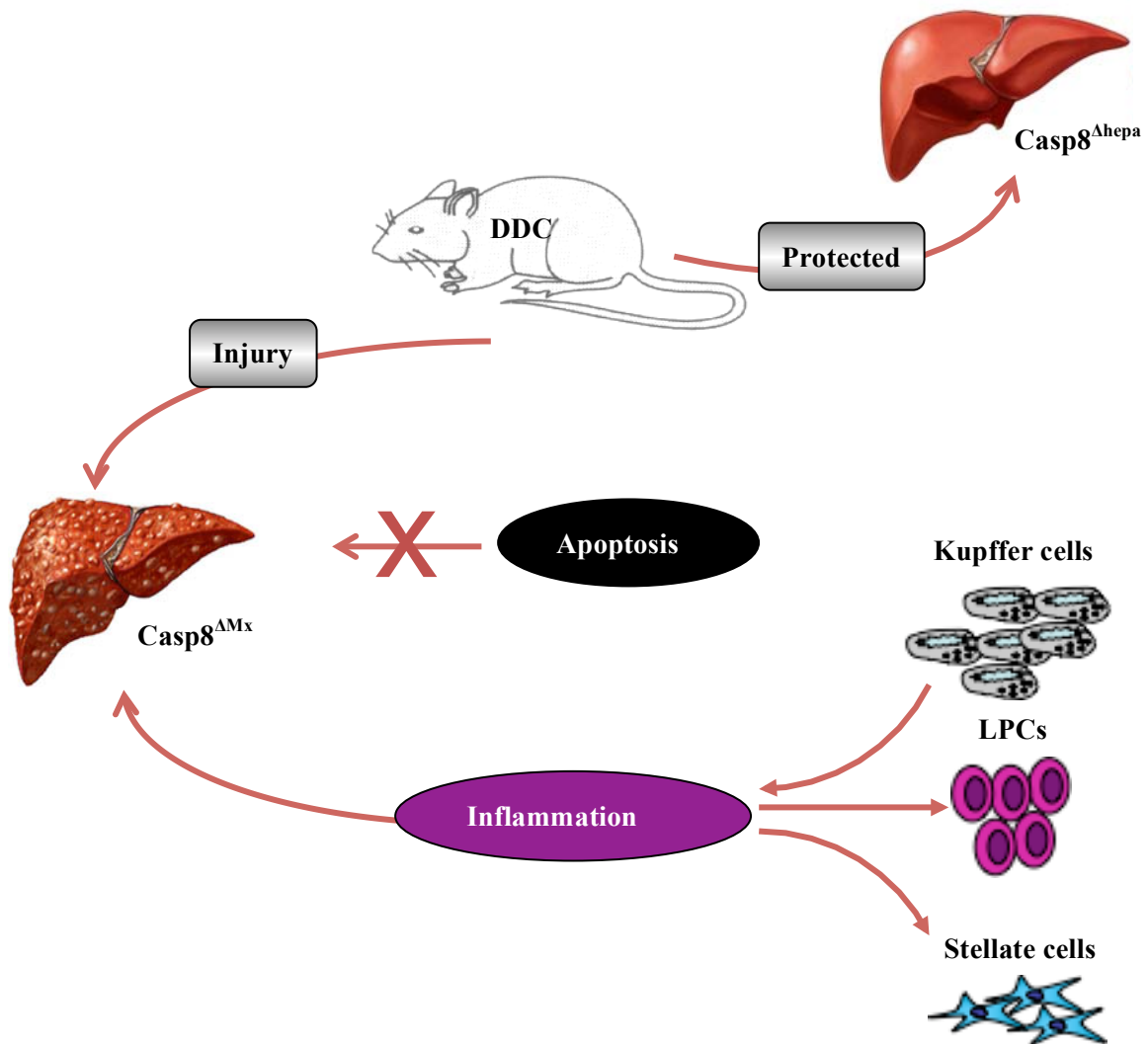
Figure 5.2 Model of chronic liver injury and LPCs activation. Hepatocyte specific Caspase-8 knockout (Casp8$^{\Delta hepa}$) provided protection from liver damage while a ubiquitous deletion of Caspase-8 (Casp8$^{\Delta Mx}$) triggered more injury and inflammation. Apoptosis is not resposnsible for liver injury in Casp8$^{\Delta Mx}$ mice. This was finally related to a significantly stronger activation of the LPCs compartment and in a stronger fibrosis progression of the underlying sclerosing cholangitis induced by DDC in Casp8$^{\Delta Mx}$ mice, as evidenced by an enhanced expression of collagen-1α and α-SMA.

6 Summary

The balance between apoptosis and proliferation represents the basis for the maintenance of tissue homeostasis. Receptor mediated cell death through the activation of Caspases has been identified as an important mechanism to control life and death in various tissues. In this study, we modulated Caspase-8 activity in individual liver cell types using hepatocyte-specific knockout mice for Caspase-8 (Casp8$^{\Delta hepa}$) and a mouse strain for a ubiquitous deletion of Caspase-8 (Casp8$^{\Delta Mx}$) in the DDC (3,5-diethocarbonyl-1,4-dihydrocollidine) model of secondary sclerosing cholangitis and liver progenitor cells (LPCs) activation.

Here, we demonstrate that mice with Caspase-8 inhibition in hepatocytes (Casp8$^{\Delta hepa}$) were protected from DDC-mediated injury, while mice with a ubiquitous conditional Caspase-8 knockout (Casp8$^{\Delta Mx}$) displayed a significantly enhanced hepatic inflammation and tissue injury. This was demonstrated by higher transaminases, bilirubin levels and finally also more liver fibrosis. Thereby Caspase-3 activity was reduced in both knockout strains, suggesting other mechanisms being responsible for the phenotype. Correlating with enhanced liver injury, Casp8$^{\Delta Mx}$ mice displayed a stronger infiltration of mononuclear immune cells and more proliferation of LPCs in periportal areas. Further analysis confirmed that these infiltrating immune cells are resistant against extrinsic apoptosis. Bone marrow transplantation (BMT) experiments demonstrated that Caspase-8-deficient bone marrow derived cells are responsible for increased liver injury in DDC fed mice.

Taken together, our in vitro and in vivo finding demonstrates a cell-specific and distinct impact of Caspase-8 on individual liver cell types. While a hepatocyte specific knockout provided protection from liver damage the ubiquitous deletion of Caspase-8 triggered more injury and inflammation. This phenotype was associated with a stronger ductular reaction and activation of the hepatic progenitor cell niche and caused through mechanism of immune-cell mediated liver injury.

7 Zusammenfassung

Das Zusammenspiel von Apoptose und Zellproliferation bildet die Basis für die Aufrechterhaltung der Gewebshomöstase. Der zur Apoptose führende sog. Rezeptor-vermittelte Zelltod wird durch die Aktivierung von Caspasen ausgelöst und stellt in vielen Geweben einen wichtigen Mechanismus für die Kontrolle der Zellfunktion dar. In der hier präsentierten Arbeit wurde die Rolle und pathophysiologische Bedeutung von Caspase-8 in verschiedenen Leberzelltypen untersucht. Dabei kamen konditionale Caspase-8 Knockout Mäuse, die entweder einen Hepatozyten-spezifischen (Casp8$^{\Delta hepa}$) oder einen ubiquitären (Casp8$^{\Delta Mx}$) Knockout aufwiesen zum Einsatz. Untersucht wurden die Mäuse im DDC (3,5-diethocarbonyl-1,4-dihydrocollidine) vermittelten Modell der sekundär-sklerosierenden Cholangitis und Lebervorläuferzell- (LPCs) Induktion.

Dabei konnte dargelegt werden, dass Mäuse mit Hepatozyten-spezifischem Caspase-8 KO im DDC-Modell geschützt waren, während eine ubiquitäre Caspase-8-Deletion zu einer vermehrten Leberentzündung und Gewebsschädigung führte. Dies wurde durch Nachweis erhöhter Transaminasen, Cholestaseparameter und schliesslich vermehrte Fibroseprogression gezeigt. Da die Aktivität der abhängigen Caspase-3 in beiden Mauslinien reduziert war, mussten andere Mechanismen für den Phänotyp verantwortlich sein. Korrelierend zur vermehrten Schädigung zeigten Casp8$^{\Delta Mx}$ Mäuse eine stärkere Infiltration mononukleärer Zellen und eine vermehrte LPCs Proliferation in periportalen Arealen. Weitere Analysen bestätigten, dass diese infiltrierenden Immunzellen resistent gegenüber extrinsischer Apoptose nach Fas-Aktivierung waren. Knochenmarktransplantationsexperimente demonstrierten dann, dass Mäuse nach Rekonstitution mit Caspase-8-defizientem Knochenmark eine vermehrte Leberschädigung nach DDC-Behandlung zeigten.

Zusammengefasst demosntrieren die dargelegten Daten, dass ein Fehlen von Caspase-8 zu Zelltyp-spezifischen distinkten pathophysiologischen Konsequenzen führt. Ein hepatozyten-spezifischer Knockout schützt die Leber, während eine ubiquitäre Deletion von Caspase-8 zu vermehrter Leberschädigung und Entzündung führt. Dieser Phänotyp war mit einer immun-vermittelten vermehrten duktalen Reaktion und der Aktivierung der hepatischen Stammzellnische verbunden.

8 References

1. Junqueira, L.C., and Carneiro, J. 2002. *Basic Histology: Text & Atlas*: McGraw-Hill/Appleton & Lange.

2. Racanelli, V., and Rehermann, B. 2006. The liver as an immunological organ. *Hepatology* 43:S54-62.

3. Fausto, N. 2004. Liver regeneration and repair: hepatocytes, progenitor cells, and stem cells. *Hepatology* 39:1477-1487.

4. Prior, P. 1988. Long-term cancer risk in alcoholism. *Alcohol Alcohol* 23:163-171.

5. Tsukuma, H., Hiyama, T., Tanaka, S., Nakao, M., Yabuuchi, T., Kitamura, T., Nakanishi, K., Fujimoto, I., Inoue, A., Yamazaki, H., et al. 1993. Risk factors for hepatocellular carcinoma among patients with chronic liver disease. *N Engl J Med* 328:1797-1801.

6. Wynn, T.A. 2008. Cellular and molecular mechanisms of fibrosis. *J Pathol* 214:199-210.

7. Guha, I.N., and Iredale, J.P. 2007. Clinical and diagnostic aspects of cirrhosis. In *Textbook of hepatology from basic science to clinical practice*. J. Rodes, J.P. Benhamou, A. Blei, J. Reichen, and M. Rizzetto, editors. Oxford: Blackwell Publishing. 604-622.

8. Conn, H.O., and Atterbury, C.E. 1993. Cirrhosis. In *Diseases of the Liver*. L. Schill, editor. Philadelphia: J.B. Lippincott. 875-934.

9. Jakubowski, A., Ambrose, C., Parr, M., Lincecum, J.M., Wang, M.Z., Zheng, T.S., Browning, B., Michaelson, J.S., Baetscher, M., Wang, B., et al. 2005. TWEAK induces liver progenitor cell proliferation. *J Clin Invest* 115:2330-2340.

10. Stumptner, C., Fuchsbichler, A., Lehner, M., Zatloukal, K., and Denk, H. 2001. Sequence of events in the assembly of Mallory body components in mouse liver: clues to the pathogenesis and significance of Mallory body formation. *J Hepatol* 34:665-675.

11. Fausto, N., and Campbell, J.S. 2003. The role of hepatocytes and oval cells in liver regeneration and repopulation. *Mech Dev* 120:117-130.

12. Michalopoulos, G.K., and DeFrances, M.C. 1997. Liver regeneration. *Science* 276:60-66.

13. Wang, X., Foster, M., Al-Dhalimy, M., Lagasse, E., Finegold, M., and Grompe, M. 2003. The origin and liver repopulating capacity of murine oval cells. *Proc Natl Acad Sci U S A* 100 Suppl 1:11881-11888.

14. Gordon, G.J., Coleman, W.B., and Grisham, J.W. 2000. Temporal analysis of hepatocyte differentiation by small hepatocyte-like progenitor cells during liver regeneration in retrorsine-exposed rats. *Am J Pathol* 157:771-786.

15. Theise, N.D. 2006. Gastrointestinal stem cells. III. Emergent themes of liver stem cell biology: niche, quiescence, self-renewal, and plasticity. *Am J Physiol Gastrointest Liver Physiol* 290:G189-193.

16. Roskams, T.A., Theise, N.D., Balabaud, C., Bhagat, G., Bhathal, P.S., Bioulac-Sage, P., Brunt, E.M., Crawford, J.M., Crosby, H.A., Desmet, V., et al. 2004. Nomenclature of the finer branches of the biliary tree: canals, ductules, and ductular reactions in human livers. *Hepatology* 39:1739-1745.

17. Roskams, T.A., Libbrecht, L., and Desmet, V.J. 2003. Progenitor cells in diseased human liver. *Semin Liver Dis* 23:385-396.

18. Roskams, T. 2006. Liver stem cells and their implication in hepatocellular and cholangiocarcinoma. *Oncogene* 25:3818-3822.

19. Wilson, J.W., and Leduc, E.H. 1958. Role of cholangioles in restoration of the liver of the mouse after dietary injury. *J Pathol Bacteriol* 76:441-449.

20. R., K. 1937. Studies on the cancerogenic chemical substances. . *Trans Soc Pathol Jpn.* 27:329–334.

21. Farber, E. 1956. Similarities in the sequence of early histological changes induced in the liver of the rat by ethionine, 2-acetylamino-fluorene, and 3'-methyl-4-dimethylaminoazobenzene. *Cancer Res* 16:142-148.

22. Paku, S., Schnur, J., Nagy, P., and Thorgeirsson, S.S. 2001. Origin and structural evolution of the early proliferating oval cells in rat liver. *Am J Pathol* 158:1313-1323.

23. Thorgeirsson, S.S. 1996. Hepatic stem cells in liver regeneration. *FASEB J* 10:1249-1256.

24. Alison, M. 1998. Liver stem cells: a two compartment system. *Curr Opin Cell Biol* 10:710-715.

25. Sell, S. 1994. Liver stem cells. *Mod Pathol* 7:105-112.

26. Sigal, S.H., Brill, S., Fiorino, A.S., and Reid, L.M. 1992. The liver as a stem cell and lineage system. *Am J Physiol* 263:G139-148.

27. Matsusaka, S., Tsujimura, T., Toyosaka, A., Nakasho, K., Sugihara, A., Okamoto, E., Uematsu, K., and Terada, N. 1999. Role of c-kit receptor tyrosine kinase in development of oval cells in the rat 2-acetylaminofluorene/partial hepatectomy model. *Hepatology* 29:670-676.

28. Omori, N., Omori, M., Evarts, R.P., Teramoto, T., Miller, M.J., Hoang, T.N., and Thorgeirsson, S.S. 1997. Partial cloning of rat CD34 cDNA and expression during stem cell-dependent liver regeneration in the adult rat. *Hepatology* 26:720-727.

29. Crosby, H.A., Kelly, D.A., and Strain, A.J. 2001. Human hepatic stem-like cells isolated using c-kit or CD34 can differentiate into biliary epithelium. *Gastroenterology* 120:534-544.

30. Petersen, B.E., Grossbard, B., Hatch, H., Pi, L., Deng, J., and Scott, E.W. 2003. Mouse A6-positive hepatic oval cells also express several hematopoietic stem cell markers. *Hepatology* 37:632-640.

31. Petersen, B.E., Goff, J.P., Greenberger, J.S., and Michalopoulos, G.K. 1998. Hepatic oval cells express the hematopoietic stem cell marker Thy-1 in the rat. *Hepatology* 27:433-445.

32. Dorrell, C., Erker, L., Lanxon-Cookson, K.M., Abraham, S.L., Victoroff, T., Ro, S., Canaday, P.S., Streeter, P.R., and Grompe, M. 2008. Surface markers for the murine oval cell response. *Hepatology* 48:1282-1291.

33. Tsuchiya, A., Heike, T., Baba, S., Fujino, H., Umeda, K., Matsuda, Y., Nomoto, M., Ichida, T., Aoyagi, Y., and Nakahata, T. 2008. Sca-1+ endothelial cells (SPECs) reside in the portal area of the liver and contribute to rapid recovery from acute liver disease. *Biochem Biophys Res Commun* 365:595-601.

34. Lemire, J.M., and Fausto, N. 1991. Multiple alpha-fetoprotein RNAs in adult rat liver: cell type-specific expression and differential regulation. *Cancer Res* 51:4656-4664.

35. Sell, S. 1978. Distribution of alpha-fetoprotein- and albumin-containing cells in the livers of Fischer rats fed four cycles of N-2-fluorenylacetamide. *Cancer Res* 38:3107-3113.

36. Suzuki, A., Zheng, Y.W., Kaneko, S., Onodera, M., Fukao, K., Nakauchi, H., and Taniguchi, H. 2002. Clonal identification and characterization of self-renewing pluripotent stem cells in the developing liver. *J Cell Biol* 156:173-184.

37. Braun, K.M., and Sandgren, E.P. 2000. Cellular origin of regenerating parenchyma in a mouse model of severe hepatic injury. *Am J Pathol* 157:561-569.

38. Rountree, C.B., Barsky, L., Ge, S., Zhu, J., Senadheera, S., and Crooks, G.M. 2007. A CD133-expressing murine liver oval cell population with bilineage potential. *Stem Cells* 25:2419-2429.

39. Solt, D., and Farber, E. 1976. New principle for the analysis of chemical carcinogenesis. *Nature* 263:701-703.

40. Higgins, G.M., and Anderson, R.M. 1931. Experimental pathology of the liver. I. Restoration of the liver of the white rat following partial surgical removal. *Archives of Pathology* 12:186-262.

41. Preisegger, K.H., Factor, V.M., Fuchsbichler, A., Stumptner, C., Denk, H., and Thorgeirsson, S.S. 1999. Atypical ductular proliferation and its inhibition by transforming growth factor beta1 in the 3,5-diethoxycarbonyl-1,4-dihydrocollidine mouse model for chronic alcoholic liver disease. *Lab Invest* 79:103-109.

42. Arai, M., Yokosuka, O., Fukai, K., Imazeki, F., Chiba, T., Sumi, H., Kato, M., Takiguchi, M., Saisho, H., Muramatsu, M., et al. 2004. Gene expression profiles in liver regeneration with oval cell induction. *Biochem Biophys Res Commun* 317:370-376.

43. Newsome, P.N., Hussain, M.A., and Theise, N.D. 2004. Hepatic oval cells: helping redefine a paradigm in stem cell biology. *Curr Top Dev Biol* 61:1-28.

44. Fausto, N. 1990. Hepatocyte differentiation and liver progenitor cells. *Curr Opin Cell Biol* 2:1036-1042.

45. Lowes, K.N., Croager, E.J., Olynyk, J.K., Abraham, L.J., and Yeoh, G.C. 2003. Oval cell-mediated liver regeneration: Role of cytokines and growth factors. *J Gastroenterol Hepatol* 18:4-12.

46. Geiger, H., Rennebeck, G., and Van Zant, G. 2005. Regulation of hematopoietic stem cell aging in vivo by a distinct genetic element. *Proc Natl Acad Sci U S A* 102:5102-5107.

47. Fujio, K., Evarts, R.P., Hu, Z., Marsden, E.R., and Thorgeirsson, S.S. 1994. Expression of stem cell factor and its receptor, c-kit, during liver regeneration from putative stem cells in adult rat. *Lab Invest* 70:511-516.

48. Rose, T.M., and Bruce, A.G. 1991. Oncostatin M is a member of a cytokine family that includes leukemia-inhibitory factor, granulocyte colony-stimulating factor, and interleukin 6. *Proc Natl Acad Sci U S A* 88:8641-8645.

49.   Kinoshita, T., Sekiguchi, T., Xu, M.J., Ito, Y., Kamiya, A., Tsuji, K., Nakahata, T., and Miyajima, A. 1999. Hepatic differentiation induced by oncostatin M attenuates fetal liver hematopoiesis. *Proc Natl Acad Sci U S A* 96:7265-7270.

50.   Kamiya, A., Kinoshita, T., Ito, Y., Matsui, T., Morikawa, Y., Senba, E., Nakashima, K., Taga, T., Yoshida, K., Kishimoto, T., et al. 1999. Fetal liver development requires a paracrine action of oncostatin M through the gp130 signal transducer. *EMBO J* 18:2127-2136.

51.   Bisgaard, H.C., Muller, S., Nagy, P., Rasmussen, L.J., and Thorgeirsson, S.S. 1999. Modulation of the gene network connected to interferon-gamma in liver regeneration from oval cells. *Am J Pathol* 155:1075-1085.

52.   Brooling, J.T., Campbell, J.S., Mitchell, C., Yeoh, G.C., and Fausto, N. 2005. Differential regulation of rodent hepatocyte and oval cell proliferation by interferon gamma. *Hepatology* 41:906-915.

53.   Akhurst, B., Matthews, V., Husk, K., Smyth, M.J., Abraham, L.J., and Yeoh, G.C. 2005. Differential lymphotoxin-beta and interferon gamma signaling during mouse liver regeneration induced by chronic and acute injury. *Hepatology* 41:327-335.

54.   Evarts, R.P., Nagy, P., Marsden, E., and Thorgeirsson, S.S. 1987. A precursor-product relationship exists between oval cells and hepatocytes in rat liver. *Carcinogenesis* 8:1737-1740.

55.   Nagy, P., Bisgaard, H.C., Santoni-Rugiu, E., and Thorgeirsson, S.S. 1996. In vivo infusion of growth factors enhances the mitogenic response of rat hepatic ductal (oval) cells after administration of 2-acetylaminofluorene. *Hepatology* 23:71-79.

56.   Nguyen, L.N., Furuya, M.H., Wolfraim, L.A., Nguyen, A.P., Holdren, M.S., Campbell, J.S., Knight, B., Yeoh, G.C., Fausto, N., and Parks, W.T. 2007. Transforming growth factor-beta differentially regulates oval cell and hepatocyte proliferation. *Hepatology* 45:31-41.

57.   Knight, B., Matthews, V.B., Akhurst, B., Croager, E.J., Klinken, E., Abraham, L.J., Olynyk, J.K., and Yeoh, G. 2005. Liver inflammation and cytokine production, but not acute phase protein synthesis, accompany the adult liver progenitor (oval) cell response to chronic liver injury. *Immunol Cell Biol* 83:364-374.

58.   Kirillova, I., Chaisson, M., and Fausto, N. 1999. Tumor necrosis factor induces DNA replication in hepatic cells through nuclear factor kappaB activation. *Cell Growth Differ* 10:819-828.

59.   Sanchez, A., Factor, V.M., Schroeder, I.S., Nagy, P., and Thorgeirsson, S.S. 2004. Activation of NF-kappaB and STAT3 in rat oval cells during 2-acetylaminofluorene/partial hepatectomy-induced liver regeneration. *Hepatology* 39:376-385.

60.   Libbrecht, L., Desmet, V., Van Damme, B., and Roskams, T. 2000. Deep intralobular extension of human hepatic 'progenitor cells' correlates with parenchymal inflammation in chronic viral hepatitis: can 'progenitor cells' migrate? *J Pathol* 192:373-378.

61.   Strick-Marchand, H., Masse, G.X., Weiss, M.C., and Di Santo, J.P. 2008. Lymphocytes support oval cell-dependent liver regeneration. *J Immunol* 181:2764-2771.

62.   Kerr, J.F., Wyllie, A.H., and Currie, A.R. 1972. Apoptosis: a basic biological phenomenon with wide-ranging implications in tissue kinetics. *Br J Cancer* 26:239-257.

63.   Strasser, A., O'Connor, L., and Dixit, V.M. 2000. Apoptosis signaling. *Annu Rev Biochem* 69:217-245.

64.   Yuan, J. 1996. Evolutionary conservation of a genetic pathway of programmed cell death. *J Cell Biochem* 60:4-11.

65.   Meier, P., Finch, A., and Evan, G. 2000. Apoptosis in development. *Nature* 407:796-801.

66.   Leist, M., and Jaattela, M. 2001. Four deaths and a funeral: from caspases to alternative mechanisms. *Nat Rev Mol Cell Biol* 2:589-598.

67.   Wyllie, A.H., Kerr, J.F., and Currie, A.R. 1980. Cell death: the significance of apoptosis. *Int Rev Cytol* 68:251-306.

68.   Budihardjo, I., Oliver, H., Lutter, M., Luo, X., and Wang, X. 1999. Biochemical pathways of caspase activation during apoptosis. *Annu Rev Cell Dev Biol* 15:269-290.

69.   Cikala, M., Wilm, B., Hobmayer, E., Bottger, A., and David, C.N. 1999. Identification of caspases and apoptosis in the simple metazoan Hydra. *Curr Biol* 9:959-962.

70.   Earnshaw, W.C., Martins, L.M., and Kaufmann, S.H. 1999. Mammalian caspases: structure, activation, substrates, and functions during apoptosis. *Annu Rev Biochem* 68:383-424.

71. Alnemri, E.S., Livingston, D.J., Nicholson, D.W., Salvesen, G., Thornberry, N.A., Wong, W.W., and Yuan, J. 1996. Human ICE/CED-3 protease nomenclature. *Cell* 87:171.

72. Yuan, J. 1997. Transducing signals of life and death. *Curr Opin Cell Biol* 9:247-251.

73. Reed, J.C. 2000. Mechanisms of apoptosis. *Am J Pathol* 157:1415-1430.

74. Danial, N.N., and Korsmeyer, S.J. 2004. Cell death: critical control points. *Cell* 116:205-219.

75. Peter, M.E., and Krammer, P.H. 2003. The CD95(APO-1/Fas) DISC and beyond. *Cell Death Differ* 10:26-35.

76. Kischkel, F.C., Hellbardt, S., Behrmann, I., Germer, M., Pawlita, M., Krammer, P.H., and Peter, M.E. 1995. Cytotoxicity-dependent APO-1 (Fas/CD95)-associated proteins form a death-inducing signaling complex (DISC) with the receptor. *EMBO J* 14:5579-5588.

77. Medema, J.P., Scaffidi, C., Kischkel, F.C., Shevchenko, A., Mann, M., Krammer, P.H., and Peter, M.E. 1997. FLICE is activated by association with the CD95 death-inducing signaling complex (DISC). *EMBO J* 16:2794-2804.

78. Ashkenazi, A. 2002. Targeting death and decoy receptors of the tumour-necrosis factor superfamily. *Nat Rev Cancer* 2:420-430.

79. Martin, D.A., Siegel, R.M., Zheng, L., and Lenardo, M.J. 1998. Membrane oligomerization and cleavage activates the caspase-8 (FLICE/MACHalpha1) death signal. *J Biol Chem* 273:4345-4349.

80. Wallach, D., Varfolomeev, E.E., Malinin, N.L., Goltsev, Y.V., Kovalenko, A.V., and Boldin, M.P. 1999. Tumor necrosis factor receptor and Fas signaling mechanisms. *Annu Rev Immunol* 17:331-367.

81. Salvesen, G.S., and Dixit, V.M. 1997. Caspases: intracellular signaling by proteolysis. *Cell* 91:443-446.

82. Salvesen, G.S., and Dixit, V.M. 1999. Caspase activation: the induced-proximity model. *Proc Natl Acad Sci U S A* 96:10964-10967.

83. Chang, D.W., Xing, Z., Capacio, V.L., Peter, M.E., and Yang, X. 2003. Interdimer processing mechanism of procaspase-8 activation. *EMBO J* 22:4132-4142.

84. Ashkenazi, A., and Dixit, V.M. 1998. Death receptors: signaling and modulation. *Science* 281:1305-1308.

85.   Scaffidi, C., Fulda, S., Srinivasan, A., Friesen, C., Li, F., Tomaselli, K.J., Debatin, K.M., Krammer, P.H., and Peter, M.E. 1998. Two CD95 (APO-1/Fas) signaling pathways. *EMBO J* 17:1675-1687.

86.   Zou, H., Henzel, W.J., Liu, X., Lutschg, A., and Wang, X. 1997. Apaf-1, a human protein homologous to C. elegans CED-4, participates in cytochrome c-dependent activation of caspase-3. *Cell* 90:405-413.

87.   Li, P., Nijhawan, D., Budihardjo, I., Srinivasula, S.M., Ahmad, M., Alnemri, E.S., and Wang, X. 1997. Cytochrome c and dATP-dependent formation of Apaf-1/caspase-9 complex initiates an apoptotic protease cascade. *Cell* 91:479-489.

88.   Ferri, K.F., and Kroemer, G. 2001. Organelle-specific initiation of cell death pathways. *Nat Cell Biol* 3:E255-263.

89.   Yamin, T.T., Ayala, J.M., and Miller, D.K. 1996. Activation of the native 45-kDa precursor form of interleukin-1-converting enzyme. *J Biol Chem* 271:13273-13282.

90.   Muzio, M., Stockwell, B.R., Stennicke, H.R., Salvesen, G.S., and Dixit, V.M. 1998. An induced proximity model for caspase-8 activation. *J Biol Chem* 273:2926-2930.

91.   Rotonda, J., Nicholson, D.W., Fazil, K.M., Gallant, M., Gareau, Y., Labelle, M., Peterson, E.P., Rasper, D.M., Ruel, R., Vaillancourt, J.P., et al. 1996. The three-dimensional structure of apopain/CPP32, a key mediator of apoptosis. *Nat Struct Biol* 3:619-625.

92.   Walker, N.P., Talanian, R.V., Brady, K.D., Dang, L.C., Bump, N.J., Ferenz, C.R., Franklin, S., Ghayur, T., Hackett, M.C., Hammill, L.D., et al. 1994. Crystal structure of the cysteine protease interleukin-1 beta-converting enzyme: a (p20/p10)2 homodimer. *Cell* 78:343-352.

93.   Wilson, K.P., Black, J.A., Thomson, J.A., Kim, E.E., Griffith, J.P., Navia, M.A., Murcko, M.A., Chambers, S.P., Aldape, R.A., Raybuck, S.A., et al. 1994. Structure and mechanism of interleukin-1 beta converting enzyme. *Nature* 370:270-275.

94.   Lamkanfi, M., Declercq, W., Kalai, M., Saelens, X., and Vandenabeele, P. 2002. Alice in caspase land. A phylogenetic analysis of caspases from worm to man. *Cell Death Differ* 9:358-361.

95.   Riedl, S.J., and Shi, Y. 2004. Molecular mechanisms of caspase regulation during apoptosis. *Nat Rev Mol Cell Biol* 5:897-907.

96.   Lippens, S., Kockx, M., Knaapen, M., Mortier, L., Polakowska, R., Verheyen, A., Garmyn, M., Zwijsen, A., Formstecher, P., Huylebroeck, D., et al. 2000. Epidermal

differentiation does not involve the pro-apoptotic executioner caspases, but is associated with caspase-14 induction and processing. *Cell Death Differ* 7:1218-1224.

97. Liedtke, C., Bangen, J.M., Freimuth, J., Beraza, N., Lambertz, D., Cubero, F.J., Hatting, M., Karlmark, K.R., Streetz, K.L., Krombach, G.A., et al. 2011. Loss of caspase-8 protects mice against inflammation-related hepatocarcinogenesis but induces non-apoptotic liver injury. *Gastroenterology* 141:2176-2187.

98. Kellendonk, C., Opherk, C., Anlag, K., Schutz, G., and Tronche, F. 2000. Hepatocyte-specific expression of Cre recombinase. *Genesis* 26:151-153.

99. Kuhn, R., Schwenk, F., Aguet, M., and Rajewsky, K. 1995. Inducible gene targeting in mice. *Science* 269:1427-1429.

100. Seglen, P.O. 1976. Preparation of isolated rat liver cells. *Methods Cell Biol* 13:29-83.

101. Livak, K.J., and Schmittgen, T.D. 2001. Analysis of relative gene expression data using real-time quantitative PCR and the 2(-Delta Delta C(T)) Method. *Methods* 25:402-408.

102. Bradford, M.M. 1976. A rapid and sensitive method for the quantitation of microgram quantities of protein utilizing the principle of protein-dye binding. *Anal Biochem* 72:248-254.

103. Mashima, T., Naito, M., and Tsuruo, T. 1999. Caspase-mediated cleavage of cytoskeletal actin plays a positive role in the process of morphological apoptosis. *Oncogene* 18:2423-2430.

104. Fausto, N. 2006. Involvement of the innate immune system in liver regeneration and injury. *J Hepatol* 45:347-349.

105. Fausto, N., Laird, A.D., and Webber, E.M. 1995. Liver regeneration. 2. Role of growth factors and cytokines in hepatic regeneration. *FASEB J* 9:1527-1536.

106. Fausto, N., and Webber, E.M. 1993. Mechanisms of growth regulation in liver regeneration and hepatic carcinogenesis. *Prog Liver Dis* 11:115-137.

107. Knight, B., Akhurst, B., Matthews, V.B., Ruddell, R.G., Ramm, G.A., Abraham, L.J., Olynyk, J.K., and Yeoh, G.C. 2007. Attenuated liver progenitor (oval) cell and fibrogenic responses to the choline deficient, ethionine supplemented diet in the BALB/c inbred strain of mice. *J Hepatol* 46:134-141.

108. Natori, S., Rust, C., Stadheim, L.M., Srinivasan, A., Burgart, L.J., and Gores, G.J. 2001. Hepatocyte apoptosis is a pathologic feature of human alcoholic hepatitis. *J Hepatol* 34:248-253.

109. Canbay, A., Higuchi, H., Bronk, S.F., Taniai, M., Sebo, T.J., and Gores, G.J. 2002. Fas enhances fibrogenesis in the bile duct ligated mouse: a link between apoptosis and fibrosis. *Gastroenterology* 123:1323-1330.

110. Rust, C., and Gores, G.J. 2000. Apoptosis and liver disease. *Am J Med* 108:567-574.

111. Yoon, J.H., and Gores, G.J. 2002. Death receptor-mediated apoptosis and the liver. *J Hepatol* 37:400-410.

112. Jacobson, M.D., Weil, M., and Raff, M.C. 1997. Programmed cell death in animal development. *Cell* 88:347-354.

113. Bettermann, K., Vucur, M., Haybaeck, J., Koppe, C., Janssen, J., Heymann, F., Weber, A., Weiskirchen, R., Liedtke, C., Gassler, N., et al. 2010. TAK1 suppresses a NEMO-dependent but NF-kappaB-independent pathway to liver cancer. *Cancer Cell* 17:481-496.

114. Plum, W., Tschaharganeh, D.F., Kroy, D.C., Corsten, E., Erschfeld, S., Dierssen, U., Wasmuth, H., Trautwein, C., and Streetz, K.L. 2010. Lack of glycoprotein 130/signal transducer and activator of transcription 3-mediated signaling in hepatocytes enhances chronic liver injury and fibrosis progression in a model of sclerosing cholangitis. *Am J Pathol* 176:2236-2246.

115. Seki, E., Brenner, D.A., and Karin, M. 2012. A Liver Full of JNK: Signaling in Regulation of Cell Function and Disease Pathogenesis, and Clinical Approaches. *Gastroenterology* 143:307-320.

116. Schattenberg, J.M., Worns, M.A., Zimmermann, T., He, Y.W., Galle, P.R., and Schuchmann, M. 2012. The role of death effector domain-containing proteins in acute oxidative cell injury in hepatocytes. *Free Radic Biol Med* 52:1911-1917.

117. Kaufmann, T., Jost, P.J., Pellegrini, M., Puthalakath, H., Gugasyan, R., Gerondakis, S., Cretney, E., Smyth, M.J., Silke, J., Hakem, R., et al. 2009. Fatal hepatitis mediated by tumor necrosis factor TNFalpha requires caspase-8 and involves the BH3-only proteins Bid and Bim. *Immunity* 30:56-66.

118. Fickert, P., Stoger, U., Fuchsbichler, A., Moustafa, T., Marschall, H.U., Weiglein, A.H., Tsybrovskyy, O., Jaeschke, H., Zatloukal, K., Denk, H., et al. 2007. A new xenobiotic-induced mouse model of sclerosing cholangitis and biliary fibrosis. *Am J Pathol* 171:525-536.

119. Van Hul, N.K., Abarca-Quinones, J., Sempoux, C., Horsmans, Y., and Leclercq, I.A. 2009. Relation between liver progenitor cell expansion and extracellular matrix

deposition in a CDE-induced murine model of chronic liver injury. *Hepatology* 49:1625-1635.

120. Chobert, M.N., Couchie, D., Fourcot, A., Zafrani, E.S., Laperche, Y., Mavier, P., and Brouillet, A. 2012. Liver precursor cells increase hepatic fibrosis induced by chronic carbon tetrachloride intoxication in rats. *Lab Invest* 92:135-150.

121. Alison, M.R., Golding, M.H., and Sarraf, C.E. 1996. Pluripotential liver stem cells: facultative stem cells located in the biliary tree. *Cell Prolif* 29:373-402.

122. Xiao, J.C., Jin, X.L., Ruck, P., Adam, A., and Kaiserling, E. 2004. Hepatic progenitor cells in human liver cirrhosis: immunohistochemical, electron microscopic and immunofluorencence confocal microscopic findings. *World J Gastroenterol* 10:1208-1211.

123. Richardson, M.M., Jonsson, J.R., Powell, E.E., Brunt, E.M., Neuschwander-Tetri, B.A., Bhathal, P.S., Dixon, J.B., Weltman, M.D., Tilg, H., Moschen, A.R., et al. 2007. Progressive fibrosis in nonalcoholic steatohepatitis: association with altered regeneration and a ductular reaction. *Gastroenterology* 133:80-90.

124. Lowes, K.N., Brennan, B.A., Yeoh, G.C., and Olynyk, J.K. 1999. Oval cell numbers in human chronic liver diseases are directly related to disease severity. *Am J Pathol* 154:537-541.

125. Clouston, A.D., Powell, E.E., Walsh, M.J., Richardson, M.M., Demetris, A.J., and Jonsson, J.R. 2005. Fibrosis correlates with a ductular reaction in hepatitis C: roles of impaired replication, progenitor cells and steatosis. *Hepatology* 41:809-818.

126. Roskams, T., Yang, S.Q., Koteish, A., Durnez, A., DeVos, R., Huang, X., Achten, R., Verslype, C., and Diehl, A.M. 2003. Oxidative stress and oval cell accumulation in mice and humans with alcoholic and nonalcoholic fatty liver disease. *Am J Pathol* 163:1301-1311.

127. Bustos, M., Sangro, B., Alzuguren, P., Gil, A.G., Ruiz, J., Beraza, N., Qian, C., Garcia-Pardo, A., and Prieto, J. 2000. Liver damage using suicide genes. A model for oval cell activation. *Am J Pathol* 157:549-559.

128. Santoni-Rugiu, E., Jelnes, P., Thorgeirsson, S.S., and Bisgaard, H.C. 2005. Progenitor cells in liver regeneration: molecular responses controlling their activation and expansion. *APMIS* 113:876-902.

129. Braun, K.M., Thompson, A.W., and Sandgren, E.P. 2003. Hepatic microenvironment affects oval cell localization in albumin-urokinase-type plasminogen activator transgenic mice. *Am J Pathol* 162:195-202.

130. Halilbasic, E., Claudel, T., and Trauner, M. 2012. Bile acid transporters and regulatory nuclear receptors in the liver and beyond. *J Hepatol*.

131. Watanabe-Fukunaga, R., Brannan, C.I., Copeland, N.G., Jenkins, N.A., and Nagata, S. 1992. Lymphoproliferation disorder in mice explained by defects in Fas antigen that mediates apoptosis. *Nature* 356:314-317.

132. Bobe, P., Bonardelle, D., Reynes, M., Godeau, F., Mahiou, J., Joulin, V., and Kiger, N. 1997. Fas-mediated liver damage in MRL hemopoietic chimeras undergoing lpr-mediated graft-versus-host disease. *J Immunol* 159:4197-4204.

133. Tanaka, M., Suda, T., Takahashi, T., and Nagata, S. 1995. Expression of the functional soluble form of human fas ligand in activated lymphocytes. *EMBO J* 14:1129-1135.

134. Tamura, A., Katsumata, M., Greene, M.I., and Yui, K. 1996. Inhibition of apoptosis and augmentation of lymphoproliferation in bcl-2 transgenic Fas/Fas ligand-defective mice. *Cell Immunol* 168:220-228.

135. Luna, G., Paez, J., and Cardier, J.E. 2004. Expression of the hematopoietic stem cell antigen Sca-1 (LY-6A/E) in liver sinusoidal endothelial cells: possible function of Sca-1 in endothelial cells. *Stem Cells Dev* 13:528-535.

136. Taube, R. 2004. Liver regeneration:from myth to mechanism. *Nat Rev Mol Cell Biol* 5:836-847.

137. Fausto, N. 2001. Liver regeneration: from laboratory to clinic. *Liver Transpl* 7:835-844.

138. Coussens, L.M., and Werb, Z. 2002. Inflammation and cancer. *Nature* 420:860-867.

139. Nathan, C. 2002. Points of control in inflammation. *Nature* 420:846-852.

140. Subrata, L.S., Lowes, K.N., Olynyk, J.K., Yeoh, G.C., Quail, E.A., and Abraham, L.J. 2005. Hepatic expression of the tumor necrosis factor family member lymphotoxin-beta is regulated by interleukin (IL)-6 and IL-1beta: transcriptional control mechanisms in oval cells and hepatoma cell lines. *Liver Int* 25:633-646.

141. Janeway, C.A., Jr., and Medzhitov, R. 2002. Innate immune recognition. *Annu Rev Immunol* 20:197-216.

142. Taub, R., Greenbaum, L.E., and Peng, Y. 1999. Transcriptional regulatory signals define cytokine-dependent and -independent pathways in liver regeneration. *Semin Liver Dis* 19:117-127.

143. Cressman, D.E., Greenbaum, L.E., DeAngelis, R.A., Ciliberto, G., Furth, E.E., Poli, V., and Taub, R. 1996. Liver failure and defective hepatocyte regeneration in interleukin-6-deficient mice. *Science* 274:1379-1383.

144. Sakamoto, T., Liu, Z., Murase, N., Ezure, T., Yokomuro, S., Poli, V., and Demetris, A.J. 1999. Mitosis and apoptosis in the liver of interleukin-6-deficient mice after partial hepatectomy. *Hepatology* 29:403-411.

145. Yamada, Y., Kirillova, I., Peschon, J.J., and Fausto, N. 1997. Initiation of liver growth by tumor necrosis factor: deficient liver regeneration in mice lacking type I tumor necrosis factor receptor. *Proc Natl Acad Sci U S A* 94:1441-1446.

9 Appendix

9.1 Abbreviations

AA	Amino acid
Ab	Antibody
Alb	Albumin
ALT	Alanine transaminase
as	Anti-sense
AST	Aspartate transaminase
ATP	Adenosine triphosphate
bp	Basepair
BM	Bone marrow
BrdU	5-Bromo-2'-deoxy-uridine
BSA	Bovine Serum Albumin
Casp	Caspase (cysteine aspartate-specific proteinases)
CCl_4	Carbon tetrachloride
Ccn	Cyclin
CDE	Choline-deficient, ethionine
cDNA	Complementary Desoyribonucleic acid
c-Kit	CD117 or c-Kit receptor
Cre	Causes recombination
Ct	Threshold Cycle
d	Day
DAB	Diaminobenzidine
DAPI	4',6-Diamidino-2-phenylindole
dATP	Desoxyadenosintriphospate
DDC	3,5-Diethoxycarbonyl-1,4-dihydro-collidine

DEPC	Diethyl pyrocarbonate
dH$_2$O	Distillated water
DMEM	Dulbecoo's Modified Eagle Medium
DNA	Deoxyribonucleic acid
dNTP	Desoxyribonucleosidtriphosphate
ds	Double-stranded
DTT	Dithiotreitol
dTTP	Desoxythmidintriphospate
EBSS	Earles basic salt solution
ECL	Enhanced Chemiluminescence
ECM	Extracellular matrix
EDTA	Ethylene Diamine Tetra-Acetic Acid
e.g.	For example (lat. exempli gratia)
EGF	Epidermal Growth Factor
et al.	And others
EtBr	Ethidium bromide
EtOH	Ethanol
FACS	Fluorescent Activated Cell Sorting, flow cytometry
FasL	Fas-ligand
FasR	Fas-receptor
FCS	Fetal calf serum
Fig.	Figure
FITC	Fluorescein isothiocyanate
fwd	Forward
g	Gram
g	Acceleration of gravity
GAPDH	Glyceraldehyde-3-Phosphate Dehydrogenase

h	Hour
HBSS	Hank's Balanced Salt Solution
HCC	Hepatocellular carcinoma
H&E	Hematoxyline/eosin
HGF	Hepatocyte growth factor
HRP	Horseraddish peroxidase
IGF	Insulin-like growth factor
IgG	Immunoglobulin G
IL	Inerleukin
i.p.	Intraperitoneal
kDa	Kilodalton
kg	Kilogram
L	Liter
loxP	Lipopolysaccharide
LPCs	Liver progenitor cells
μ	Micro
M	Molar
MACS	Magnetic Assorted Cells Sorting
min	Minute
mg	Miligram
ml	Milliliter
mM	Milimolar
mRNA	Messenger Ribonucleic Acid
Mx	Myxovirus resistance
NF-κB	Nuclear factor-kappa B
ng	Nanogram

NID	Non-ionic detergent
NIH	National Institutes of Health
nm	Nanometer
NPC	Non parenchymal cell
NP40	Nonidet P40
OD	Optical Density
p-	Phosphor-
p53	Protein 53 or tumor protein 53
PBS	Phosphate buffered saline
PCNA	Prolifeating Cell Nuclear Antigen
PCR	Polymerase Chain Reaction
PE	Phycoerythrin
PerCP	Peridinin Chlorophll Protein
PFA	Paraformaldehyde
pH	Potential Hydrogenii
PI	Propidium iodide
pIpC	Polyriboinosinic-polyribocytidylic
PMSF	Phenylmethyl sulfonyl flurodie
P/S	Penicillin/streptomycin
rev	Reverse
RNA	Ribonucleic acid
rpm	Rounds per minute
RT	Room temperature
RT-PCR	Real-Time Polymerase Chain Reaction
S	Sense
SD	Standard deviation
SDS PAGE	Sodium Dodecyl Sulfate Polyacrylamide Gel Electrophoresis

SMA	Smooth Muscle Actin
STAT	Signal Transducer and Activator of Transcription
TAE	Tris-acetat-EDTA
Taq	*Thermus aquaticus*
TBS	Tris buffered saline
TBS-T	Tris buffered saline supplemented with Tween 20
TE	Tris-EDTA
TEMED	N,N,N',N'-Tetramethylethylendiamin
TNF-α	Tumornecrosis factor alpha
TRIS	Tris(hydroxymethyl)aminomethane
TUNEL	Terminal Deoxynucleotidyl Transferase dUTP Nick End Labeling
U	Unit
UKA	Universitatsklinikum Aachen
v	Volume
vs.	Versus
w	Week
wt	Weight
WT	Wild-type

Eidesstattliche erklärung

Hiermit erkläre ich, Kunal Chaudhary, dass ich die Dissertation mit dem Titel:

Differential Role of Caspase-8 in Hepatocytes and Non-Parenchymal Liver Cells in a Model of Chronic Liver Injury and Progenitor Cell Activation

selbständig verfasst habe.

Bei der Anfertigung wurden folgende Hilfen Dritter in Anspruch genommen:

• In der Abteilung Gastroenterologie und Stoffwechselkrankheiten der medizinischen Klinik III im Universitätsklinikum Aachen habe ich die Versuche mit den im Kapitel „Material und Methoden" aufgeführten Hilfen und Hilfsmitteln durchgeführt.

• Die Anfertigung erfolgte unter der Leitung von P.D. Dr. med. Konrad Streetz, Abteilung Gastroenterologie und Stoffwechselkrankheiten der medizinischen Klinik III im Universitätsklinikum Aachen, die fachliche Betreuung wurde von Prof. Dipl. Ing. Dr. Werner Baumgartner Abteilung Zelluläre Neurobionik Institut für Biologie II der RWTH Aachen übernommen.

Ich habe keine entgeltliche Hilfe von Vermittlungs- bzw. Beratungsdiensten in Anspruch genommen. Niemand hat von mir unmittelbar oder mittelbar entgeltliche Leistungen für Arbeiten erhalten, die im Zusammenhang mit dem Inhalt der vorgelegten Dissertation stehen. Die Synthesen der verwendeten Primer, Sonden und Antikörper wurden von den jeweils erwähnten Firmen durchgeführt

Ich habe die Dissertation an folgenden Instituten angefertigt:

Abteilung Gastroenterologie und Stoffwechselkrankheiten der medizinischen Klinik III im Universitätsklinikum Aachen

Die Dissertation wurde bisher nicht für eine Prüfung oder Promotion oder für einen ähnlichen Zweck zur Beurteilung eingereicht.

Ich versichere, dass ich die vorstehenden Angaben nach bestem Wissen vollständig und der Wahrheit entsprechend gemacht habe.

_____ **Aachen, 25 September 2012**

Acknowledgment

Publications

Teile dieser Arbeit wurden bereits vorab veröffentlicht oder zur Publikation eingereicht:

- **Chaudhary, K.,** Liedtke, C., Trautwein, C., Streetz, K.L., Heterologous roles for caspase-8-signalling in hepatocytes and non-parenchymal cells in a model of liver stem cell activation and sclerosing cholangitis. Oral presentation at the International Liver Congress^{TM} 2012 by EASL. April 2012. Barcelona, Spain.

- **Chaudhary, K.,** Liedtke, C., Trautwein, C., Streetz, K.L., Differential roles of caspase-8-signalling in hepatocytes and non-parenchymal cells in a model of liver progenitor cell activation and sclerosing cholangitis, The Liver Congress 2011 by AASLD, Nov. 2011, *Hepatolog*y, 54 (4), p.959a, 2011. San Francisco, USA.

- **Chaudhary, K.,** Liedtke, C., Trautwein, C., Streetz, K.L., Hepatocyte protection by conditional caspase8-deletion hampers activation of the liver progenitor cell compartment in a model of sclerosing cholangitis, The Liver Congress 2010 by AASLD, Oct.-Nov. 2010, *Hepatology*, 52 (4), p.967a, 2010. Boston, USA.

Lebenslauf

Name:	Kunal Chaudhary
Geburtsdatum:	25.09.1979
Geburtsort:	Kota, Indien
Familienstand:	Verheiratet

Schulausbildung: 1996-1998

Higher Secondary School, Gujarat, Indien

Studium: 1998-2002

Bachelor of Science (B.Sc)

Navinchandra Mafatlal College of Agril. Sciences, Gujarat, Indien

2003-2006

Master of Science (M.Sc)

Georg-August Universität. Göttingen, Deutschland

2006-2007

Master of Science (M.Sc)

Gent Universität, Gent, Belgien

Wissenschaftliche **2008-2008**

Tätigkeit: Wissenschaftlicher Assistent

Deutsch Primatenzentrum (DPZ GmbH), Leibniz Institut für Primatenforschung, Göttingen, Deutschland

2008-2009

Wissenschaftlicher Assistent

Cardiovascular Research Institute Maastricht, Universitätsklinik Maastricht, Niederlande

2009-2012

Doktorand

Forschunglabor der Medizinischen Klinik III in der Arbeitsgruppe von PD. Dr. med. Konrad Streetz

Universitätsklinikum Aachen, RWTH Aachen, Deutschland